

# Project X Initial Configuration Document - 2

**V1.0**  
**March 17, 2010**

## **The Project X Collaboration:**

**Argonne National Laboratory**  
**Brookhaven National Laboratory**  
**Cornell University**  
**Fermi National Accelerator Laboratory**  
**Lawrence Berkeley National Laboratory**

**Oak Ridge National Laboratory/SNS**  
**Michigan State University**  
**Thomas Jefferson National Accelerator Facility**  
**SLAC National Accelerator Laboratory**  
**ILC/America's Regional Team**

**Bhabha Atomic Research Laboratory,**  
**Mumbai**  
**Inter-University Accelerator Center, Delhi**

**Raja Ramanna Center for Advanced**  
**Technology, Indore**  
**Variable Energy Cyclotron Center, Kolkata**

ICD-2 Version 1.0 Approval



---

Stephen D. Holmes, Acting Project Manager

## Table of Contents

<b>I</b>	<b>Introduction.....</b>	<b>2</b>
<b>II</b>	<b>Technical Goals and Assumptions .....</b>	<b>5</b>
II.1	Technical Goals .....	6
II.2	Operational Scenario and Assumptions.....	6
<b>III</b>	<b>Physics Design and Parameters .....</b>	<b>9</b>
III.1	CW Linac.....	9
III.2	2 GeV Beam handling.....	25
III.3	Rapid Cycling Synchrotron .....	36
III.4	Recycler/Main Injector.....	64
<b>IV</b>	<b>Requirements and Initial Configuration of Major Subsystems .....</b>	<b>65</b>
IV.1	CW Linac .....	66
IV.2	Collimators and Beam Dump .....	69
IV.3	Rapid Cycling Synchrotron .....	72
IV.4	MI/RR .....	87
IV.5	Cryogenics.....	88
IV.6	Instrumentation .....	89
IV.7	Controls: .....	91
IV.8	LLRF .....	91
IV.9	Safety and radiation shielding.....	92
IV.10	Conventional Facilities .....	96
<b>V</b>	<b>Appendix A: Longitudinal Beam Motion in a Flat-Bottom Potential Well.....</b>	<b>100</b>

## I Introduction

Project X is a high intensity proton facility conceived to support a world-leading program in neutrino and flavor physics over the next two decades at Fermilab. Project X is an integral part of the Fermilab Roadmap as described in the Fermilab Steering Group Report of August 2007 (<http://www.fnal.gov/pub/directorate/steering/index.shtml>) and of the Intensity Frontier science program described in the P5 report of May 2008 ([http://www.er.doe.gov/hep/files/pdfs/P5\\_Report%2006022008.pdf](http://www.er.doe.gov/hep/files/pdfs/P5_Report%2006022008.pdf)).

The primary elements of that research program to be supported by Project X include:

- *A neutrino beam for long baseline neutrino oscillation experiments.* A new 2 megawatt proton source with proton energies between 50 and 120 GeV would produce intense neutrino beams, directed toward a large detector located in a distant underground laboratory.
- *Kaon and muon based precision experiments running simultaneously with the neutrino program.* These could include a world leading muon-to-electron conversion experiment and world leading rare kaon decay experiments.
- *A path toward a muon source for a possible future neutrino factory and, potentially, a muon collider at the Energy Frontier.* This path requires that the new proton source have significant upgrade potential.

These elements are expected to form the basis of the Mission Need statement as is required for Critical Decision 0 (CD-0), and must be incorporated into the design criteria for Project X.

The initial Project X goals and associated design concept<sup>1</sup> were primarily driven by the Project X synergy with the ILC and the 2-MW operation of the Main Injector for the long baseline neutrino program. The details of operation with a slow extracted beam at 8 GeV were not considered in the first proposal. While some enhancements were introduced in the Project X ICD-1<sup>2</sup> it still follows the same path as the initial Project X proposal but with an increased beam current. The accelerator complex defined in ICD-1 can drive the long-baseline neutrino program, and provide enhanced capabilities in the muon-to-electron conversion experiment (mu2e); however, it does not provide a flexible platform to pursue a broader research program in rare muon and kaon processes based on high duty-factor beams.

Motivated by the lack of flexibility in ICD-1, and as part of the standard DOE planning process, the Project-X design team is considering additional configurations that can meet the research goals of the expected Mission Need statement. This document, Initial Configuration Document-2 (ICD-2), describes such a design.

ICD-2 is comprised of a 2-GeV superconducting CW (continuous wave) linac, a 2-8 GeV rapid cycling synchrotron (RCS), and the existing (but modified) Recycler and Main Injector to provide in excess of 2 MW of beam power throughout the energy range 60 – 120 GeV, simultaneous with 2 MW at 2 GeV and 80-190 kW at 8 GeV. **The ICD-2 scope can be described as follows: from the ion source to the RF separator at 2 GeV and to the extraction kicker in the Main Injector.** A schematic layout is shown in Figure I-1. It is anticipated that the final configuration and operating parameters of the complex will be refined through the R&D program in advance of CD-2.

The intent of this configuration is to strengthen the rare processes physics program. This program typically requires a high duty-factor beam<sup>3</sup>, with a beam energy above the kaon production threshold (1.6 GeV). In ICD-1 this may be achieved with a slow-extracted beam at 8 GeV, although the slow-extracted beam delivery is outside of the ICD-1 scope. A re-configuration of the low-energy portion of Project X superconducting linac from a pulsed to the CW regime opens new possibilities. Using high efficiency RF separation of the beam allows for a simultaneous operation of several experiments so that each experiment receives the desired beam intensity and structure. In particular, it allows one to run simultaneously two of the highest priority experiments: the muon-to-electron conversion and the rare kaon decays. The requirements of these experiments determine the energy of the CW linac to be 2 GeV (kinetic). In addition, depending on the MI operating energy (60 or 120 GeV), 60 to 200 kW of single-turn extracted protons are available from the Recycler at 8 GeV to support experiments such as g-2 (which requires muons at 3.1 GeV and therefore at least 8 GeV protons). In contrast, the high beam power available at 8 GeV in ICD-1 is not readily usable by the rare processes experiments that require a slow extraction of the beam. The slow extraction process has intrinsic limits because of space charge tune-shifts and particle losses; it also typically precludes running simultaneously more than one experiment with differing beam structure requirements.

---

<sup>1</sup> Project X-doc-79

<sup>2</sup> ICD-1, <http://projectx.fnal.gov/>

<sup>3</sup> [http://www.fnal.gov/pub/projectx/pdfs/ICD-2\\_Research\\_Program\\_Task\\_Force\\_v6.pdf](http://www.fnal.gov/pub/projectx/pdfs/ICD-2_Research_Program_Task_Force_v6.pdf)

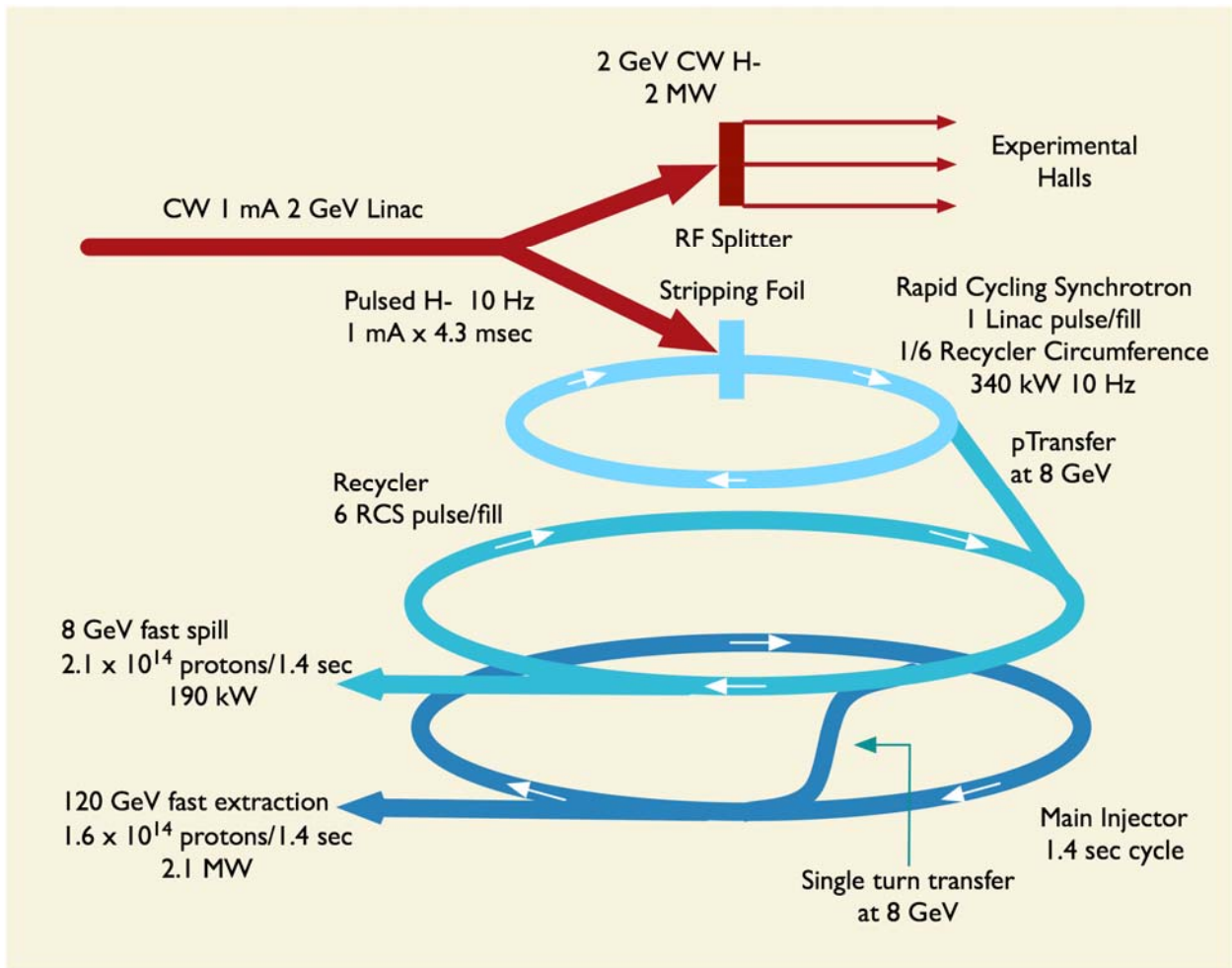


**Figure I-1: The schematic layout of ICD-2**

A CW linac provides several important advantages to the rare processes experimental program while preserving the beam characteristics for the long baseline neutrino program. The beam quality and the duty factor of a CW linac are significantly better than that for slow extracted beams. The linac beam intensity does not have the fluctuations inherent in slow extracted beam and has nearly 100% duty factor. The bunch length in a linac ( $<10$  ps RMS) is much smaller than can be reasonably achieved in a ring, which allows one to use high accuracy time of flight measurements for particle identification. The beam power in a CW linac is set by high energy physics requirements (ability to use this power by experiments) rather than by technical or accelerator physics limitations. A reduction of particle yield due to decrease of the beam energy from 8 to 2 GeV can be compensated by a larger linac power. More importantly, the unwanted physics backgrounds tend to decrease (with beam energy) significantly faster than the particle yield resulting in better overall experimental conditions<sup>4</sup>.

<sup>4</sup> Ibid.

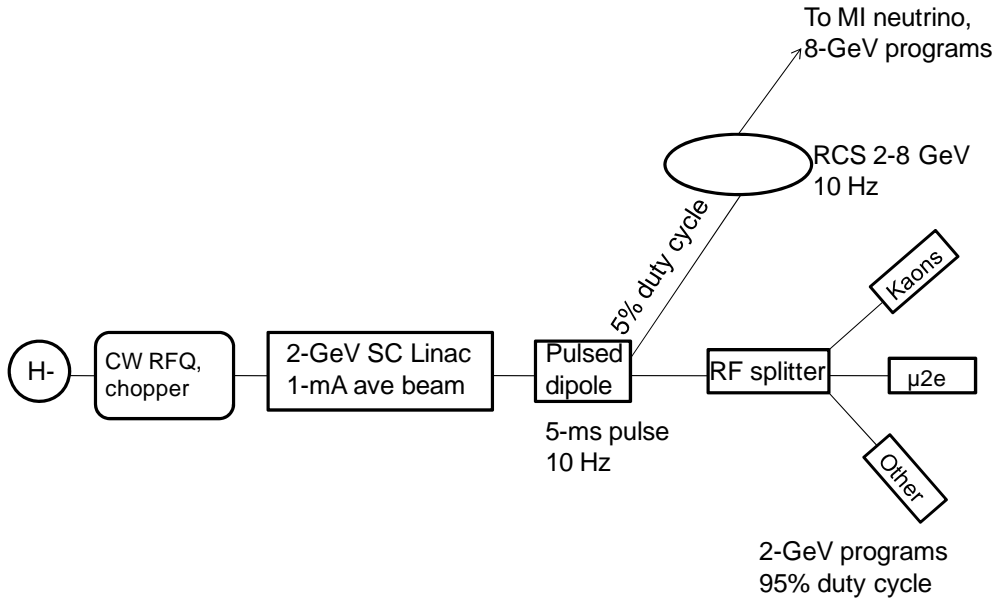


**Figure I-2:** A more detailed schematic layout of the linac portion of the ICD-2 accelerator complex.

Figure I-2 presents a more detailed schematic of the ICD-2 accelerator complex. The beam originates from a 1-10 mA DC  $H^-$  source. The beam is then bunched and accelerated by a CW normal-conducting RFQ to 2.5 MeV and the bunch structure is formatted by a chopper following a pre-programmed timeline. From 2.5 MeV to 2 GeV the  $H^-$  bunches are accelerated by a CW superconducting RF (SRF) linac. The average beam current in the SRF linac is 1 mA. For this conceptual study we reuse designs of cavities, cryomodules and beam optics (to the extent possible) developed for the pulsed linac in ICD-1. For the ILC-like portion of the CW linac ( $\beta=1$ ) we have selected the maximum accelerating cavity gradient of 17 MV/m. About 5% of the linac duty cycle (5 ms at 10 Hz) is diverted by a pulsed magnet to a 550-m long rapid cycling synchrotron (RCS) with  $2.6 \times 10^{13}$   $H^-$  ions per pulse. The rest of the duty cycle (about 1.9 MW) is delivered to the rare decay experiments at 2 GeV. At injection into the RCS the  $H^-$  ions are stripped in a manner that “paints” the beam both transversely and longitudinally to reduce space charge forces. Following the 4.3 ms injection, the proton beam is moved off the stripping foil, is accelerated, and transferred in a single turn into the Recycler. Six such pulses are box-car stacked in the Recycler and then transferred in a single turn into the Main Injector. These protons are then accelerated to 120 GeV and fast extracted to a neutrino target. The 120 GeV Main Injector cycle takes 1.4 seconds, producing 2.1 MW of beam power. At lower proton energies the Main Injector cycle is shorter. Remaining RCS pulses are available for an 8 GeV program (between 2 and 8 pulses depending upon the target Main Injector energy). The total 8 GeV beam power is in the range of 60-200 kW with Main Injector operations at  $\sim 2$  MW.

## II Technical Goals and Assumptions

The overall goal of ICD-2 is to provide a basis for a cost estimate necessary as part of the Critical Decision 0 (CD-0) process, the first step in the critical decision tree mandated by DOE order 413.3. CD-0 requires a cost range and discussion of alternatives. The cost range will be

established via initial cost estimates for ICD-1 and ICD-2 completed under common ground rules and assumptions.

## II.1 Technical Goals

High level performance goals associated with Project X ICD-2 are listed in Table II-1.

The proposed experimental program determines the energy of the linac. The linac energy of 2 GeV is believed to be sufficient to meet the requirements of both the muon conversion program and a kaon programs.

Description	Req.	Unit
MI Beam Power	2	MW
Linac Beam Power	2	MW
RCS Beam Power	340	kW
Available (outside of MI) 8 GeV Beam Power	60	kW
MI Availability	80	%
8 GeV Availability	85	%
2 GeV Availability	90	%

**Table II-1: Performance Goals for the Project X Accelerator Facility**

## II.2 Operational Scenario and Assumptions

In the operational scenario, the facility provides beam to multiple end users concurrently. The pulsed beam from the Main Injector is delivered to a long baseline neutrino oscillation experiment (50-120 GeV) and, if desired, from the Recycler to other users at 8-GeV. The CW beam is delivered to three users simultaneously by way of selectively filling appropriate RF buckets at the front end of the linac and then RF separating them to three different target halls<sup>5</sup>. The design of target halls and the experimental apparatus is outside of the project scope. For the initial scenario we have used a muon conversion experiment and a rare kaon decay experiment as the two of the three CW beam users. The third user is not yet determined at the time of this report writing.

For the long baseline neutrino experiment, the H<sup>-</sup> source provides  $2.6 \times 10^{13}$  ions to the RCS, where they are stripped, stored and accelerated before a single turn transfer to the Recycler. 6 such pulses are boxcar stacked in the Recycler, then transferred in a single turn to the Main Injector. The Main Injector ramps to 120 GeV and delivers the beam through a single turn fast extraction to a transport line (outside the scope of this project). This cycle repeats every 1.4 seconds. A possible alternative is for the Main Injector to ramp to 60 GeV, in which case the cycle repeats every 0.8 seconds (see Figure II-1).

---

<sup>5</sup> In this document we consider 3 end users. However the number of users can be increased if required by installation of additional RF separators, serially to the existing one/ones. These separators, if required, can be added to the project at any time.

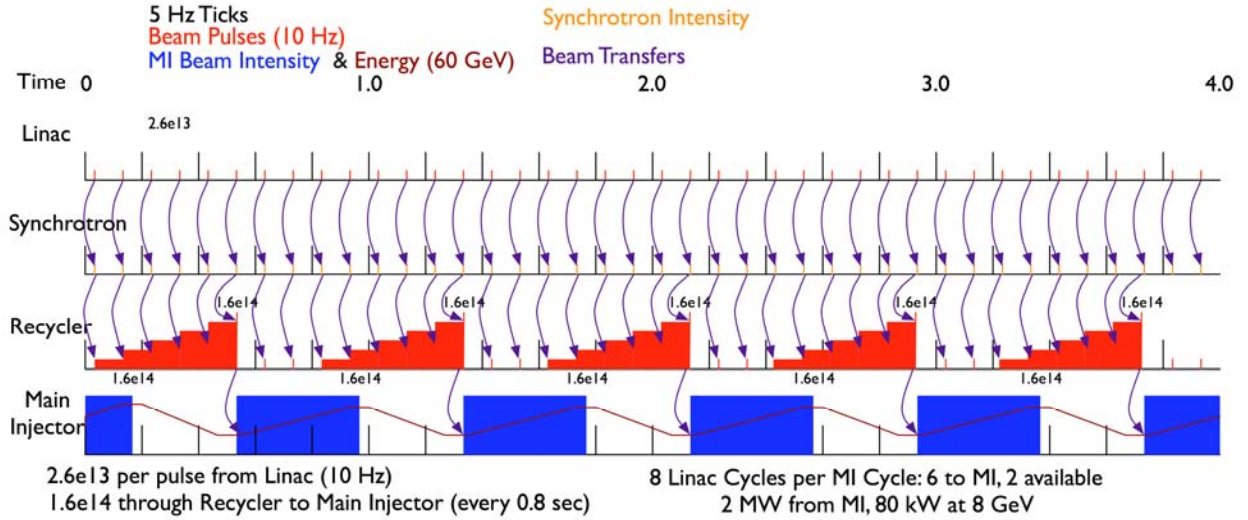


**Figure II-1: Initial LBNE scenario over 4 seconds, assuming a 60 GeV (0.8 sec) MI cycle.**

For the rare-decay program, the facility will provide 1 mA (average) of  $H^-$  ions at 2 GeV with variable and adjustable bunch structures. For the initial configuration we have used beam requirements developed for the “Muon conversion” and “Kaon” experimental programs. Table II-2 presents these requirements.

	Train Frequency	Pulse Width (nanoseconds)	Inter-Pulse Extinction
Kaon experiments	20-30 MHz	0.1-0.2	$10^{-3}$
Muon conversion experiment	0.5-1.0 MHz	50	$10^{-9}$

**Table II-2: Bunch train requirements for the kaon and muon rare decay programs**

Several front end beam subsystems will be employed to provide beam users with a variable bunch pattern concurrently. These subsystems will be described in detail in the following sections. Here, we will briefly touch upon the main considerations. For the optimal linac operation the power of RF system should be matched to the required beam power. This minimizes the operational cost; and, for constant beam intensity, it results in no energy variations related to the beam intensity. If the average beam intensity stays constant but the peak intensity varies with time so that the beam power (temporarily) exceeds the power of the RF system, the beam energy begins to droop. Fortunately, SC cavities have a comparatively large stored energy that strongly suppresses the energy variations if the beam intensity variations are sufficiently fast. For the accelerating gradient of 17 MV/m, suggested for the ILC section of the CW linac, the stored energy in a Tesla-type cavity is  $\sim 30$  J/cavity. This means that for an average beam current of 1 mA, any intensity redistribution within  $\sim 3$   $\mu$ s results in energy gain variation of less than 0.1%. All presently suggested experiments require significantly faster beam intensity variations (or bunching patterns) leading to these variations being “invisible” for the accelerating structures. In our configuration we are proposing to use a variable intensity DC ion source, capable of delivering 0-10 mA of  $H^-$  ions. After bunching at 162.5 MHz the beam is chopped so

that each experiment would receive a desired beam pattern. The only limitations are that (1) the average beam current should not exceed 1 mA, (2) all bunches (which are not chopped out) have the same intensity, and (3) the pattern period for each experiment would not exceed a few microseconds.

As an example, Figure II-2 presents a possible beam structure to support a muon conversion experiment, rare kaon experiments, and a third unspecified program. Using an RF separator running at nine/fourths of the bunch frequency (365.625 MHz), every other pulse is available to the muon experiment, so a burst of 10 81.25-MHz bunches (~100 nsec) of  $1.25 \times 10^8$  ppb can be provided. The other RF buckets are equally split between two other experiments. To match the 20-30 MHz desired bunch spacing, further chopping can be done and provide beam at 20.3 MHz. In this example the CW linac provides 400 kW of 2 GeV  $H^-$  ions for the muon conversion experiment and 800 kW to the two additional locations simultaneously. In this example the  $H^-$  ion source delivers about 3.3 mA DC. The average current is then reduced to 1 mA by chopping.

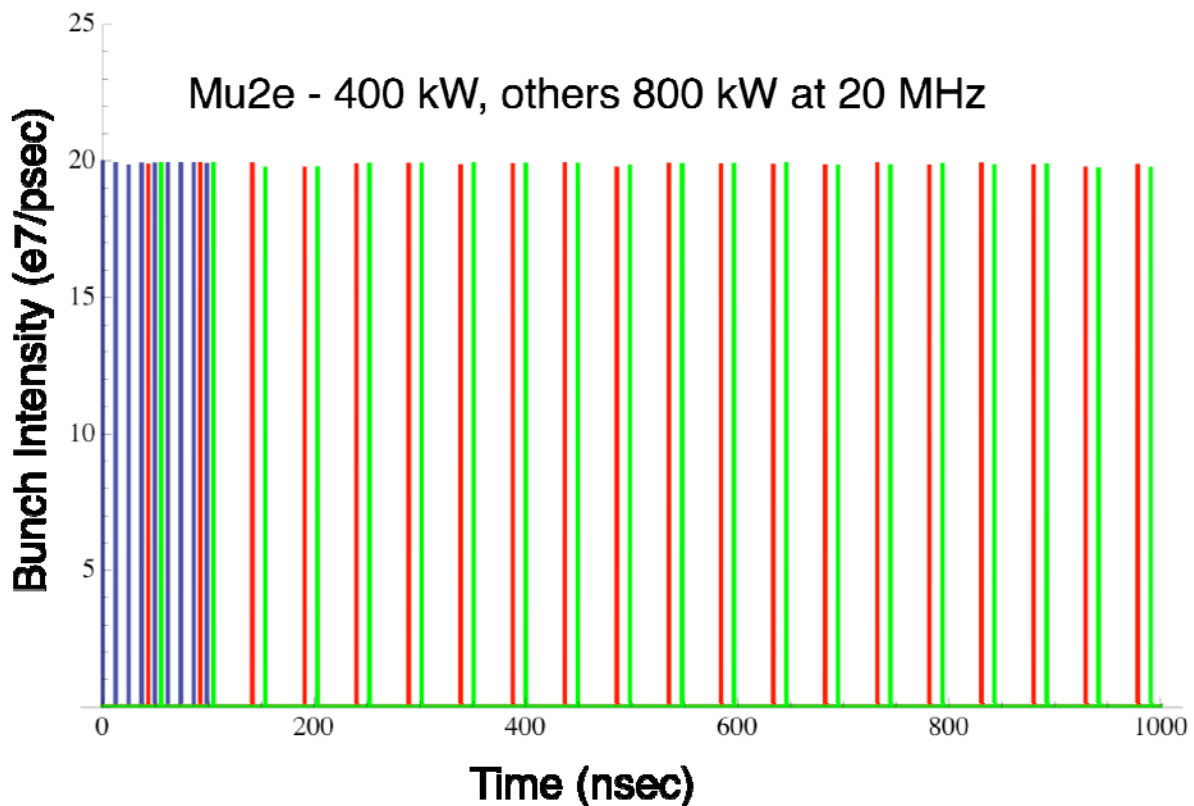


**Figure II-2: 1  $\mu$ sec period for linac, with blue pulses for the muon conversion experiment, red for rare kaon decay experiments, and green for other experiments. The integral bunch intensity is  $1.25 \times 10^8$  with a 10 psec RMS.**

For this operating scenario, and to meet the technical goals, the following assumptions are made about the state of operations at Fermilab for the initial configuration:

- The existing Linac and Booster will not be operational once Project X becomes fully operational.
- The existing Tevatron and supporting utilities will not be operational.
- The existing test beam facility in Meson, based on 120 GeV beam from the Main Injector, will remain available at low duty factor.

- A neutrino beam-line directed towards LBNE will be operating with beam power on target of 700 kW, with shielding and infrastructure designed to accommodate up to 3 MW.
- For the purpose of this document, the interface to the LBNE beam-line is defined as the Main Injector extraction kicker and the interface to the 2 GeV experimental programs is the RF transverse separator.

### III Physics Design and Parameters

#### III.1 CW Linac

The beam originates from a 1-10 mA DC H<sup>+</sup> source. The beam is then bunched and accelerated by a CW normal-conducting RFQ to 2.5 MeV and a chopper, following a pre-programmed timeline, formats the bunch pattern. Figure III-1 shows this linac timeline schematically. There are two timeline periods: (1) the long time period associated with a 10-Hz injection rate to RCS and (2) the short time period (~ μs) associated with the rare-decay experiments (see Figure II-2).

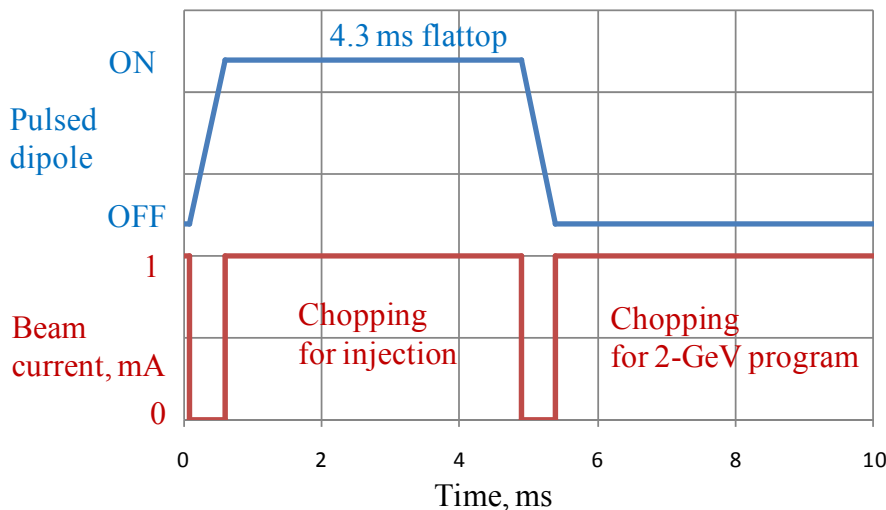


**Figure III-1: A schematic timeline for linac beam current (first 10 ms of the 100 ms cycle). The pulsed magnet's rise and fall time is assumed to be 0.5 ms.**

From 2.5 MeV to 2 GeV the H<sup>+</sup> bunches are accelerated by a CW superconducting RF (SRF) linac. The average beam current in the SRF linac is 1 mA. For this conceptual study we reuse designs of cavities, cryomodels and beam optics (to the extent possible) developed for the pulsed linac in ICD-1. For the ILC-like portion of the CW linac ( $\beta=1$ ) we have selected the maximum accelerating cavity gradient of 17 MV/m with a Q-factor of  $1.5 \times 10^{10}$  at 2K. Since the linac average beam current is 1 mA and the beam current at the ion source can be as high as 10 mA, up to 90% beam has to be removed by a chopper in the MEBT section. The power of removed beam is quite high, on order 25 kW, and thus it will require a dedicated beam dump. The beam energy of 2.5 MeV was chosen in part because it is below the neutron production threshold for most materials.

The 2-GeV CW linac has an average current (over few microseconds) of 1 mA, with a pulsed current of up to 10 mA. Since the pulsed 8-GeV Project X linac (ICD-1) has a well developed optics model operating at this current range, it is possible to use the same structure of the linac and same break points as in the pulsed linac with the necessary modifications to operate in a CW regime.

The CW linac (see Figure III-2) consists of a low-energy 325 MHz SRF section (2.5 - 450 MeV) containing three different families of single-spoke resonators (SSR0, SSR1, SSR2) and one family of a triple-spoke resonator (TSR), and the high energy 1.3-GHz SRF section (450 MeV – 2 GeV) containing squeezed elliptical  $\beta_G=0.81$  cavities (S-ILC), and ILC-type  $\beta_G=1$  cavities.

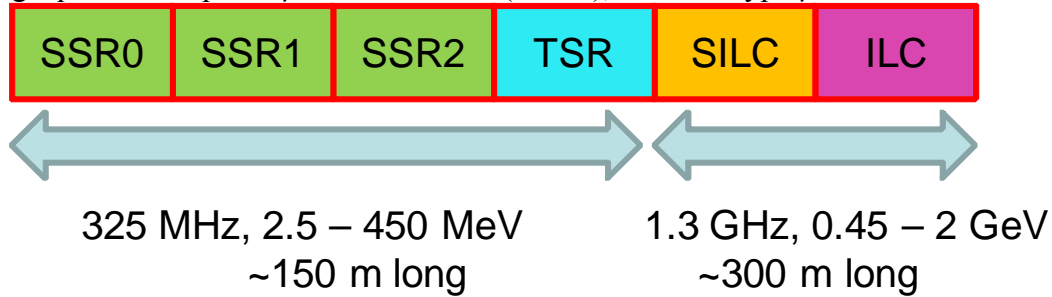


**Figure III-2: The schematic of the CW linac (2.5 MeV – 2 GeV).**

The RMS normalized beam emittance budget is as follows: 0.25 mm-mrad at the ion source, 0.4 mm-mrad at the exit of the CW linac, and 0.5 mm-mrad at the injection foil of the RCS.

The focusing lattice elements are shown in Table III-1. In the initial part of the low-energy linac, focusing is provided by solenoids. Starting with the TSR section, a standard FODO lattice is used. All magnets are superconducting with built-in dipole correctors for beam steering.

Cavities and focusing elements are grouped in cryomodules. For the high energy linac, ILC Type-4 cryomodules are used with minor modifications.

Section	SSR-0	SSR-1	SSR-2	TSR	S-ILC	ILC
Focusing	SR	SR	SR <sup>2</sup>	FRDR	FR <sup>2</sup> DR <sup>2</sup>	FR <sup>5</sup> DR <sup>5</sup>

**Table III-1: The linac focusing lattice: S – solenoid, R resonator, F and D - quadrupoles.**

The diagnostics includes a BPM in each magnet package. The SRF linac will include several warm sections with a matching section in one of them. These sections will be used for optics matching and diagnostics, such as bunch transverse and longitudinal profile monitors, beam loss monitors, etc. Warm sections will also contain collimation sections necessary to avoid uncontrolled beam loss and protect SC cavities and quads. These warm insertions will be determined by requirements of safe and reliable operations, diagnostics, collimation, and cryogenic segmentation constraints.

### III.1.1 Ion sources, RFQ and MEBT

The H<sup>+</sup> ion source should provide 10mA DC current. The transverse emittance is required to be less than 0.25 mm-mrad (RMS normalized) and beam halo must be controlled to prevent unacceptable resultant beam losses at high energies. The CW RFQ section provides bunching of the beam at 162.5 MHz and acceleration to 2.5 MeV.

For this conceptual study, we assumed the bunch repetition rate within a train to be 162.5 MHz, however not all of the RF buckets would contain bunches. There are two principal time structures needed for the linac operation: (1) a pulsed 5 ms structure at 10 Hz and (2) CW with a bunch structure variation at the microseconds level. The pulsed time structure is required to provide 4.3-ms long trains of bunches at 10 Hz for the injection into the Rapid Cycling Synchrotron (RCS). The bunch structure must incorporate the RCS RF bucket frequency (50.33 MHz) structure to facilitate pseudo bunch-to-bucket transfer (Figure III-3) and also the RCS revolution frequency (0.513 MHz) structure to provide a 200-ns extraction gap in the RCS ring. The CW bunch structure is determined by rare decay experiments, an example is shown in Figure II-2. In summary, the beam bunches can occupy arbitrary RF buckets as long as the average current does not exceed 1 mA. It is likely that such a time structure will be provided by two choppers, the first one (a pre-chopper) immediately after the ion source and the second in the MEBT section after the beam acceleration in the RFQ.

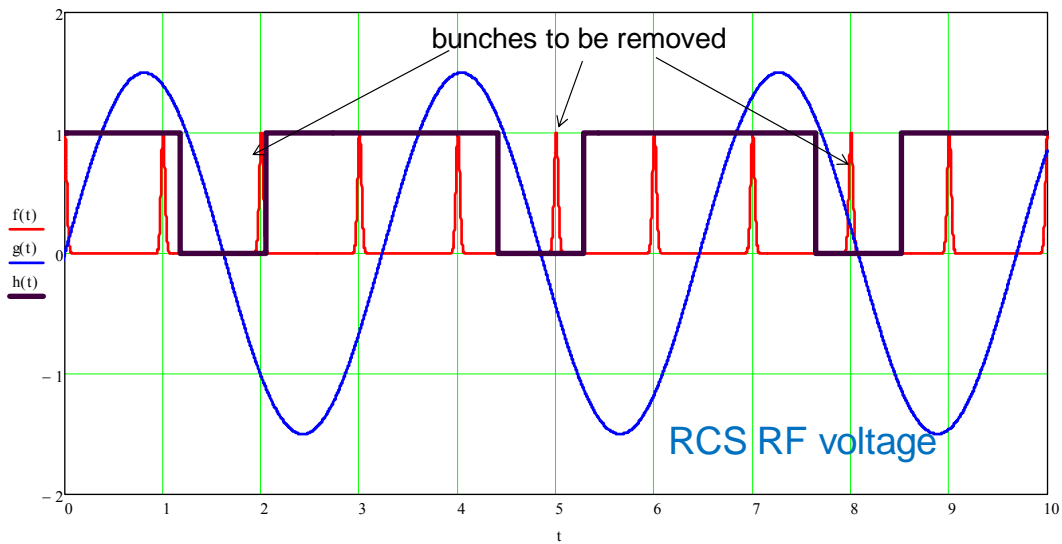


**Figure III-3: An example of the bunch chopping pattern for the RCS injection. The x-axis is in units of the bunch period ( $1/162.5$  MHz), the y-axis is an arbitrary scale. The bunch repetition rate is 162.5 MHz (red), while the RCS RF cavity voltage frequency is 50.33 MHz (blue). Bunches outside of the  $\pm 7.3$ -ns long gate (black) are to be removed by the chopper.**

For the purposes of this document, we will assume that the chopper is capable of removing individual bunches or groups of bunches. Such a chopper may be made of a single or multiple kickers. Preliminary simulations of the RFQ shows that the 100% bunch length is 1 ns while the spacing between the bunches is 6.15 ns. The chopper pulse should deflect the bunch by about 10 mrad. In order to absorb the deflected beam, the beam displacement should be at least 4 RMS beam sizes at the absorber location. Figure III-4 shows a schematic chopper pulse. The pulse flattop should be 1.5 ns or more. Such a scheme requires a wide band chopper with bandwidth of  $\sim 1$  GHz. A possible design can be based on a meander line proposed for the SPL in CERN<sup>6</sup>.

<sup>6</sup> T. Kroyer, F. Caspers, E. Mahner, “The CERN SPL Chopper Structure: A Status Report”, CARE-Report-06-033-HIPPI, Geneva, Switzerland, October 2006

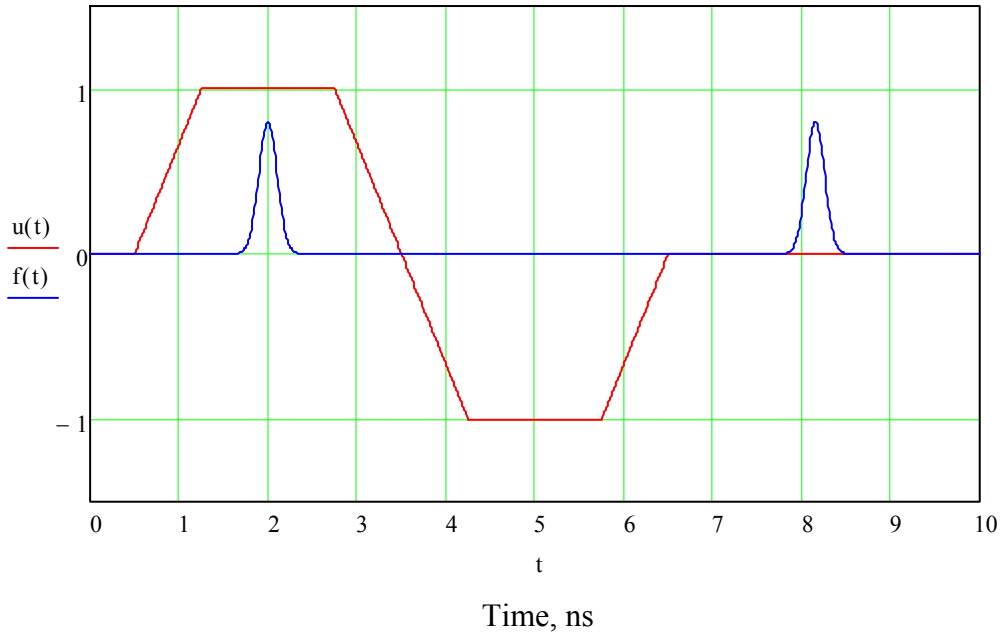


**Figure III-4: A schematic chopper pulse (red) and two consecutive beam bunches (blue).**

The MEBT section will contain the above mentioned chopper, several bunching SRF cavities in order to condition the beam for injecting it into the 325-MHz linac section, and beam diagnostics instrumentation.

### III.1.2 Low-beta section

The major modification between ICD-1 and ICD-2 in the low energy (325-MHz) part includes replacing buncher cavities and 16 room temperature crossbar cavities with the SC spoke cavities. The break points between sections containing the cavities of different types are shown in Table III-2. The MEBT bunching cavities together with focusing solenoids are presented. The number of focusing elements and cryomodules are also shown.

Section	Energy range MeV	$\beta$	Number of cavities/ lenses/CM	Type of cavities and focusing element	Maximal power/cavity, kW ( $I_{av}=1$ mA)
Bunching SSR0 ( $\beta_G=0.11$ )	2.5	0.073	2/3/2	Single spoke cavity, Solenoid	>0.1
SSR0 ( $\beta_G=0.11$ )	2.5-10	0.073-0.146 0.073-0.145	16/16/2	Single spoke cavity, Solenoid	0.8
SSR1 ( $\beta_G=0.22$ )	10-32	0.146-0.261 0.145-0.255	18/18/2	Single spoke cavity,	1.5

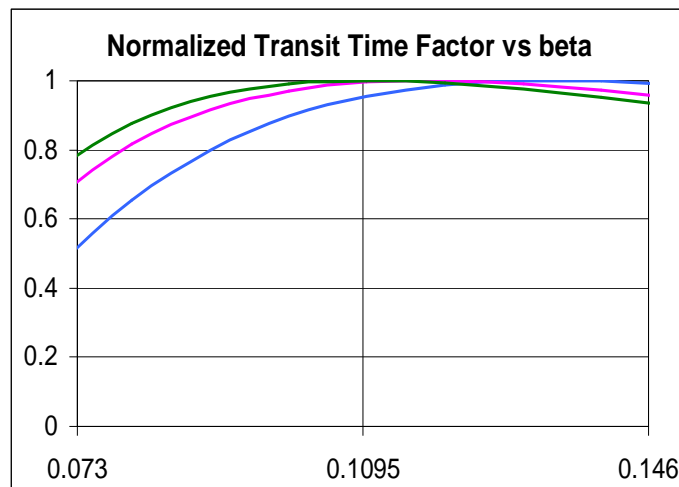
				Solenoid	
SSR2 ( $\beta_G=0.4$ )	32-117	0.261-0.5 0.255-0.458	33/17/3	Single spoke cavity, Solenoid	3.2
TSR ( $\beta_G=0.6$ )	117-466	0.5-0.744 0.458-0.744	48/48/8	Triple spoke cavity, quads	8.5

**Table III-2: Break points between the sections in the low-energy part of the linac.  $\beta_G$  is cavity geometrical phase velocity**

**2.5-10 MeV section:** A single family of CW Spoke SC cavities (SSR0) will be used for acceleration for the beam energy from 2.5 MeV to 10 MeV. The SSR cavity for  $\beta = 0.073-0.146$  was optimized, and the results of optimization are shown in Table III-3, where  $E_{acc^*} = E_{acc}(\beta_G) \times TTF$  and TTF is the transit-time factor. The transit time factor versus  $\beta$  and the field patterns are shown in Figure III-5.

Operating frequency	325	MHz
$\beta_G$	0.117	
Cavity diameter	200	mm
R/Q	120	$\Omega$
Average transit time factor (TTF)	0.94	
Electric field enhancement factor, $(E_{max}/E_{acc}) / (E_{max}/E_{acc^*})$	5.5/5.85	
Magnetic field enhancement factor, $(H_{max}/E_{acc}) / (H_{max}/E_{acc^*})$	6.5/6.9	[mT/MV/m]
Cavity effective length, $D_{eff} = 2 * \beta \lambda / 2$	108	mm

**Table III-3: Parameters of the low-beta spoke cavities (SSR0)**



a)

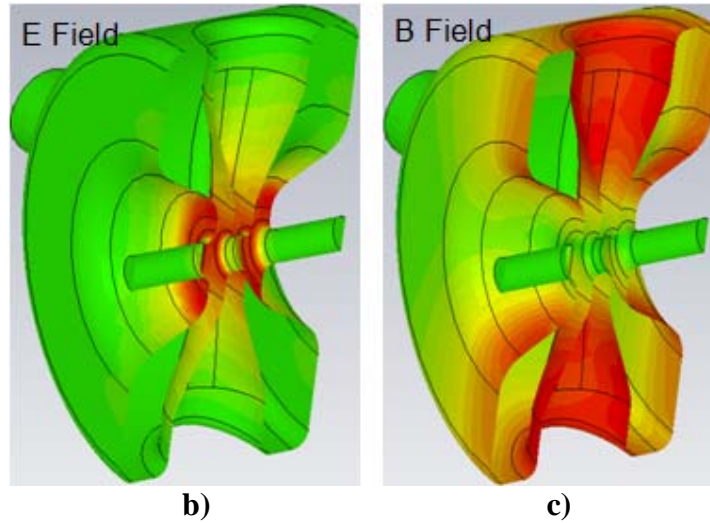


**Figure III-5: The transit time factor vs. proton beta for three different cavities having  $\beta_G=0.135$  (blue),  $\beta_G=0.117$  (pink), and  $\beta_G=0.11$  (green) (a); and cavity layout with field pattern for compromise cavity with  $\beta_G=0.117$  (b,c). One can see (figure c) that the surface magnetic field is distributed homogeneously on the spoke surface.**

A single spoke 325 MHz cavity (SSR1-02) having  $\beta_G = 0.22$  was designed and built for the HINS project. Our experience with this cavity shows that it is possible to achieve a maximum gradient of 25 MeV/m at 4°K and 33 MeV/m at 2°K (see Figure III-6). The gradient of  $E_{acc} = 15$  MeV/m looks reasonable for CW operation. It corresponds to the maximum surface electric field  $E_{max} \approx 40$  MV/m and magnetic field  $H_{max} \approx 60$  mT. For fixed  $H_{max} = 60$  mT the energy gain vs.  $\beta$  is shown in Figure III-7. The green curve corresponds to the gain per cavity for the RT cavities of the ICD-1 pulsed linac. One can see that the chosen design can provide the required gain per cavity.

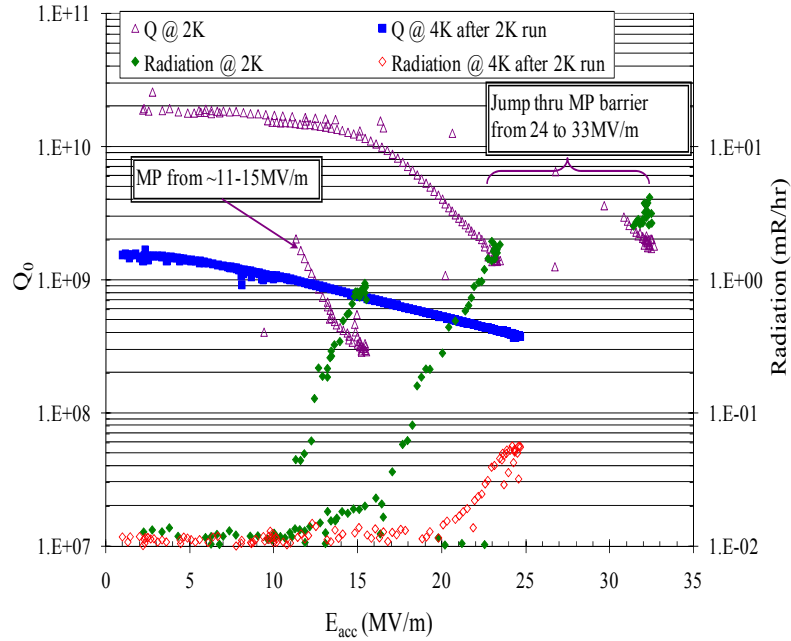


**Figure III-6:  $Q_0$  vs. acceleration gradient  $E_{acc}$  from the first cold test of SSR1-02 single-spoke cavity ( $\beta = 0.22$ ). Magenta points present the quality versus the gradient shown on different stages of the cavity conditioning at 2 K. In blue the quality vs. the gradient is shown at 4 K after 2K run. Maximal  $E_{acc} = 25$  MeV/m @4K; 33MeV/m@2K.**

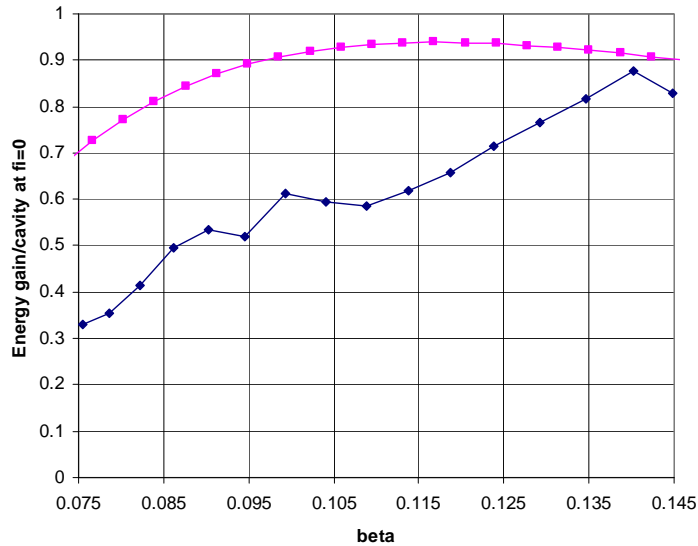


**Figure III-7: The energy gain per cavity for SSR0 resonator (pink) at the surface magnetic field of 60 mT, and for room-temperature cross-bar cavity of the ICD-1 pulsed linac (blue).**

**10-466 MeV section:** Other parts of 325 MHz SC linac are the same (SSR1, SSR2, TSR) as in the ICD-1 8 GeV linac. Parameters of the cavities are shown in

cavity type	F [MHz]	$U_{acc, max}$ [MeV]	$E_{max}$ [MV/m]	$B_{max}$ [mT]	R/Q $\Omega$	G $\Omega$	$Q_{0,2K} \times 10^9$	$Q_{0,4K} \times 10^9$	$P_{max,2K}$ [W]	$P_{max,4K}$ [W]
SSR0	325	0.78	53	59.5	120	57	9.5	0.7	0.77	10.4
SSR1	325	1.53	34.4	50.8	242	84	14.0	1.0	0.94	13.2
SSR2	325	3.16	33	54	322	112	18.0	1.3	2.07	28.6
TSR	325	8.5	31.4	67	554	117	19.0	1.4	7.9	106.9

Table III-4.

cavity type	F [MHz]	$U_{acc, max}$ [MeV]	$E_{max}$ [MV/m]	$B_{max}$ [mT]	R/Q $\Omega$	G $\Omega$	$Q_{0,2K} \times 10^9$	$Q_{0,4K} \times 10^9$	$P_{max,2K}$ [W]	$P_{max,4K}$ [W]
SSR0	325	0.78	53	59.5	120	57	9.5	0.7	0.77	10.4
SSR1	325	1.53	34.4	50.8	242	84	14.0	1.0	0.94	13.2
SSR2	325	3.16	33	54	322	112	18.0	1.3	2.07	28.6
TSR	325	8.5	31.4	67	554	117	19.0	1.4	7.9	106.9

**Table III-4: Parameters of the single cavities SSR1 and SSR2, and triple – spoke cavities TSR.**

The SSR1 cavity layout is shown in Figure III-8. Results of the cavity tests are shown in Figure III-6. The surface resistance dependence on the temperature is shown in Figure III-9. The resistance at 4 K is more than ten times higher than at 2K, and thus the quality factor is more than 10 times lower. As the conversion factor for cryogenics for 2 K is 700 W/W versus 200 W/W for 4 K (see also Table III-4), from an efficiency point of view, it is preferable to work at 2 K. In addition, at 2 K the level of microphonics is much smaller. Note though that the average RF power requirements for CW operation are higher, and the coupler needs to be redesigned.



**Figure III-8: SSR1 cavity layout and photo.**

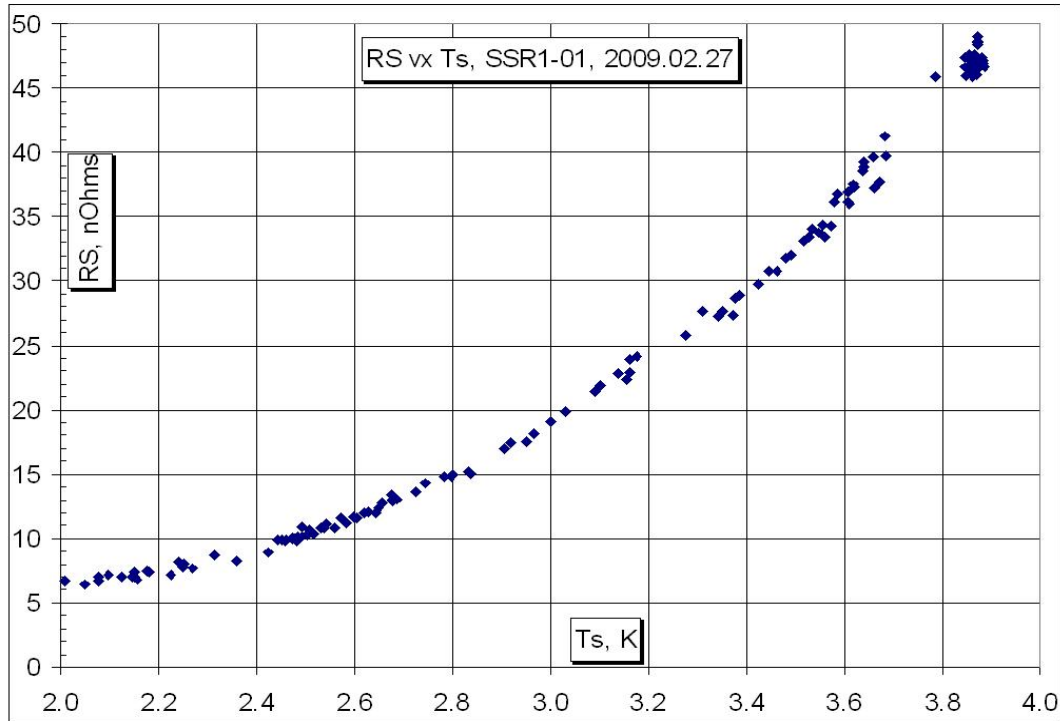


**Figure III-9: Temperature dependence of the surface resistance for SSR1 cavity.**

A single spoke 325 MHz cavity (SSR2) having  $\beta_G = 0.4$  was developed for the HINS project as well. The cavity layout is shown in the Figure III-10. The EM optimization as well as mechanical design was completed including a piezo tuner and a helium vessel. The triple-spoke cavity TTR operating at 325 MHz was also developed. An example is shown in Figure III-11. Each cavity of SSR0, SSR1, SSR2 and TSR types may be powered by separate RF source. Inductive output tubes (IOTs) or solid state amplifiers are feasible for the required power consumption at 325 MHz.

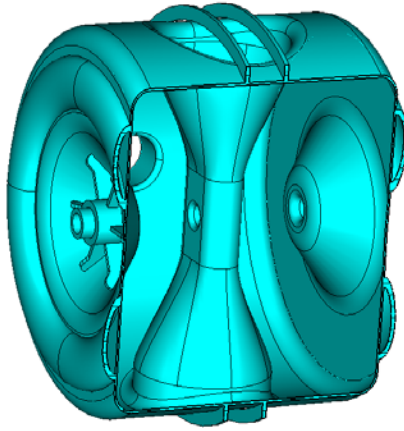


**Figure III-10: SSR2 cavity layout.**

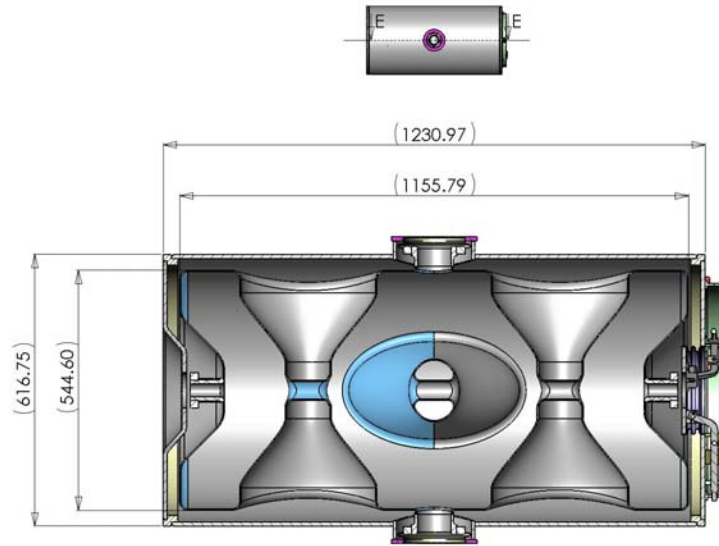


**Figure III-11: TTR cavity layout.**

### III.1.3 The 1.3-GHz section

**466-2000 MeV section:** The acceleration from 466eV to 2 GeV may be provided at 1300 MHz using the same configuration as developed for the ICD-1 8-GeV pulsed linac. This configuration contains two sections, denoted S-ILC and ILC. The S-ILC section is based on an elliptical squeezed cavity with  $\beta_G = 0.81$ . In the ILC section, standard  $\beta_G = 1$  ILC cavities are

used. The same type-4 ILC cryomodule is used in both sections. In this case, in order to use the cryomodule space effectively, an 11-cell  $\beta_G = 0.81$  squeezed cavity is suggested. The cavity layout is shown in Figure III-12 as well as its parameters and cell dimensions.

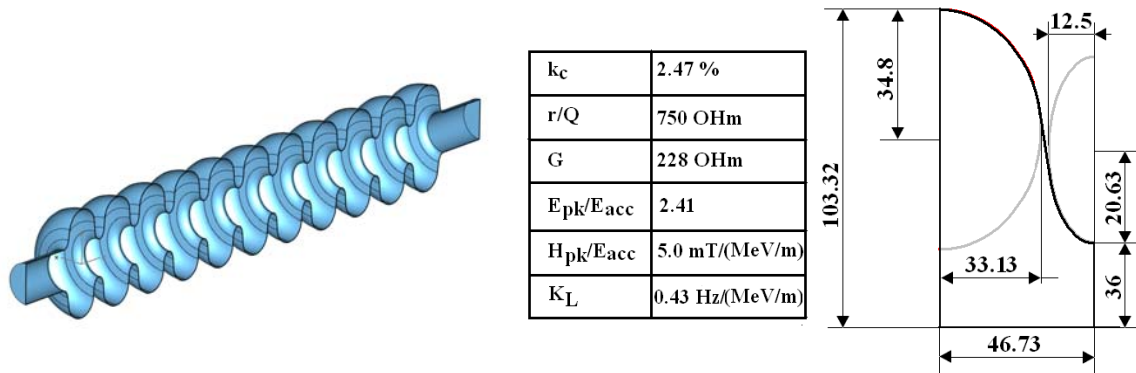


**Figure III-12: 11-cell  $\beta_G = 0.81$  cavity layout, parameters, and cell dimensions. Note that the coupling coefficient  $k_c$  is increased to 2.47% compared 1.87% for the TESLA cavity, in order to provide the same field flatness for larger number of cells. It leads to the surface field (electric and magnetic) enhancement factor increase. However, 11-cell cavity provides a higher energy gain per cavity than the cavities with smaller number of cells, see [N. Solyak, et al, PAC2009, TU5PFP063].**

The gradient for this section was chosen to be 14.4 MeV/m. It corresponds to the surface magnetic field of 72 mT (see Table III-5 and Figure III-12). This magnetic field corresponds in turn to the gradient of 19 MeV/m for a standard ILC section, that should be acceptable for CW regime. For this gradient, the Q-factor for ILC cavity is not smaller than  $1.5 \times 10^{10}$ , see Figure III-13<sup>7</sup>, where the test results for different TESLA structures are summarized. For the S-ILC structure the Q-factor will be about  $1.3 \times 10^{10}$  taking into account that for this case G-factor is 228 Ohm versus 270 Ohm for the ILC structure, see Figure III-12. The RF losses are about 30 W/cavity (Table III-5).

<sup>7</sup> taken from J. Sekutowicz, Meas. Sci. and Tech., 18(2007), 2285-2292

**DESY data (last test) - status March 2009**

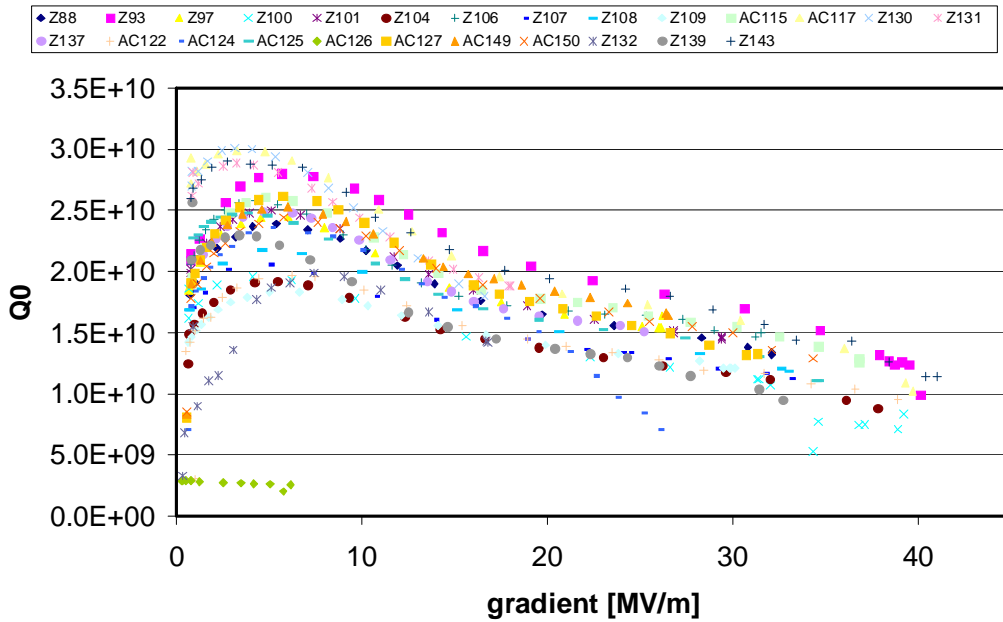


**Figure III-13: Q-factor versus acceleration gradient for 9-cell standard TESLA cavities.**

cavity type	f [MHz]	$E_{acc}$ [MV/m]	$L_{eff}$ , mm	$E_{max}$ [MV/m]	$B_{max}$ [mT]	R/Q $\Omega$	G $\Omega$	$Q_{0,2K} \times 10^9$	$Q_{0,4K} \times 10^9$	$P_{2K}$ [W]	$P_{4K}$ [W]
11-cell, $\beta=0.81$	1300	14.4	1028	35	72	750	228	12.7	n/a	22.4	n/a
9-cell, ILC	1300	16.9	1038	34	72	1036	270	15.0	n/a	19.0	n/a

**Table III-5: Parameters for the cavities of the high-energy sections, SILC and ILC.**

The number of cavities (preliminary) necessary in this section is 66, or 11 cryomodules. In Figure III-14 the modified Type-4 CM schematic is shown: each cryomodule in the SILC section contains 6 squeezed elliptical cavities and 3 quads.

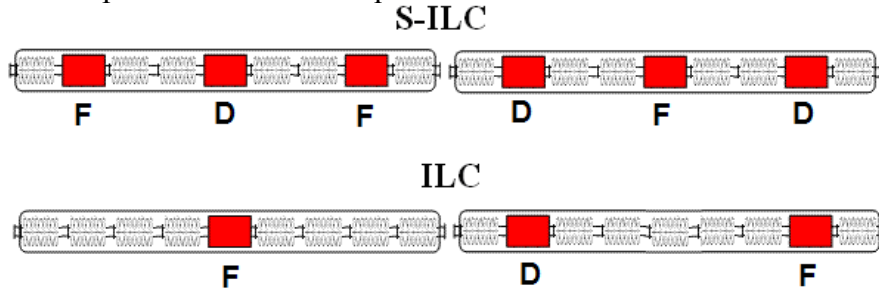
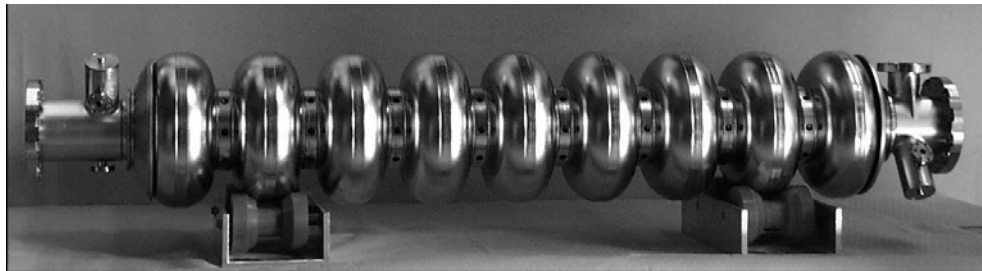
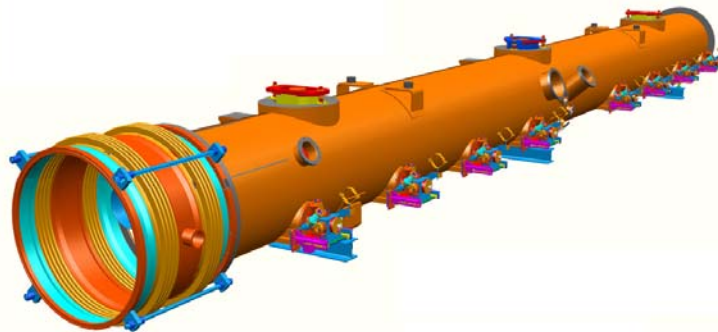


**Figure III-14: Modified Type-4 ILC cryomodule schematics. The cryomodule in S-ILC section contains three quads in the positions of 2<sup>nd</sup>, 5<sup>th</sup>, and 8<sup>th</sup> cavities, and six 11-cell cavities. The ILC cryomodule has the two different quad locations: in 5<sup>th</sup> position, and in 2<sup>nd</sup> and 8<sup>th</sup> positions.**

Acceleration from 1.2 MeV to 2 GeV may be provided by section with 68 standard well-tested  $\beta_G = 1$  ILC cavities, or 9 cryomodules (see Figure III-15). The gradient is 18 MeV/m. Maximal surface magnetic field is about the same as in the S-ILC section, 77 mT. The RF losses are about 22.5 W/cavity (see Table III-5). There are two types of the ILC cryomodules following one after another as shown in Figure III-14, so that the pair of cryomodules contains 15 ILC-type 9-cell cavities, and 3 quads. Note that the ILC-type cavity is not optimal for acceleration from 1.2 to 2 GeV (the beta range from 0.9 to 0.95), but it is well developed, and there is a long-term experience of the cavity operation at DESY. The parameters of the sections including the number of quads, cavities and cryomodules are presented in Table III-7.



a)



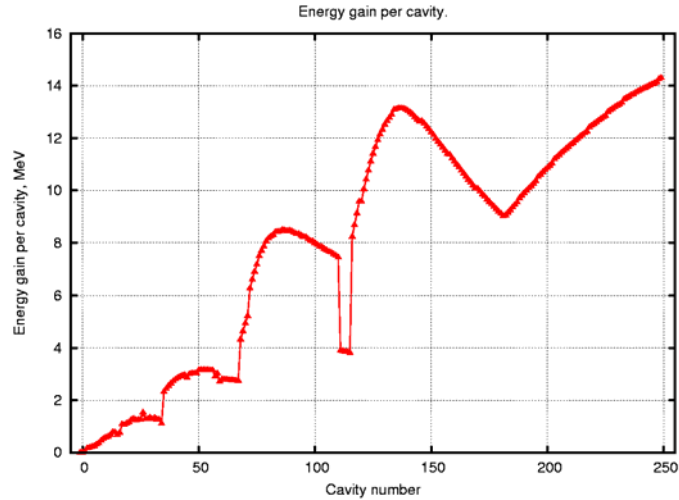
b)

**Figure III-15: A standard 1.3 GHz,  $\beta_G = 1$  TESLA structure (a) and Type-4 ILC cryomodule (b).**

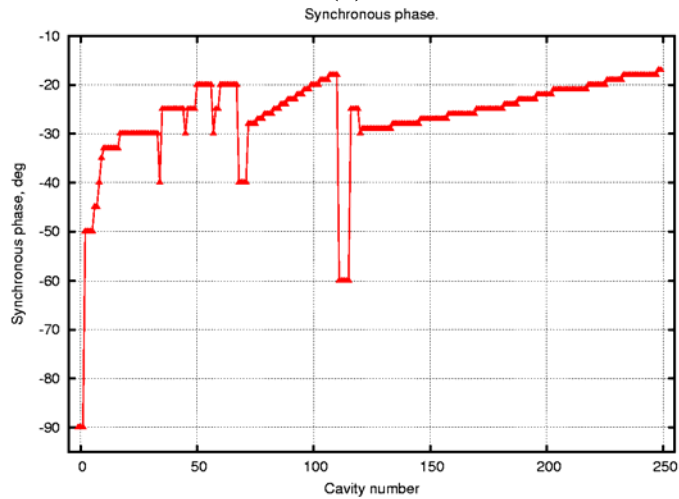
Section	Energy range MeV	$\beta$	Number of cavities/ quads/CMs	Type	Max Power/cavity, kW( $I_{av}=1$ mA)
S-ILC( $\beta_G=0.81$ )	466-1200	0.744-0.9	66 / 42 / 11	Squeezed elliptical	13
ILC ( $\beta_G=1$ )	1200-2000	0.9-0.95	68 / 13 / 9	9-cell ILC	15

**Table III-6: Break point between the sections in the high-energy part of the linac.**

Figure III-16 (a) presents the average energy gain per cavity along the linac. The equilibrium phases are shown in the Figure III-16 (b).



(a)



(b)

**Figure III-16: The energy gain per cavity (a) and equilibrium phases (b). Cavities 1-117 are 325 MHz, 118-251 are 1.3 GHz. One can see that the last five cavities (112-117) in the 325 MHz section have very big (60-70°) equilibrium phase and, thus, small energy gain (<4 MeV/cavity), in order to match the beam longitudinal dynamics to the 1.3 GHz section.**

Maximal required average power per cavity in the high-energy section is no more than ~20 kW. IOTs with this power are available at 1300 MHz, thus the RF distribution system is simple and similar to the SNS SC linac with one RF source per cavity.

The power loss in the cavity walls has to be compensated by the cryogenic system. Corresponding power losses are shown in Table III-7.

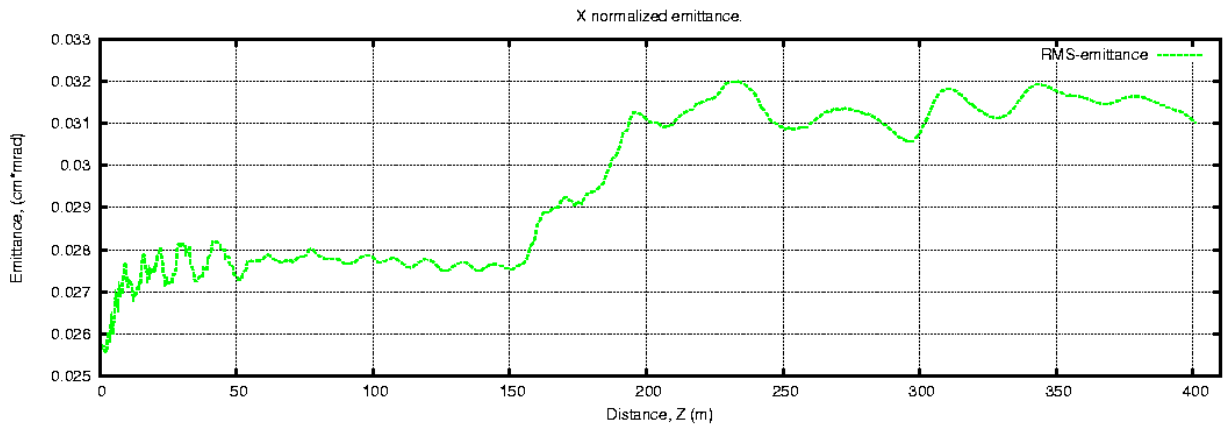
Power losses				
	Power loss per cryomodule at 2	Power loss per cryomodule at	Power loss per	Power loss per

	K,W	4K, W	section at 2 K,W	section at 4 K,W
S SR0	1.33/4.7	18.2/63.8	6.05	82.1
S SR1	6.11/6.27	85.6/87.7	12.4	173.3
S SR2	22.73/22.73/19.2	314.8/314.8/265.9	64.7	895.4
T SR	47.3	641.3	378.0	5130.4
S ILC	138	N/A	1520.9	N/A
I LC*	160/149	N/A	1360.0	N/A

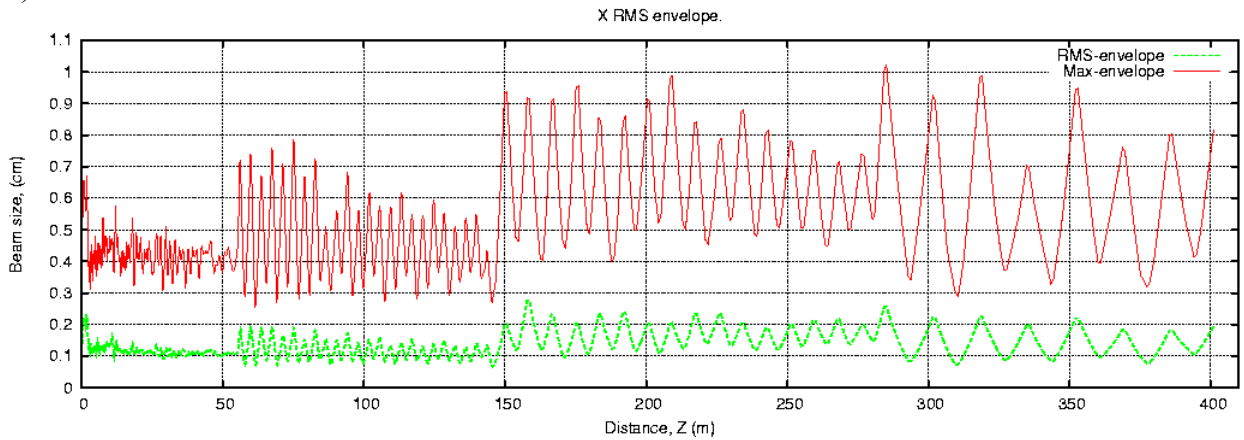
\*There are two types of the ILC cryomodules, see Figure III-14.

**Table III-7: Power losses in the low energy and high energy sections of the linac.**

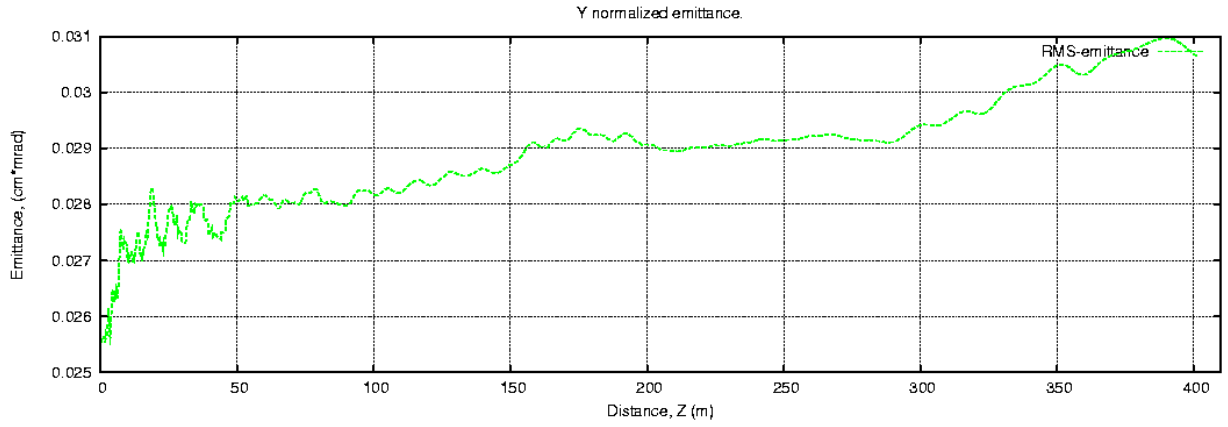
The results of the beam dynamics simulations are shown in Figure III-17.



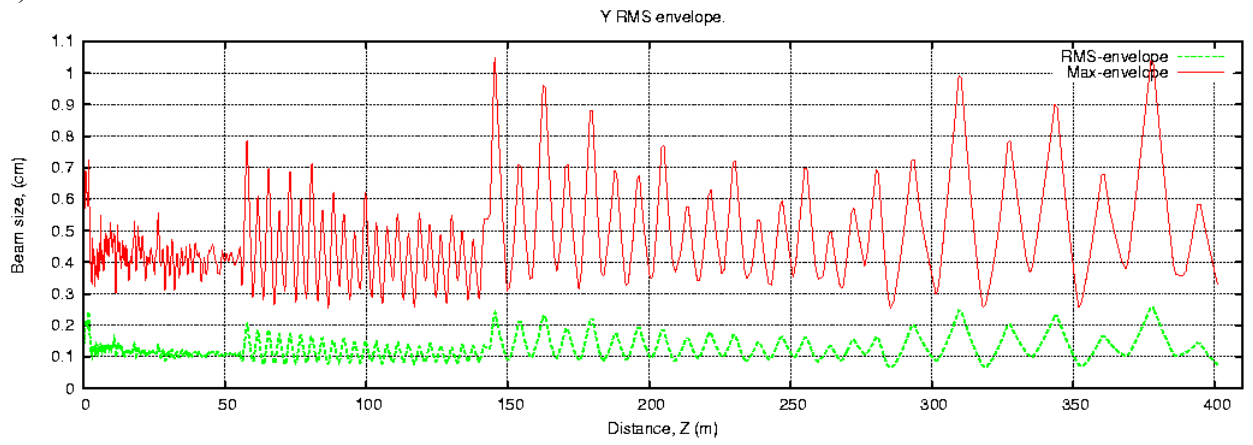
a)



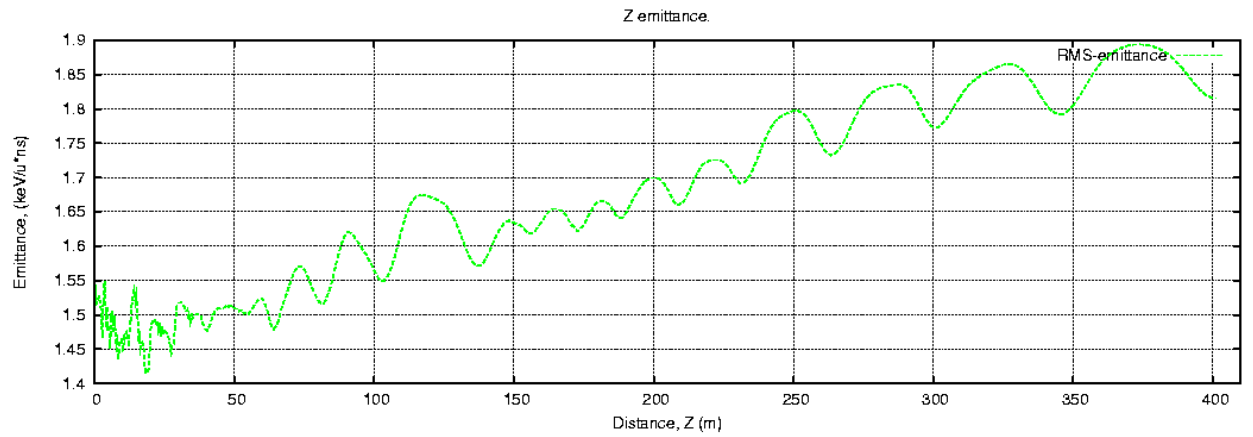
b)



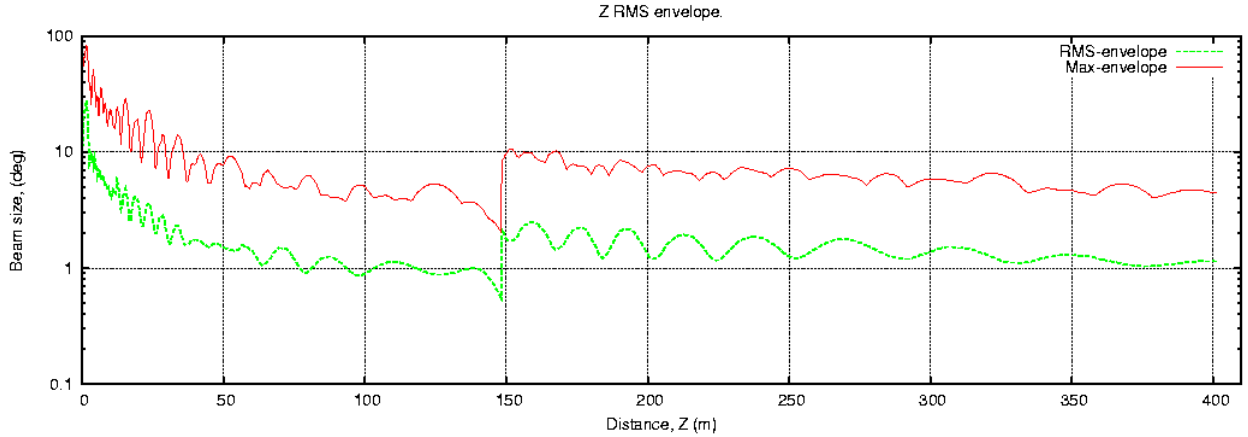
c)



d)



e)



f)

**Figure III-17: Results of the beam dynamics simulations. (a) – horizontal RMS emittance evolution along the linac; (b) – horizontal beam maximal and RMS envelope; (c) – vertical r.m.s emittance evolution along the linac; (d) – vertical maximal and RMS beam envelope; (e) – longitudinal r.m.s emittance evolution along the linac; (f) – longitudinal maximal and RMS bunch length**

### III.2 2 GeV Beam handling

The CW linac accelerates  $H^-$  ions having the base bunch frequency of 162.5 MHz set by the RFQ. The beam may be steered toward the RCS, to the experimental area, or to the beam dump as shown in **Figure III-18**. The injection to the RCS is controlled by switching on a pulsed switch magnet for 4.3 ms. It is located immediately after the matching section between the linac and transfer line. The beam directed to the RCS is stripped at the injection, accelerated to 8 GeV and then transferred to the Recycler. If this pulsed magnet is off and a DC selection magnet, one cell downstream, is energized the  $H^-$  will be transported to the Experimental Area for further distribution to the experiments. If both switch magnets are off, the beam goes to the Linac dump. Beam line layouts are shown in **Figure III-18**.

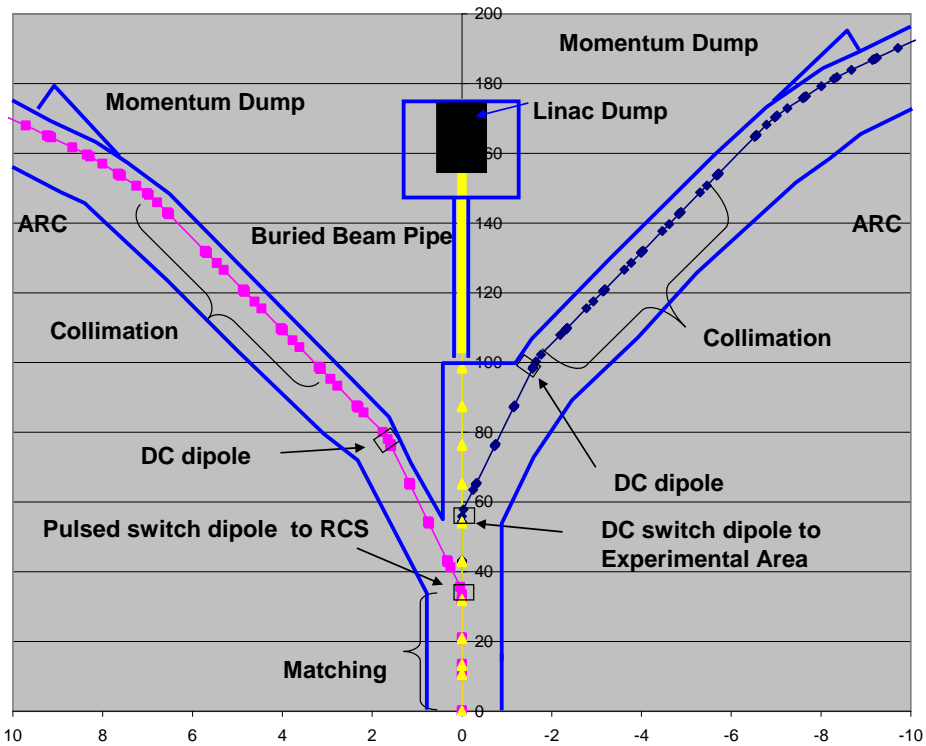
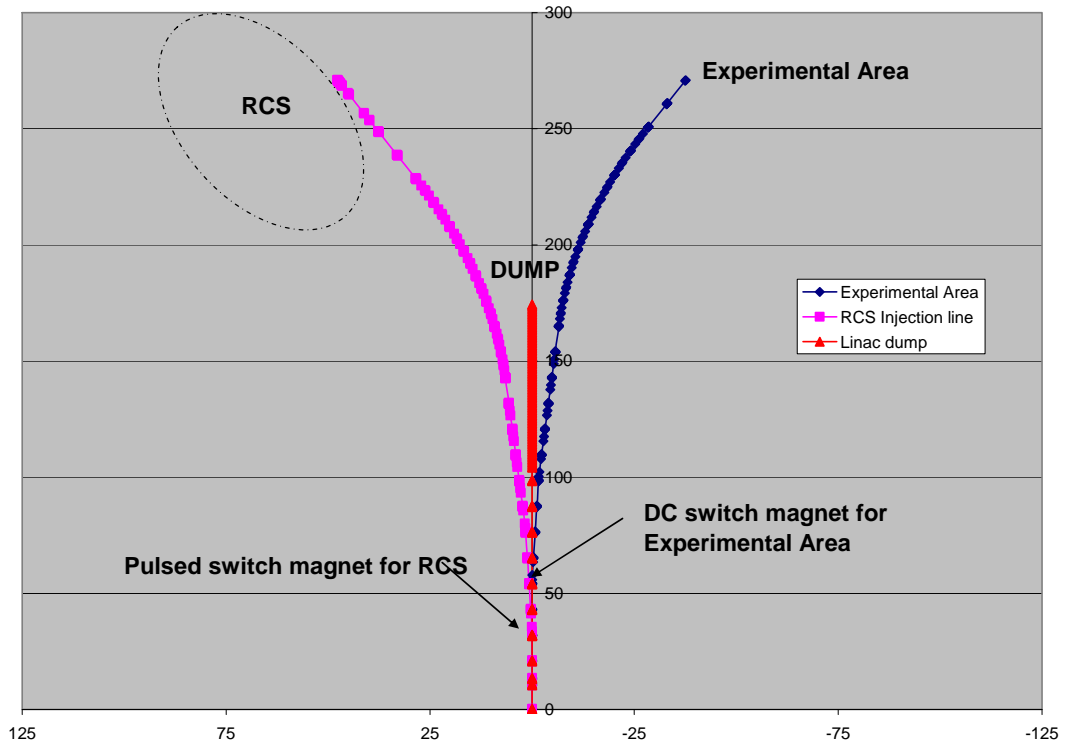


Figure III-18 (top): Layout of the transport lines from the end of the linac to the RCS (magenta), the 2 GeV experimental area (dark blue), and the linac dump (red). (bottom)

**Expanded view of the upstream end of the transport lines to the RCS, dump, and Experimental Area. Potential transport enclosure is indicated in blue.**

**III.2.1 Beam Loss**

The configuration of transport lines supports H<sup>-</sup> beam transport both to the RCS (85 kW) and to the Experimental Area (2 MW). The requirements to the fractional beam loss are dominated by higher intensity beam transport to the Experimental Area.

The H<sup>-</sup> transport should have sufficiently small loss to minimize residual radiation in the tunnel. It is highly desirable to keep residual radiation level well below 20 mRem/hr. At 2 GeV, a loss of  $3.2 \times 10^9$  p/m/s corresponds to approximately 1 W/m loss rate and produces a contact residual dose rate of ~100 mRem/hr on a bare beam pipe. Setting a desirable activation level to 10 mRem/hr results in a loss goal of 0.1 W/m, and, consequently, fractional part loss of  $2.8 \times 10^{-7} \text{ m}^{-1}$  and  $5 \times 10^{-8} \text{ m}^{-1}$  for 85 kW beam to RCS and 2 MW beam to the experiments, correspondingly.

The single particle mechanisms contributing to the beam loss are the Lorentz stripping in dipoles, the beam stripping in the residual gas, and the photo detachment by blackbody radiation in the beam pipe.

Beam motion in a magnetic field excites an electric field in the beam frame. If this electric field is sufficiently strong, it can detach the weakly bound outer electron (Lorentz stripping). Figure III-19 shows the lifetime in the laboratory frame and the loss rate per meter for a 2 GeV kinetic energy H<sup>-</sup> as a function of magnetic field. One can see that a dipole field of 1.8 kG produces a fractional loss of  $6.4 \times 10^{-8} \text{ m}^{-1}$ . As the dipoles occupy a comparatively small fraction of the beam line length, we will use this value as the maximum acceptable dipole field. The loss rate is a steep function of field: a field increase to 2 kG increases the fractional loss to  $1.1 \times 10^{-6} / \text{m}$ , while its decrease to 1.6 kG reduces the fractional loss to  $1.8 \times 10^{-9} / \text{m}$ .

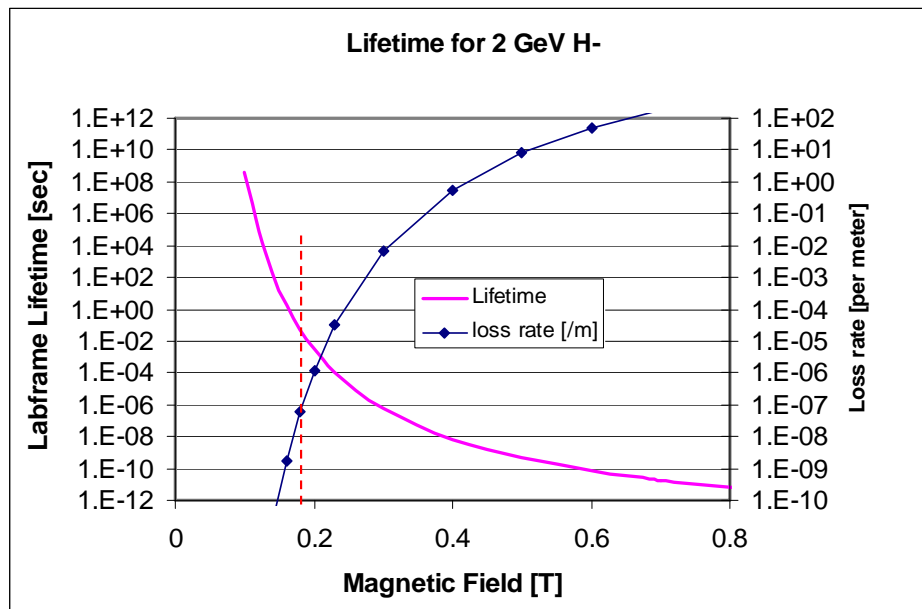


**Figure III-19: Fractional loss for a 2 GeV H<sup>-</sup> ion traveling in a dipole field. The dashed line marks a magnetic field of 1.8 kG.**

The loss rate due to  $H^-$  scattering on the residual gas molecules is proportional to their density and the ionization cross section of the molecules present. The cross section decreases proportional to  $\beta^{-2}$ . The analysis carried out for the 8 GeV Proton Driver<sup>8</sup> yielded that for a typical transport line pressures of  $10^{-8}$  Torr, the fractional loss at 2 GeV is expected to be about  $1 \times 10^{-8} m^{-1}$ . That sets a requirement to the desired vacuum to be  $<10^{-8}$  Torr.

The contribution from the blackbody photons at 2 GeV at room temperature is  $4 \times 10^{-8} m^{-1}$  as seen in Figure III-20. It is well within specifications for transport to the RCS, where the beam power is limited to 85 kW, however for transport of 2 MW beam power it is just inside the specs.

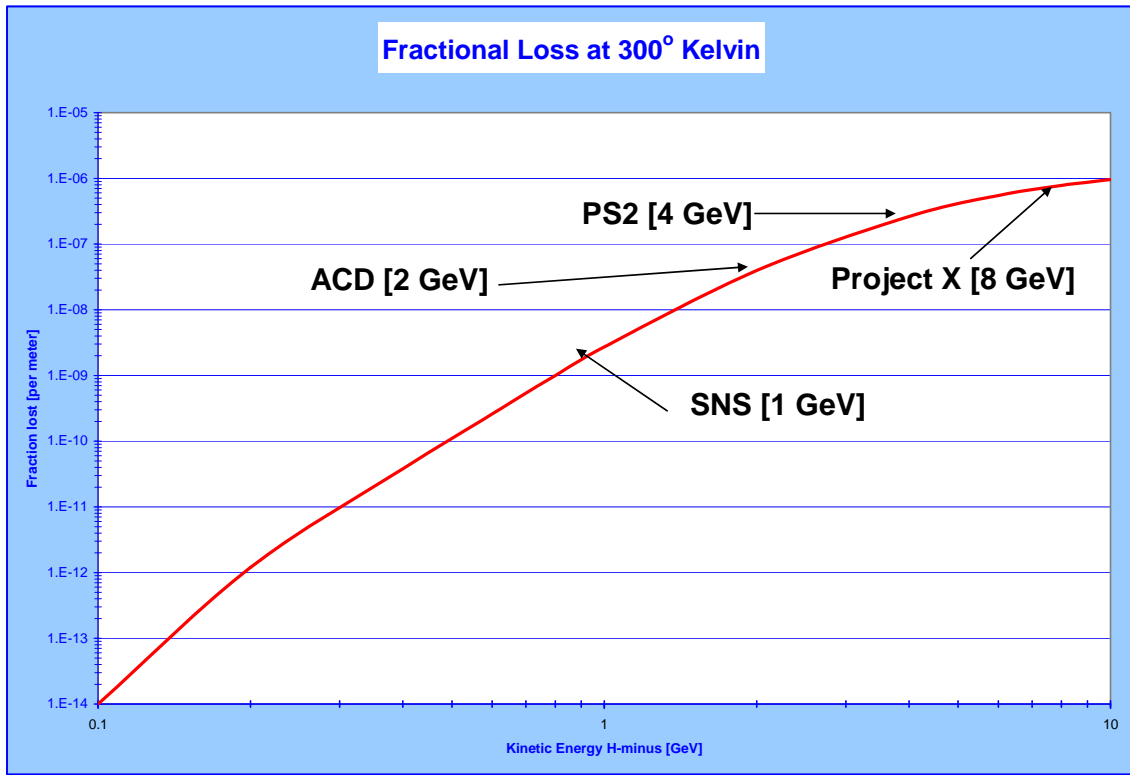


**Figure III-20: Loss rate [ $m^{-1}$ ] due to the interaction of 300°K blackbody photons as a function of  $H^-$  kinetic energy.**

One can see that the black body radiation is expected to make a major contribution. Summing the three contributions, the single particle fractional loss is expected to be  $\sim 7.5 \times 10^{-8} m^{-1}$ , yielding the average residual radiation (on contact on a bare beam pipe) of  $\sim 2.5$  mRem/hr for the RCS transport line and about  $\sim 15$  mRem/hr for the Experimental Area transport line.

### III.2.2 Transport line functionality

In addition to controlling the single particle loss the transport line should provide a mechanism for controlling loss from large amplitude particles, linac energy errors, and alignment/ power supply errors.

Based upon experience from SNS, a two stage transverse collimation system is considered for installation in the upstream end of the transfer line. This system consists of a movable thick carbon foil (100% stripping efficiency) upstream of a transport line quad and an absorber

<sup>8</sup> [http://protondriver.fnal.gov/SCRF\\_PD\\_v56.doc](http://protondriver.fnal.gov/SCRF_PD_v56.doc)

downstream of the quad to intercept the large amplitude protons generated from  $H^-$  passing through the foil. With an expected  $90^\circ$  cell structure of the transport line, two horizontal and two vertical systems would be required for all phase coverage. Although only the largest amplitude particles will be intercepted, a prudent design will size the capacity for the system at 5% or 4.25 kW (~1% for each of the 4 collimation systems) due to the uncertainty of halo production in the CW linac. Due to the differing requirements of the RCS and Experimental Area transport lines, collimation is necessary in both of the transport lines.

To protect the RCS from errant beam energies, a momentum collimation system will be installed at the dispersion peak of the achromatic horizontal bend module. A thick movable foil is placed between the central quad and the downstream dipoles. The foil will convert  $H^-$  with wrong energy to protons, which will be swept out of the transport line to a momentum dump by the following dipoles. This implies that these two dipoles need to be of a c-magnet design with an open side-leg. Requirements for the Experimental Area are to be reviewed to determine if momentum collimation is required.

Typical alignment errors achieved during accelerator and transport line installation are 0.25mm transverse and 0.5mr roll. It is expected that these tolerances will be adopted for the installation tolerances in this project. A dipole corrector system will be utilized to correct any orbit distortions caused by misalignments. These will likely be new correctors, similar in design to existing beam line trims.

### III.2.3 $H^-$ Transport to RCS

To fill the RCS, the chopper will create notches in the CW beam at 2.5 MeV for the rise and fall time of a pulsed switch magnet with a 4.3 ms flattop to divert  $2.7 \times 10^{13}$  particles into the RCS transport line. In addition, the chopper will need to create the micro-bunch structure to fill 88 out of the 98 50.33 MHz RCS RF buckets and to remove the linac bunches which do not completely fit into the RCS RF buckets.

Running at the full 10 Hz rep rate corresponds to  $2.7 \times 10^{14}$  particles/sec for a maximum beam power of 85kW (340 kW at 8 GeV). Since only 6 of the 10Hz cycles are used to fill the Recycler for each MI cycle, the average beam power can be reduced depending on the flattop energy of the MI, its cycle time, and beam requests from the 8 GeV program. For a 120 GeV MI cycle, with a cycle time of 1.4 sec, the average injected beam power at 2 GeV is 37 kW. For the 60 GeV MI cycle, with a cycle time of 0.8 sec, the average injected beam power is 64 kW. The four cycles not used for the MI neutrino program are available for an 8 GeV program off the RCS or Recycler. For beam loss specifications, we will use the maximum beam power.

#### III.2.3.1 Initial 2 GeV Transfer line layout

**An initial layout for the 2 GeV  $H^-$  transfer line that captures the requirements discussed above is shown in**

Figure III-21. The plot shows the lattice functions from the end of the linac matched to the injection straight section of the RCS. These are not optimized and are only meant to illustrate the functionality of the transfer line. The transfer line consists of the following sections: 1) matching

from the linac to the transfer line, 2) pulsed dipole switch (red ellipse), 3) a second dipole to create a localized achromat with the dipole separator, 4) a transverse collimation system (blue ellipse) in a four half-cell span, 5) a four cell (360°) main dipole achromatic bend, 6) a momentum collimation system (green ellipse) at the dispersion peak, and 7) a matching section into the RCS (magenta ellipse). The choice for the magnitude of the lattice functions is predicated by the choice of a half-cell length of 11.112 m to minimize the number of elements. The achromatic arc in this example consists of 16 RCS dipoles, with 2 dipoles per half-cell. For a field of ~ 0.95 kG, this arc produces a 20° bend which combined with the separator dipole(s) places the linac at an angle of 24.2° with respect to the injection straight section. The RCS dipoles were chosen for this example to minimize cost of designing a new dipole. The selection dipoles have a bend angle of 38 mr and are configured in a horizontal achromat. The first dipole will be pulsed and the second dipole is DC. The dipole field is 1.725 kG and has a length of 2 m. The field of these dipoles can be increased to 1.8 kG giving approximately 70° of bend. All quads in the transport line are standard RCS quads. Further details on the RCS magnets can be found in Section IV.3.1.

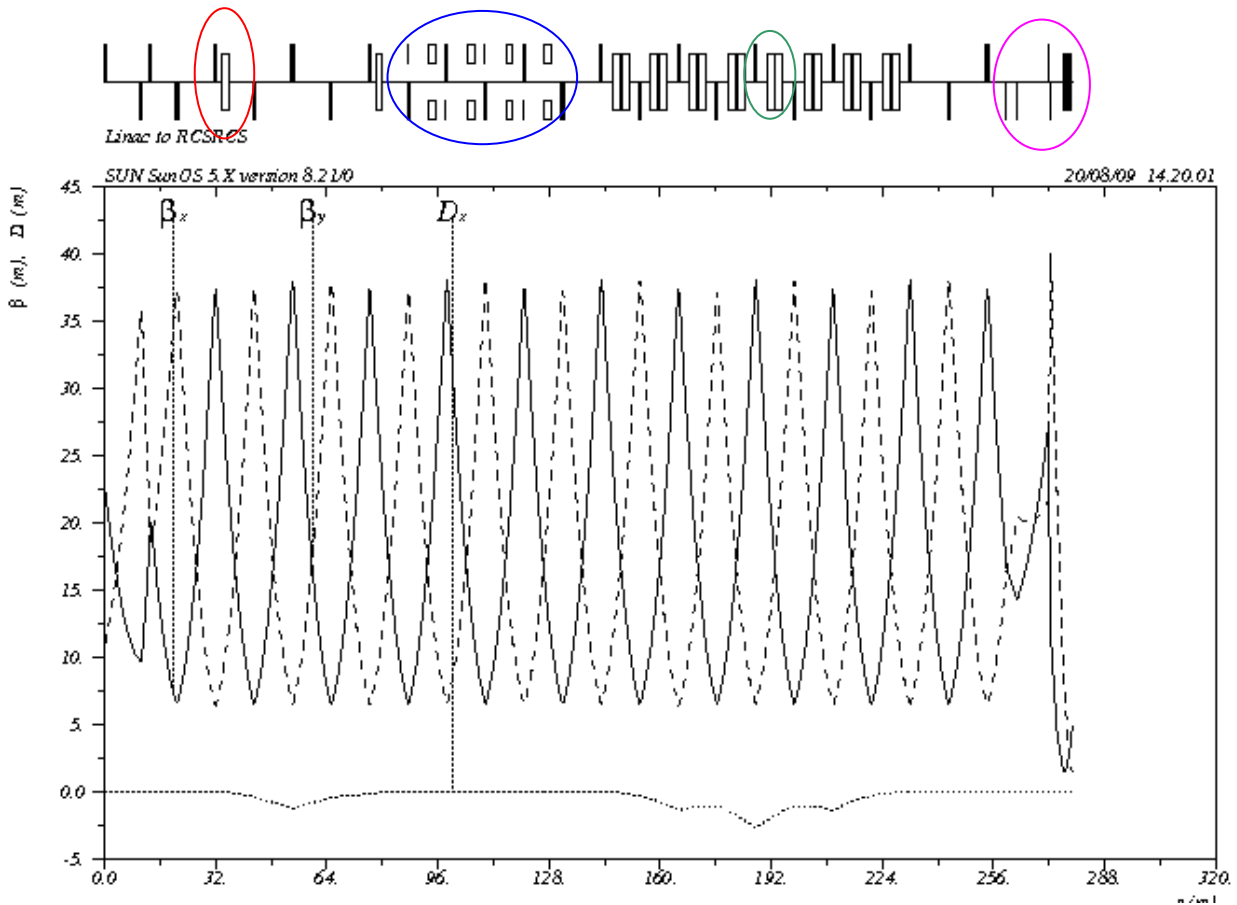


**Figure III-21:Initial concept for the RCS injection transfer line.**

The gradients of the quads are ~20 kG/m, well below that in the RCS. Since the transport line runs DC (except for the pulsed switch magnet), the steel laminations utilized for the RCS magnets are not strictly required.

Optimization of magnet parameters and design has not been done. The length of the different sections of the transfer line may be adjusted to accommodate civil construction issues. For this

example the matching section to the RCS has assumed the same transport line lattice functions discussed in the phase space painting discussion in Section III.3.4.2.

**Assuming an RMS emittance out of the linac of  $0.5 \pi$ -mm-mr and longitudinal emittance of  $8 \times 10^{-6}$  eV-s, the beam sigma and  $6\sigma$  for the line between the linac and RCS is shown in**

Figure III-22.

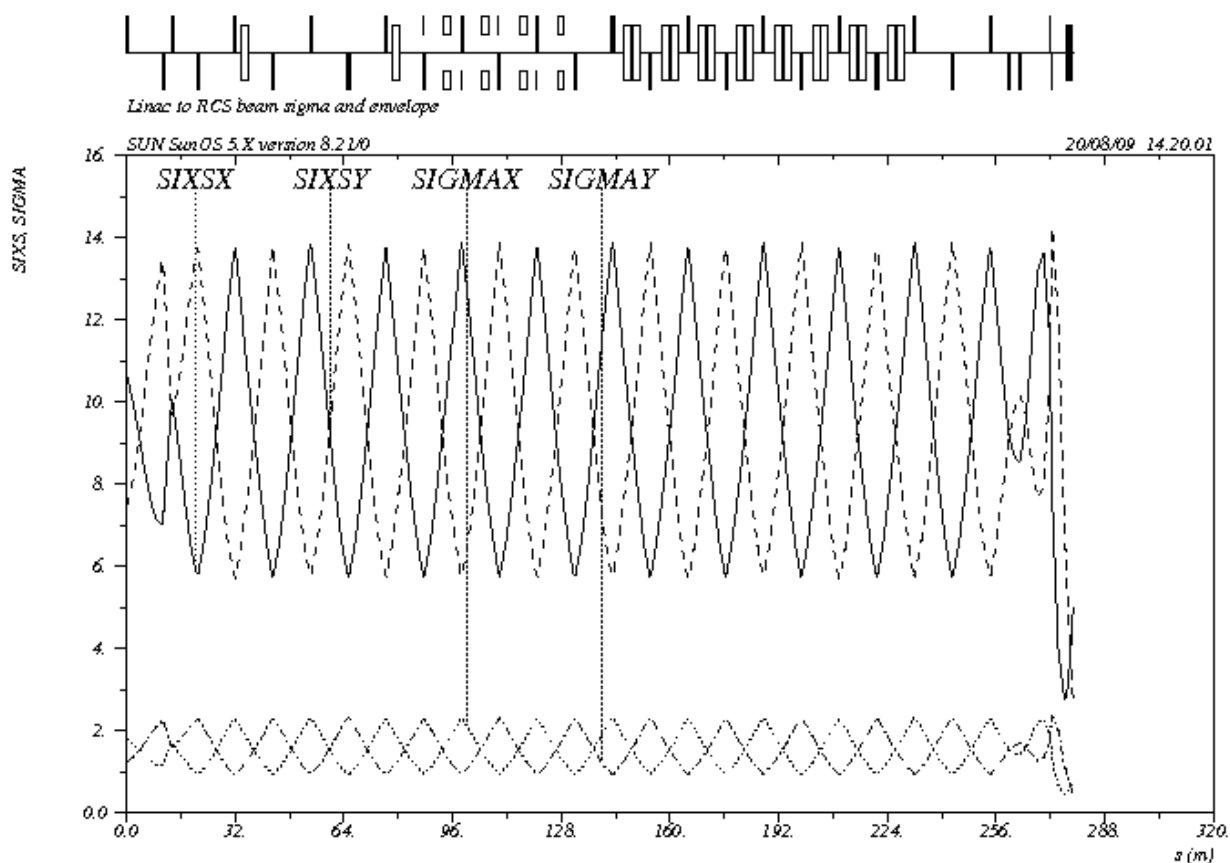


**Figure III-22: Beam sigma and 99% beam size for the linac to RCS transfer line.**

The initial concept for the beam pipe is to utilize an "elliptical" beam pipe similar to that utilized in the Main Injector or Recycler with a 2 inch vertical and 4 to 5 inch horizontal dimension. The beam pipe should be able to achieve a vacuum level of low  $10^{-8}$  Torr and the bellows should have an RF shield. The vacuum chamber should have an allowance for the horizontal beam size increase due to  $\pm 0.5\%$  beam momentum change during injection ( $\pm 1.25$  cm for 2.5 m maximum dispersion in the linac-to-RCS transfer line).

The separation dipole is currently set at a 38 mrad bend angle (1.764 kG) which produces about 0.25 m separation at the next quad to allow installation of a quad in the RCS line, thus keeping the same quad spacing as the rest of the transport line.

It is assumed all magnets in the transport line to the RCS will be powered magnets since the injection energy into the RCS may be adjusted to accommodate linac energy shifts due to reduced accelerating gradients.

The transverse collimation system is located immediately after the switch achromat and consists of four stripping and absorber pairs, two in each plane.

### III.2.4 H<sup>-</sup> Linac Dump

A straight-ahead beam dump is provided for tune up. The transport line to the dump is the same FODO lattice used in the linac-to-RCS transport line. At an appropriate distance a lattice quad is moved upstream 1/2 cell length and tuned to produce a round beam. The beam dump is located in a separate enclosure at a distance of approximately 150 to 160 meters from the end of the linac. A buried beam pipe connects the beam-line enclosure to the beam dump enclosure. The lattice is shown in Figure III-6. For an expected linac RMS emittance of 0.5 pi-mm-mr the spot size on the face of the dump with a beta of 200 m is about 32 mm.

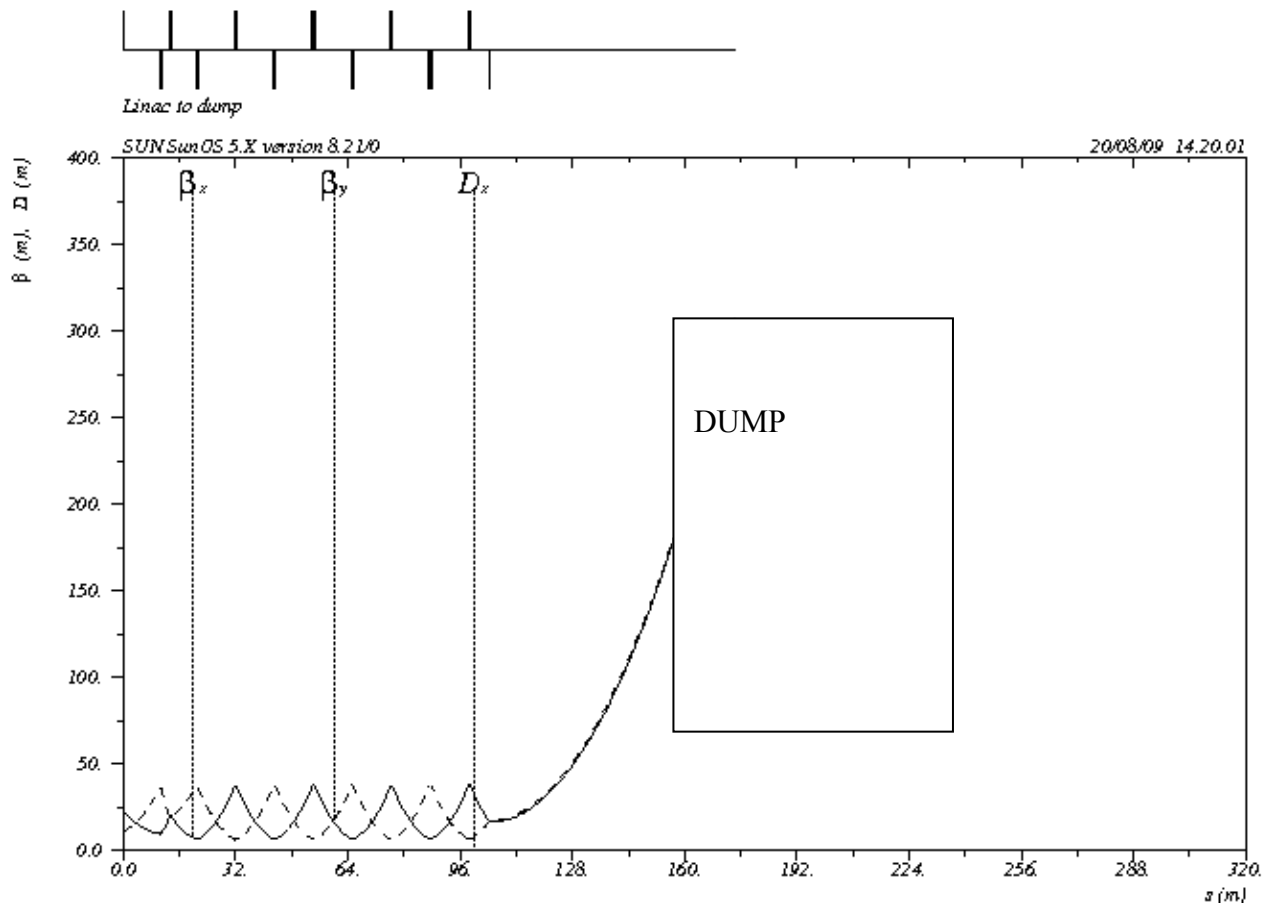


Figure III-23: Lattice functions for the linac straight ahead dump line.

### III.2.5 H<sup>-</sup> Transport to Experimental Area

If the RCS switch magnet is off and the DC Experimental Area switch magnet is on, the CW linac H<sup>-</sup> beam will be directed toward the Experimental Area. The beam power in this transport line is 2 MW. It is critical to minimize single particle losses, provide sufficient aperture, and provide collimation to remove large amplitude particles that could become lost in unprotected areas. It is expected that a H<sup>-</sup> stripping station will be provided at the end of the transport line, but before the RF separator.

#### III.2.5.1 Initial Transport Line Configuration

The optics of the Experimental Area transport line are identical to those of the linac to RCS transport line. Immediately after splitting off the dump line, a collimation system for the H<sup>-</sup> is provided. This collimation system is identical in functional design to the RCS transport line collimation but the beam power handling capability needs to be significantly larger, thus requiring significantly larger absorbers.

The dipoles and quads for this line are of the same design used in the linac-RCS and the linac dump line.

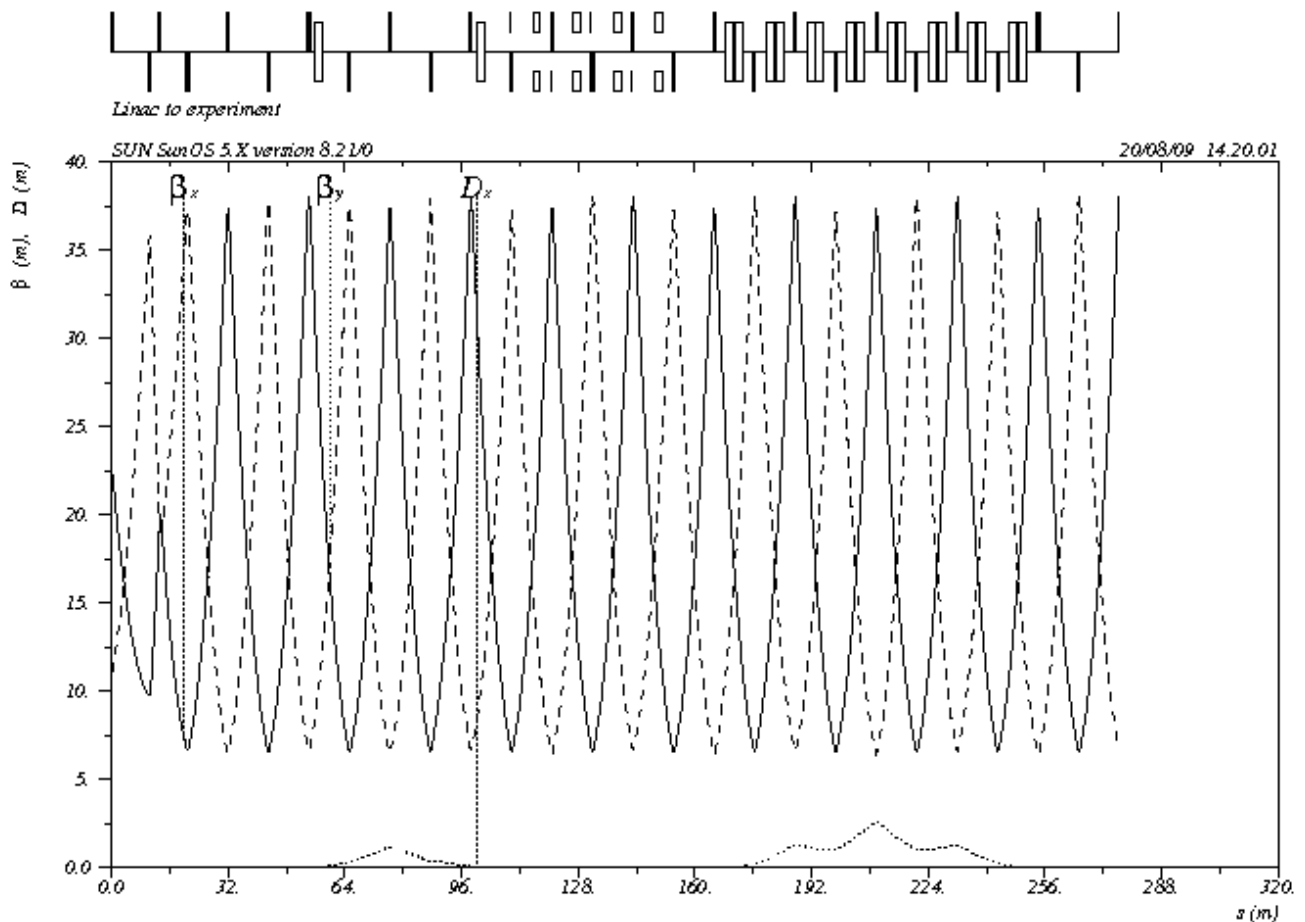


**Figure III-24: Lattice functions for the Experimental Area transport line.**

### III.2.6 RF Beam Separation for 2 GeV Experimental Program

To reduce the power required for the RF beam separation in CW regime a SRF structure with the deflecting  $TM_{110}$  mode is assumed. The structure should operate at the frequency  $f_0(m \pm 1/4)$ , where  $f_0$  is the bunch sequence frequency ( $f_0 = 162.5$  MHz). In the 3.9 GHz deflecting structure developed at FNAL<sup>9</sup>, the deflection strength is 7 MeV/m. To reduce the emittance growth related to different kicks applied to the bunch tail and head we choose lower frequency of 365.625 MHz ( $m=2$ ). Figure III-25 presents a schematic of bunch RF separation. For the deflection strength of 15 MeV a deflection angle is  $\pm 5$  mrad. Assuming a 20 m long drift space, the beam separation is  $\pm 100$  mm. With a beta function near the end of accelerator of 20 m and an expected emittance of  $2 \times 10^{-7}$  m, the RMS beam size at the separator is approximately 2 mm and increases by the end of the drift distance by 50%. Due to sufficiently small frequency the differential head-to-tail kick makes negligible contribution to the horizontal emittance growth ( $\Delta\epsilon/\epsilon < 0.1\%$ )

#### Transverse Kick / Intensity

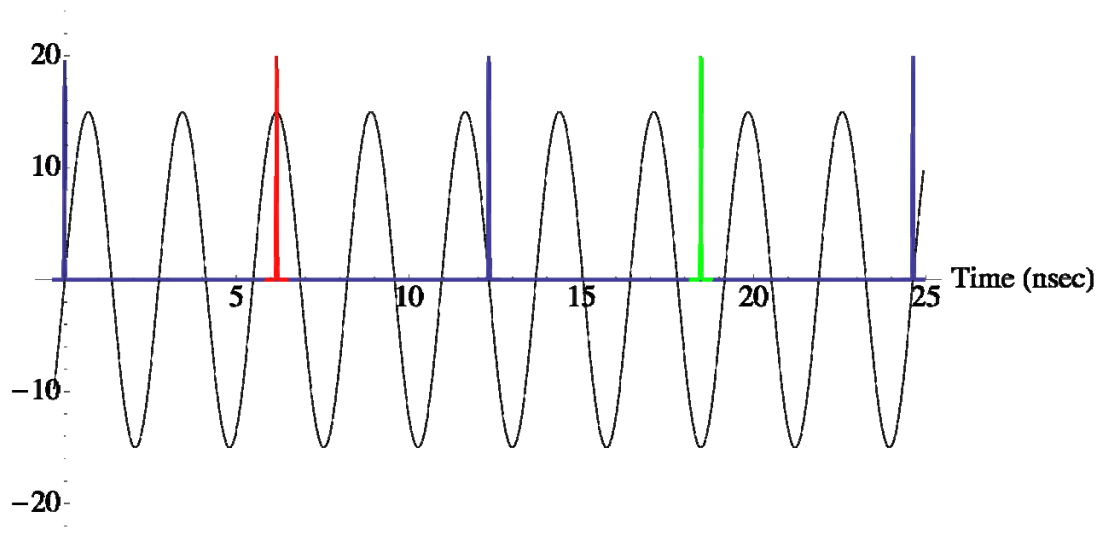


**Figure III-25: Transverse deflecting kick at 365.625 Mhz. The blue pulses are not deflected, the red pulse is deflected to the right, and the green pulse is deflected to the left.**

KEK-B utilizes a 500 MHz crab cavity with a squashed-cell shape and has achieved a separating gradient of 30 MV/m at 4.2 K. The cavity operates at 21 MV/m (a kick voltage of 1.44 MV). Scaling to a cavity of 365.625 MHz, the operating parameters in Table III-8 appear feasible. 4 cavities with a kick of 3.75 MeV are needed for a total kick of 15 MeV over a total length of approximately 4.5 m. The surface magnetic field for this gradient is 72 mT. Figure

<sup>9</sup> L. Bellantoni, *et al.*, FERMILAB-Conf-01/103-E July 2001.

III-26 shows a representative drawing of the separator cavities, including input power couplers and mode couplers.

The total power load in the cavity is a combination of the power necessary to maintain the RF field, power necessary to overcome beam loading from misalignments, and power necessary to handle microphonic detuning. With an assumed  $Q_0$  of  $10^9$ , the power load is dominated by the microphonics contribution (20 kW/cavity), followed by beam loading compensation (9 kW/cavity). The field is maintained with 260 W/cavity. In total, the 4 separator cavities will need approximately 150 kW at 365.625 MHz.

<b>Parameters</b>	
<b>E (surface field) MV/m</b>	<b>29.3</b>
<b>B (surface) mT</b>	<b>72</b>
<b>R/Q (Ohm)</b>	<b>27</b>
<b>Longitudinal size (mm)</b>	<b>440</b>
<b>Vertical size (mm)</b>	<b>865</b>
<b>Horizontal size (mm)</b>	<b>962</b>
<b>Operating Frequency (MHz)</b>	<b>365.625</b>
<b>Power (W)/cavity</b>	<b>260</b>
<b>Transverse kick/cavity (MeV)</b>	<b>3.75</b>

**Table III-8: Operating parameters of separator cavity at 365.625 MHz. 4 cavities for a total transverse kick of 15 MeV are required.**

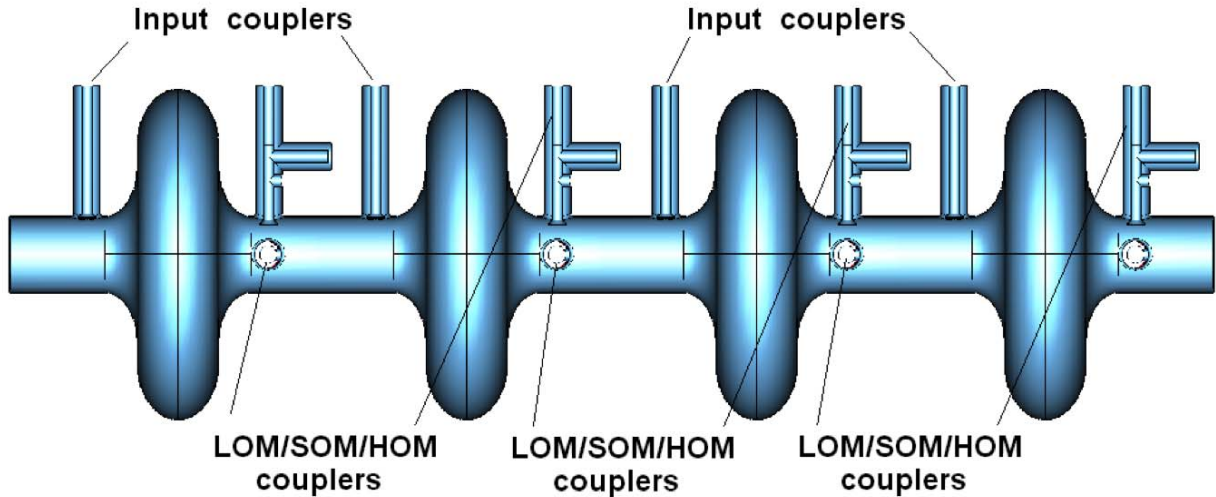


**Figure III-26: Representative drawing of a separator cavity section, including power and mode couplers.**

### III.3 Rapid Cycling Synchrotron

#### III.3.1 Choice of main parameters

To support the 2 MW Main Injector (MI) neutrino program, a rapid cycling synchrotron (RCS) has to deliver  $1.6 \times 10^{14}$  particles to Recycler during one MI cycle, which can vary in length from 0.8 sec (60 GeV flattop energy) to 1.4 sec (120 GeV flattop energy). The RCS has a shorter circumference than Recycler and therefore several RCS cycles are required to fill Recycler. Balancing the impacts of beam space charge, instabilities, magnetic field strength, and repetition rate, the circumference is chosen to be 1/6 of the MI circumference and the repetition rate is chosen to be 10 Hz. During one 0.8 s MI cycle 6 RCS pulses go to MI and the other two are available for an 8 GeV physics program. The main parameters of the RCS are presented in Table III-9.

**Table III-9: Main Parameters of RCS**

Energy, min/max, GeV	2/8
Repetition rate, Hz	10
Circumference, m (1/6 <sup>th</sup> of the MI)	553.2
Tunes, $\nu_x/\nu_y$	18.42 / 18.44
Transition energy (kinetic), GeV	13.3
Number of particles	$2.6 \times 10^{13}$
Beam current at injection, A	2.2
Transverse 95% normalized emittance at injection, mm mrad	$22^{10}$
Space charge tune shift, inj.	$0.07^{11}$

<sup>10</sup> 12% emittance dilution is implied in the course of acceleration and transfer to Recycler, where the design value for the emittance is 25 mm mrad

Normalized acceptance at injection, mm mrad	40
Harmonic number for main RF system, $h$	98
Harmonic number for 2-nd harmonic RF system	196
RF bucket size at injection, eV s	0.38
Injection time for 1.04 mA linac current, ms	4.3
Required correction of linac energy (kinetic) during injection	1.2%
Total beam power required from linac, kW	90 <sup>12</sup>
Total beam power delivered by RCS, kW	340

Reliable and efficient operation of the RCS leads to some specific design decisions. To avoid transition crossing, the transition energy is chosen to be outside the machine energy range. The lattice needs to be relatively insensitive to focusing errors and synchro-betatron resonances. The latter is achieved by having zero dispersion in the straight sections where RF cavities are located. A FODO lattice with a missing dipole for dispersion suppression is a natural choice resulting in simple requirements for magnets and vacuum chamber and strongly suppressed nonlinear resonances. However to avoid stripping foil overheating by injected beam (see Section III.3.4) the beta-functions at the foil location need to be increased relative to their nominal values of the FODO structure. Therefore the optics for seven half-cells in vicinity of the injection point are modified. That resulted in an increase of the geometric mean of beta-functions at foil,  $\sqrt{\beta_x \beta_y}$ , from 5.5 m to 20.5 m with corresponding decrease of foil heating by more than an order of magnitude.

The ring is designed as a racetrack (two long straights and two 180° arcs) with the same distance between centers of quads through the entire ring with exception of the injection region. One long straight section is for the RF cavities and the other is used for injection, extraction, and beam collimation. The F and D quads have the same focusing strength and are connected serially with the dipoles. Eight quadrupoles, four in the injection and four in the extraction regions, have larger aperture and length but they have the same integral strength. Tune and optics corrections are performed via additional corrector coils wound in each quadrupole. Figure III-27 presents the  $\beta$ -functions, the dispersion, and the beam envelopes for the half of the ring. The injection region is shown at the left side of the plot, where two quadrupole doublets replace six quadrupoles of the FODO structure. The rest of the ring, including another straight line not shown in the picture, has the regular FODO structure. The betatron phase advance per cell is 102°. Strong focusing results in small beam sizes and small dispersion. That, in its turn, results in a small synchrotron beam size and, consequently, a small difference between horizontal and vertical beam envelopes through the entire ring.

---

<sup>11</sup> This value is computed for the KV-like transverse distribution and the longitudinal bunching factor of 2.2 that are obtained by the beam painting as presented below in Section III.3.5.

<sup>12</sup> We imply here 4% loss of the injected beam. See details below.

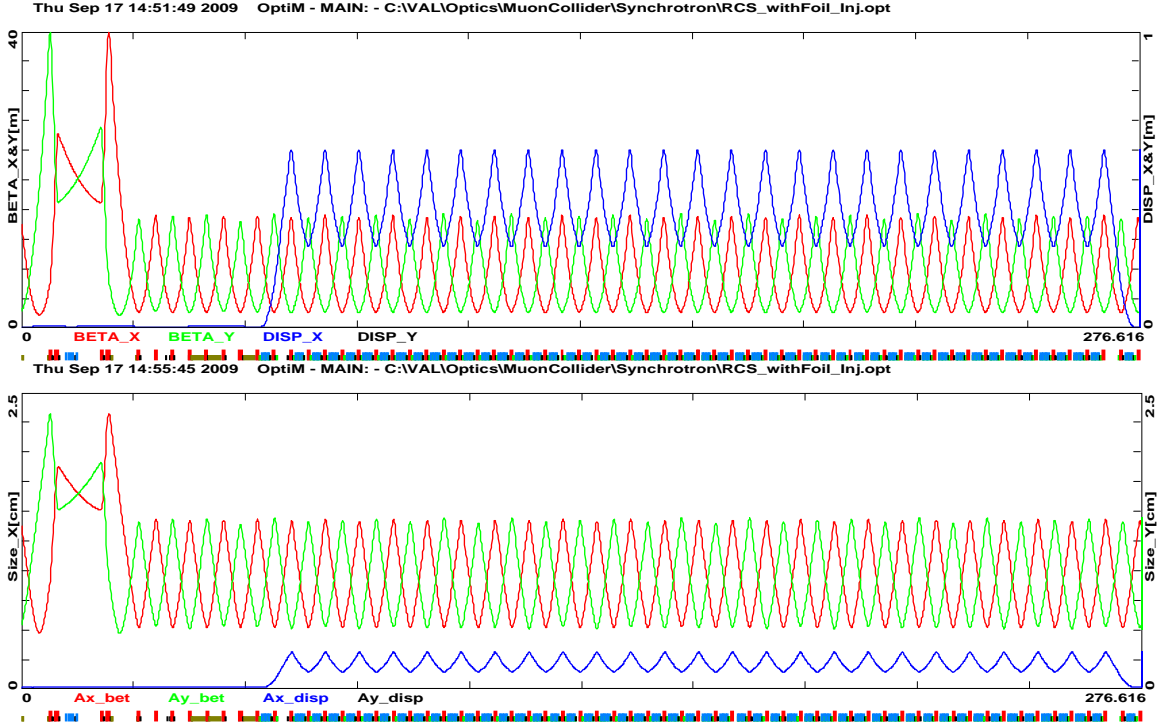


**Figure III-27: The beta-functions and dispersion (top) and the beam envelopes (bottom) for a half of the ring (the injection & extraction straight and downstream arc.) The beam envelopes are presented for  $\varepsilon_n=40$  mm mrad,  $E_k = 2$  GeV,  $\Delta p/p = 5 \times 10^{-3}$ .**

Table III-10 presents the structure of machine period. The FODO structure is built so that for a perfectly periodic lattice it would have 66 cells with two 7-cell long straight sections. Taking into account that 7 half cells of the injection straight are used for injection region and they have 4 quads instead of 6 one obtains that altogether there are 130 quadrupoles and 100 dipoles. To ease the power supply voltage requirements the dipoles and quadrupoles of each cell are included into a resonance circuit. Every quadrupole has an associated corrector package (denoted sF and sD in Table III-10). The general corrector package contains a trim dipole coil (horizontal near the F quads and vertical near the D quads) and a sextupole coil at locations with non-zero dispersion. Table III-10 presents the required strength of the trim magnets.

In this document all quadrupoles and corresponding downstream half-cells are numbered so that for the perfectly periodic FODO structure the counting would go from 1 to 132 (in the beam direction) starting from the second quadrupole of the injection straight. Taking into account that two quads are missing in the injection region optics, actual counting starts from 3 and goes to 132. Thus, the quads 132 and 3 to 14 belong to the injection straight; the quads 66 to 80 belong to the RF straight; and each two of the quads 15, 16, 64, 65, 81, 82, 130 and 131 belong to one of four short straights with missing dipole.

**Table III-10: Structure of periodicity element for 8 GeV kinetic energy**

Name	S[cm]	L[cm]	B[kG]	G[kG/cm]	S[kG/cm/cm]
qF	65.9	65.9	0	1.7675	0
o2	85.9	20			
sF	105.9	20	0	0	0.185

o1	135.9	30			
bD	349.116	213.216	8.7375	0	0
o	419.116	70			
qD	485.016	65.9	0	-1.7634	0
o2	505.016	20			
sD	525.016	20	0	0	-0.324
o1	555.016	30			
bD	768.232	213.216	8.7375	0	0
o	838.232	70			

Two groups of dipole correctors perform orbit correction: the regular correctors and the injection correctors. There are altogether 124 regular dipole correctors: 62 horizontal and 62 vertical correctors located near focusing and defocusing quads, correspondingly. Their strength is determined by accuracy of dipole fields ( $<0.3\%$ ) and quadrupole alignment ( $<1$  mm) resulting in the strength of 11 kG cm. The corrector ramping rate is determined by duration of the cycle and was chosen to be 1 kG cm/ms. The regular dipole correctors are located in the locations from 8 to 131. There are four injection correctors in each plane independently controlling the beam position and angle on the striping foil. They are located on both sides of the injection straight. The injection correctors perform the linac beam painting into transverse aperture of the ring (see below). They have larger strength (30 kG cm) and much larger ramping rate (30 kG cm/ms). There is also permanent orbit bump in the extraction region. The bump is introduced by vertical displacement of 3 quadrupoles and therefore does not require special correctors.

To ease the betatron tune correction the trim coils in quadrupoles are split into two large quadrupole families, F and D, which do not include trim coils in 36 quadrupoles assigned for optics correction. Each F and D family includes coils in 47 quads and is powered from one power supply. The optics correction quads are located at the both ends of each long straight, and in the middle and both ends of each arc. Thus the optics correction quads are: 3-6, 11-14, 16, 18, 37-42, 62, 64, 66-69, 77-80, 82, 84, 103-108, 128 and 130. The strength of the trim quadrupoles is determined by (1) focusing errors determined by finite accuracy of quadrupole production ( $\sim 2 \cdot 10^{-3}$ ), (2) different dependence of magnet strength on the power supply current for dipoles and quadrupoles due to different magnetization of their cores ( $\leq 5 \cdot 10^{-4}$ ), (3) different field correction for dipoles and quads excited by eddy currents in the vacuum chamber ( $5 \cdot 10^{-4}$ ), and (4) sufficiently large tune correction span. For the F and D families the correction value of  $\pm 1\%$  ( $\int GdL = 1.1$  kG) was chosen resulting the tune correction range of  $\pm 0.25$  for both planes. The optics correction trim quads have a larger strength of 2.2 kG. Note that all large aperture quads belong to the group of optics correction quads and, consequently, have correcting coils.

There are 98 sextupoles in the ring. They are located at positions 16-64 and 82-130 and are split into two families F (50 sextupoles) and D (48 sextupoles). The sextupole strengths required to correct the natural machine chromaticities  $\xi_x \approx \xi_y \approx -25$  to zero are  $\int S_F dL = 3.7$  kG/cm and  $\int S_D dL = -6.8$  kG/cm at the energy of 8 GeV. Taking into account the RCS will operate with chromaticities in the ranges of -10 to -20 we choose maximum strength to be 4 kG/cm. That still leaves sufficiently large margin between the operational and maximum strengths of sextupoles.

Table III-11 presents parameters of different trim coil packages required in this design.

**Table III-11:** Parameters of trim packages

Name	Quantity	L[cm]	B <sub>H</sub> [G]	B <sub>V</sub> [G]	S[G/cm <sup>2</sup> ]
------	----------	-------	--------------------	--------------------	-----------------------

Regular H	50	20	550	-	200
Regular V	48	20	-	550	200
Straight line H	12	20	550	-	-
Straight line V	14	20	-	550	-
Injection	4	30	1000	1000	-

To minimize the vertical dispersion and  $x$ - $y$  coupling twelve skew-quadrupole correctors are installed in the positions 3, 15, 16, 64, 65, 66, 67, 81, 82, 130, 131 and 132. These correctors have length 20 cm, and the integral strength of 5 kG.

The small current of CW linac results in long injection time. For 1.04 mA linac current it is equal to 4.3 ms or 2200 turns. To minimize the required linac energy correction the injection begins 2.15 ms before magnetic field reaches the maximum. The linac kinetic energy has to vary in time with the RCS field, with a total correction of 1.2%.

### III.3.2 RCS Vacuum chamber

The vacuum chamber for the RCS needs to satisfy a set of contradictory requirements. To minimize effects from eddy currents in a conductive beam pipe, a thin wall small radius pipe would be optimum. To maximize mechanical stability a thick wall pipe would be optimum. To minimize transverse impedance, a high conductivity wall with large radius pipe would be optimum. In detail, the competing effects are:

the shielding and distortion of the dipole bending field by eddy currents excited in the vacuum chamber;

the vacuum chamber stability under atmospheric pressure;

the vacuum chamber heating by the eddy currents;

the transverse impedance due to wall resistivity;

the ring admittance.

The compromise solution resulted in a round stainless steel vacuum chamber with external radius of 22 mm and the wall thickness of 0.7 mm. Details are discussed below.

The complex amplitude of magnetic field produced by eddy currents excited in the vacuum chamber of radius  $a_w$  with the wall thickness  $d_w$  and the wall conductivity  $\sigma_w$  by the AC component of dipole magnetic field alternating with frequency  $\omega_{ramp}$  is:

$$\Delta B_y(0,y) = iB_{AC} \left( 1 + \frac{\pi^2}{12} + \frac{\pi^4}{240} \frac{y^2}{a_w^2} + \dots \right) \frac{a_w d_w}{\delta_w^2}, \quad \delta_w = \frac{c}{\sqrt{2\pi\sigma_w\omega_{ramp}}} \ll a_w \quad (3.1)$$

The field correction is shifted by 90° relative to the AC component of magnetic field. The first addend in the parenthesis is related to the eddy currents excited in the wall by bending field and the other two addends are related to the multiple reflections of this current in the poles of a dipole. For the magnetic field changing as  $B(t) = B_{DC} - B_{AC} \cos(\omega_{ramp}t)$  the last addend corresponds to the sextupole field with the sextupole gradient equal to:

$$S(t) = B_{AC} \frac{\pi^4}{120} \frac{d_w}{a_w \delta_w^2} \sin(\omega_{ramp}t) \quad (3.2)$$

The relative value of dipole correction of the field (sum of the first two addends in Eq. (3.1)) is equal to zero at the cycle beginning and end. It achieves the maximum of  $|\Delta B/B| = 8.5 \times 10^{-4}$  at 16 ms within the acceleration cycle. Similarly, in the case of changing quadrupole field in a quadrupole magnet there is a quadrupole field correction with a relative value approximately half of the dipole

correction. Consequently, keeping constant tunes during the acceleration cycle requires a quad current correction  $\Delta I/I \approx 4.3 \times 10^{-4}$ . As for the field correction in a dipole, the sextupole field correction is zero at the cycle beginning and end. At 16 ms it results in the maximum contribution to the machine chromaticity:  $\Delta \xi_x \approx 1.03$  and  $\Delta \xi_y \approx -0.85$ . These values are small fraction of the natural machine chromaticity and can be easily compensated by machine sextupoles. Note that the sign of the sextupole is focusing in the acceleration part of the cycle and defocusing at the deceleration part. Tracking studies show that if only the machine sextupoles and the eddy current sextupoles are taken into account the dynamic aperture exceeds the machine aperture by about factor of 4.

There has to be sufficiently large safety margin for the mechanical stresses of vacuum chamber to warranty the reliable operation for the long lifetime of the machine. For a perfectly round vacuum chamber, the stress in the material due to atmospheric pressure,  $P_{atm}$ , is determined by

$$\sigma_{mpr} = P_{atm} \frac{a_w}{d_w} , \quad (3.3)$$

and is equal to 3.1 N/mm<sup>2</sup>. If the chamber is weakly elliptic there is additional bending stress equal to

$$\sigma_{bend} = \frac{9}{4} P_{atm} \frac{\Delta a_w}{a_w} \left( \frac{a_w}{d_w} \right)^2 , \quad (3.4)$$

where  $\Delta a_w$  determines the ellipse semi-axes to be equal to  $a_w \pm \Delta a_w$ . Assuming a comparatively conservative ellipticity of the chamber  $\Delta a_w / a_w = 0.02$ , corresponding to  $a - b = 0.88$  mm,  $\sigma_{bend} = 8.9$  N/mm<sup>2</sup>. The sum of these stresses is equal to 12 N/mm<sup>2</sup>. It is ~20 times smaller than the maximum acceptable stress (yield stress) for the stainless steel of ~200 N/mm<sup>2</sup>. A further reduction of vacuum chamber thickness is still possible but a thickness below 0.5 mm would jeopardize the long-term stability of the chamber.

The eddy currents produce vacuum chamber heating. The power per unit length is

$$\frac{dP}{dz} = \frac{\pi \sigma_R d_w a_w^3 \omega_{ramp}^2}{c^2} B_{AC}^2 . \quad (3.5)$$

For the nominal parameters the heating is equal to 10 W/m. This power level does not require water or forced air cooling. A conservative air cooling estimates for the case of convective cooling is based on the heat transfer coefficient  $10^{-3}$  W/cm<sup>2</sup>/K. If one neglects the thermal conductivity of the chamber it results in the temperature increase of 15° C on the sides of the chamber where the current is concentrated. Further increase of the ramp frequency or the AC component of magnetic field would require forced air cooling.

At low frequencies ( $f \leq 0.5$  GHz), the transverse impedance is dominated by the wall resistivity. For a thin wall chamber and the frequency range corresponding to the lowest betatron sidebands the real part of the impedance per unit length can be approximated by the following equation:

$$Z_{\perp}(\omega) = Z_0 \frac{c^2}{4\pi^2 \sigma_R \omega a_w^3 d_w} , \quad \delta_w = \frac{c}{\sqrt{2\pi\sigma_w \omega}} , \quad \sqrt{a_w d_w} \geq \delta_w \geq d_w , \quad (3.6)$$

where  $Z_0 \approx 377 \Omega$  is the impedance of free space. Comparing Equations (3.5) and (3.6) one can see that the transverse impedance and the vacuum chamber heating are closely related:

$$Z_{\perp}(\omega) \frac{dP}{dz} = \frac{Z_0}{4\pi} \frac{\omega_{ramp}^2}{\omega} B_{AC}^2 ; \quad (3.7)$$

so that their product does not depend on the vacuum chamber radius, thickness and material. Varying parameters to reduce the heating term results in an increase of the impedance term and vice versa. **Figure III-28** compares impedances of the nominal stainless steel vacuum chamber and a vacuum chamber similar to the Booster (where the poles of laminated dipole are the vacuum chamber wall). The high value of  $\mu$  and laminations greatly increase the impedance at high frequencies. In particular there is a large difference for frequencies above 50 MHz where active transverse damping is very difficult. Note that the calculations of the transverse impedance of the steel poles assume  $\mu=500$  over the entire frequency range. This assumption is not justified for frequencies above  $\sim 10$  MHz where the skin depth becomes comparable to the domain size. Consequently, the impedance is somewhat smaller at very high frequencies but is still well above the impedance of stainless steel chamber. Figure III-29 presents the betatron tune shifts due to beam interaction with stainless steel vacuum chamber in the approximation of zero betatron tune spread. The growth time for the lowest betatron sideband is about 150 turns. A bunch-by-bunch transverse damper can suppress this instability easily. Instabilities at frequencies corresponding to intra-bunch motion ( $f > 50$  MHz) are damped by chromaticity (see below).

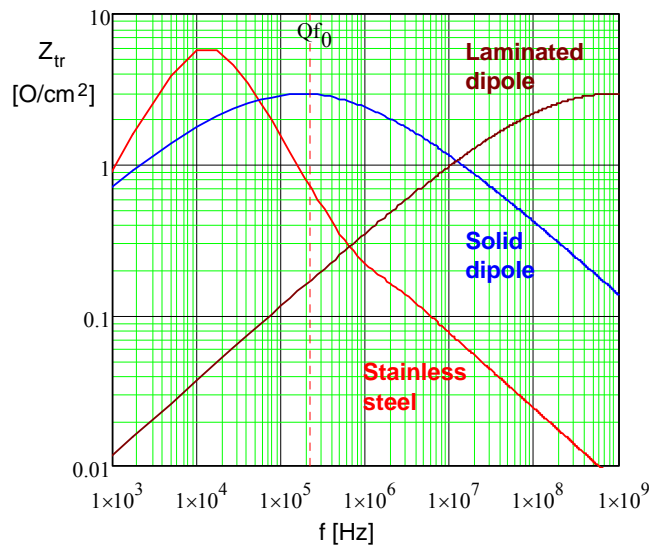


**Figure III-28:** Dependence of the transverse impedance per unit length on frequency; red line - thin stainless steel vacuum chamber with radius 22 mm and wall thickness of 0.7 mm; blue and brown lines – vacuum chamber walls are poles of solid and laminated dipoles correspondingly with gap of 44 mm and  $\mu=500$ , lamination thickness of 0.63 mm.

From the above discussion, there are many reasons to keep the vacuum chamber size being sufficiently small. It also shows that a ceramic vacuum chamber is not really helpful (while significantly more expensive): a reduction of conducting layer thickness could reduce the vacuum chamber heating but it results in an increase of transverse impedance being the same as for a stainless steel chamber. If the vacuum chamber walls are too thin or absent as in the Booster the beam interacts with the steel laminations of magnets resulting in much higher impedances and instability growth rates.

There is a sufficiently large margin between the 95% normalized emittance of 25 mm mrad and the beam boundary set at 40 mm mrad. At injection the beam boundary corresponds to the maximum beam size of 14 mm leaving 6 mm for orbit distortions in both planes. This value is

within normal operational orbit distortions of the Booster. The sagitta in the dipole is equal to 1.7 cm. To avoid aperture loss the vacuum chamber in dipoles has to be bent to follow the beam bending with 33.9 m radius.

To prevent the multipactoring of electrons by the beam fields and the resulting e-p instability a thin film of TiN or carbon coats the inner wall of vacuum chamber.

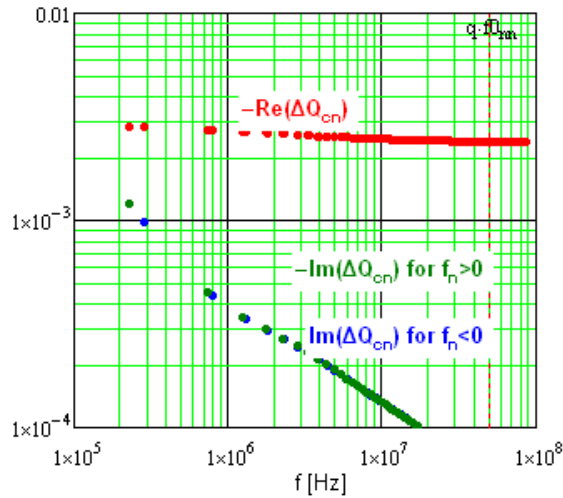


**Figure III-29:** Real and imaginary tune shifts for stainless steel vacuum chamber;  $a_w=22$  mm,  $d_w=0.7$  mm.

### III.3.3 RCS RF Systems

Figure III-30 presents time dependences of beam and RF system parameters in the course of acceleration and Table III-12 shows the main parameters of the RF system. To reduce the betatron tune shifts due to the beam space charge at injection and through acceleration we plan to use a double harmonic RF system so that the voltages of the fundamental (first harmonic) RF system and an additional RF system operating at its second harmonic could create a longitudinal potential well with a flat bottom through the entire accelerating cycle<sup>13</sup>. Presently we plan to inject the beam into the ring with flat-bottom potential well and, then, gradually reduce the second harmonic RF voltage in the second half of the accelerating cycle; so that the beam would be matched to the Recycler RF which is not planned to have the second harmonic RF on at injection. The match also implies that the longitudinal emittance needs to be increased from 0.35 to 0.4 eV s (or if necessary even to 0.6 eV s) in the course of acceleration. It can be achieved by manipulations with the longitudinal quadrupole damper similarly to how it is done now in the Booster. However if necessary the scenario can be changed so that both RSC and Recycler will have the second harmonic RF on during beam transfer resulting in a well matched bucket-to-bucket beam transfer and smaller bunching factor. The maximum RF voltage is chosen so that

<sup>13</sup> Relationships used for calculations of the double harmonic RF system are shown in Appendix A.

the nominal RF voltage could be achieved even if 2 of 16 (1 of 10) cavities do not operate for the first (second) harmonic RF systems.

The beam-induced voltage significantly exceeds the RF system voltage required for the beam acceleration and capture. Even at the RF voltage maximum of 1.2 MV the beam induced voltage (at resonance) exceeds the required RF voltage by a factor of 2.6. This ratio achieves its maximum of about 50 at the end of the accelerating cycle where the RF voltage, depending on scenario, can achieve its minimum of about 60 kV. A relative misphasing of the first and second harmonic RF systems deteriorates the flat bottom potential well resulting in an increase of longitudinal density or/and shallowing the potential well and, subsequently, leading to a particle loss. The required accuracy of relative phasing is about 5° of the first harmonic frequency. Addressing the voltage stability and relative phasing will require a sophisticated low level RF.

**Table III-12:** Main Parameters of RF system

	1 <sup>st</sup> harmonic	2 <sup>nd</sup> harmonic
Harmonic number	98	196
Maximum voltage, MV	1.6	0.7
Minimum voltage, kV	20	10
Frequency sweep, MHz	50.33-52.81	100.66 – 105.62
Number of first harmonic cavities	16	10
Shunt impedance, kΩ	100	100

The injection to the Recycler, and, subsequently, to MI requires injection gaps of 3 buckets in the bunch structure of MI. The beam abort and the extraction from the MI at the maximum energy require an abort gap of 45 buckets in MI and set the extraction gap in RCS to 10 buckets. Consequently, only 88 of 98 buckets have to be filled at the injection to RCS. To minimize adverse effects of the beam loading, feed forward correction of the RF voltage will be used.

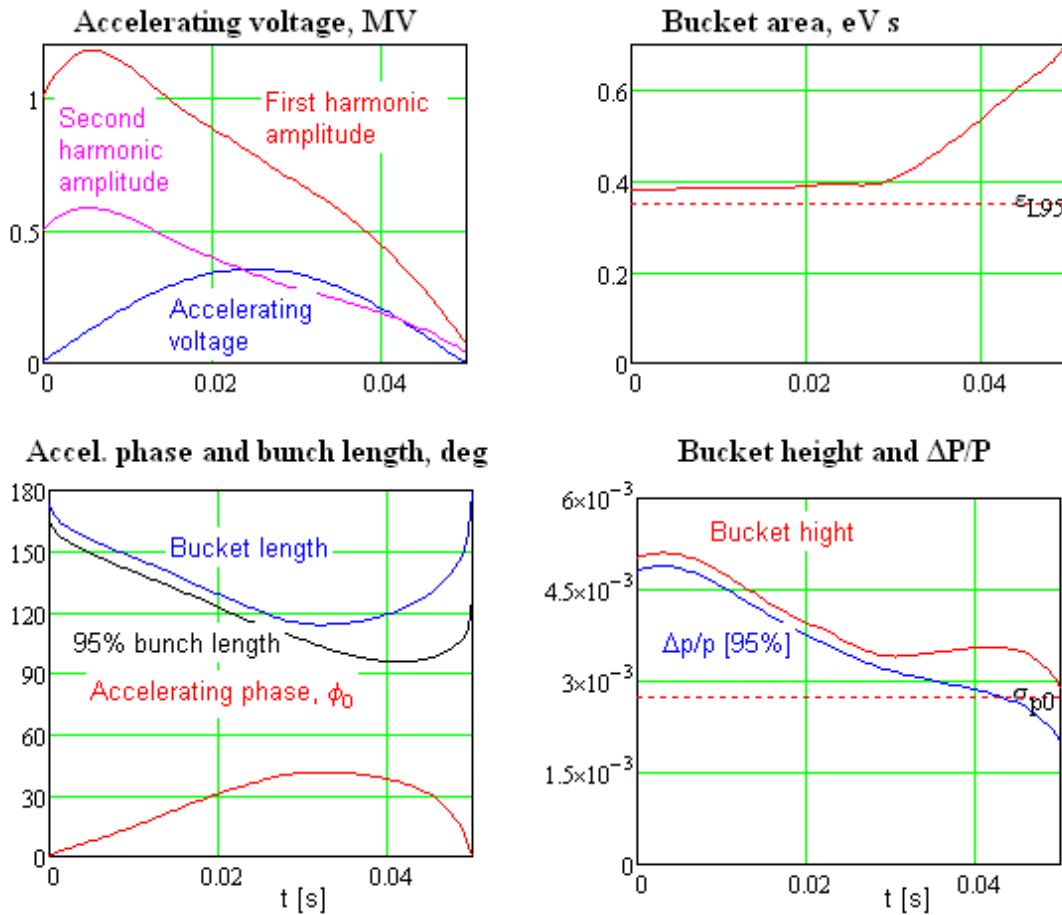


**Figure III-30:** Beam and RF system parameters during acceleration. For this plot, the longitudinal emittance is equal to 0.35 eV s and is not changed in the course of acceleration. The total RF power is presented for the case when 2 of 16 and 1 of 10 RF cavities are not operating for the first and second harmonic RF systems, correspondingly.

### III.3.4 Beam Stability for RCS

A beam is stable, if for its every coherent mode a sum of the Landau damping and the damper-induced rate exceeds the impedance-associated growth rate. Landau damping is extremely sensitive to a ratio of the effective space charge tune shift to the synchrotron tune<sup>14</sup>. For the discussed parameters, this ratio  $q=2.4$  for a 3D Gaussian beam, and  $q=1.6$  for KV model at injection energy. Since the space charge parameter  $q$  is not extremely high, the strong space charge theory<sup>14</sup> can be used only as a rather rough approximation. According to that, 0<sup>th</sup> head-tail mode does not have any Landau damping at all, while the first mode has rather fast damping rate  $\Lambda_1 \approx (0.2 - 0.4)Q_s$ , and higher modes should not be seen at all.

The coherent growth rate can be estimated by the air-bag model (see<sup>15</sup>, Eq. (6.188)):

<sup>14</sup> A. Burov, Phys. Rev. ST Accel. Beams 12, 044202 (2009)

<sup>15</sup> A. Chao, "Physics of collective beam instabilities", J. Wiley & Sons, 1993.

$$\text{Im}\Omega = \frac{Nr_0c}{2\gamma T_0^2 \omega_b} \sum_{p=-\infty}^{\infty} Z^\perp(\omega') J_l^2(\omega'z/c - \chi), \quad \omega' = pM\omega_0 + \mu\omega_0 + \omega_b.$$

For the thick-wall resistive impedance it results in the growth rate equal to:

$$\text{Im}\Omega / \omega_0 = \frac{Nr_0 \delta_0 \bar{\beta}_x}{2\pi \gamma a^3} \Gamma(l, \chi, \mu);$$

$$\delta_0 = c / \sqrt{2\pi\sigma\omega_0};$$

$$\Gamma(l, \chi, \mu) \equiv \sum_{p=-\infty}^{\infty} \sqrt{\frac{\omega_0}{|\omega'|}} J_l^2(\omega'z/c - \chi) \text{sgn}(\omega')$$

The most unstable coupled-bunch mode for the betatron tune  $\nu_b=18.44$  is the mode  $\bullet = -19$ . The mode-factors  $\bullet$  for this coupled-bunch number are presented in Figure III-31. Without a damper, the 0<sup>th</sup> head-tail mode can be only stabilized for the head-tail phase  $\bullet$ . Assuming  $\bullet=1.5$ , the growth rate for the 1<sup>st</sup> head-tail mode is calculated to be  $\text{Im}(\bullet)/\bullet=0.01Q_s$ , which is 20-40 times smaller than the Landau damping rate for this mode. Thus, there is a significant safety factor for the beam coherent stability.

For the extraction energy, the synchrotron frequency goes fast to its minimal value at the very end of the cycle. This results in  $q=10$  at extraction, making the first 3-4 head-tail modes formally unstable. However, the growth times of these modes are calculated as 20 ms or higher and are too long to cause concern, since the entire acceleration time is 50 ms.

The longitudinal microwave stability threshold (Keil-Schnell) is calculated as 10-20 times above the nominal beam current (at all energies), so this instability should not to be a problem.

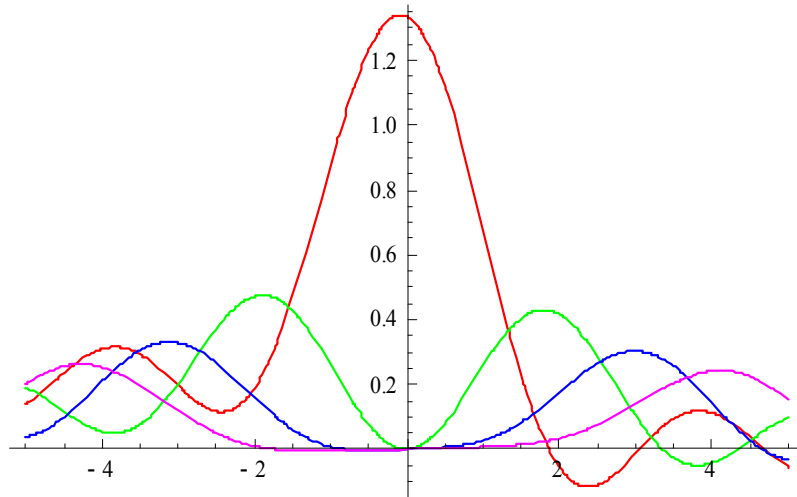


**Figure III-31: Mode factors  $\bullet$  as functions of the head-tail phase  $\bullet$  for the head-tail modes 0 (red), 1 (green), 2 (blue) and 3 (magenta), and the coupled-bunch mode number -19.**

### III.3.5 Beam injection and extraction

Figure III-32 presents the beam envelopes in the injection-extraction straight line. It also shows the injection and extraction bumps and the aperture limitations. The beam envelope represents the beam boundary corresponding to the normalized emittance of 40 mm mrad at the injection energy. The vertical lines show vacuum chamber aperture for corresponding quadrupoles, positions of the

stripping foil, and collimators. The assignment for each half cell is presented in Table III-13. Injection and extraction are in the horizontal plane from radially outside and to radially outside, correspondingly.

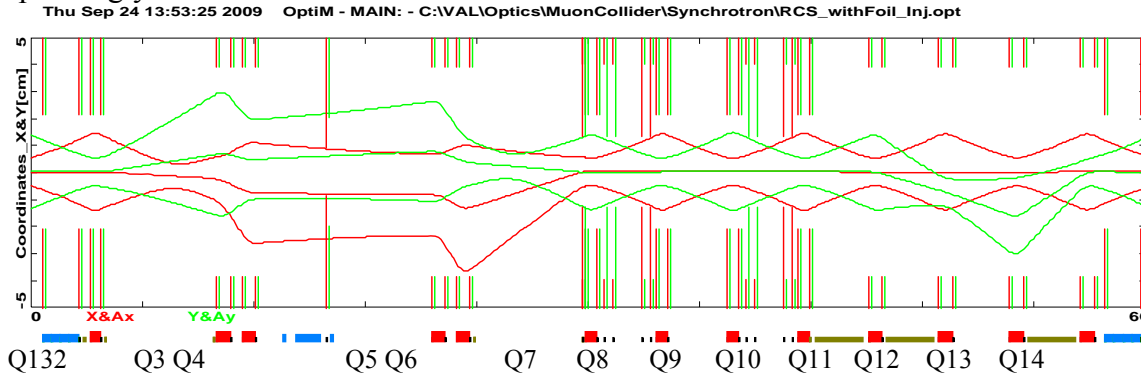


**Figure III-32: The beam envelopes and the aperture limitations in the injection-extraction straight line. The vertical line between Q4 and Q5 marks the position of the stripping foil. Horizontal and vertical collimators are shown between quads Q7 – Q8 and Q9 – Q10. The injection bump is shown at the end of injection process after the beam is horizontally displaced from the foil.**

Cell number	Assignment
132	TBD
4	Injection
6	Primary collimators
7	Vertical and Horizontal collimators
8	TBD
9	Vertical and Horizontal collimators
10-11	Extraction kickers
12	TBD

**Table III-13: Half Cell Assignments for the injection-extraction straight section.**

### III.3.5.1 H- Multi-turn injection

The RCS will utilize the multi-turn charge exchange injection. Due to the long injection time of 4.3 ms (2200 turns), the transverse and longitudinal phase space painting techniques are required to minimize the impact of the foil on the circulating beam (and vice versa) as well as to minimize the beam density for mitigation of space charge effects. In the course of injection, the linac energy has to follow the RCS energy that varies by 1.2% (kinetic) during the injection time.

The horizontal transverse injection system consists of a 3 dipole DC chicane located in the 10.43 meter straight section between Q4 and Q5 quads. The optics structure of the injection half-cell is presented in

. At the injection energy the chicane displaces the reference orbit outward approximately 17.5 mm in the middle of the merging chicane dipole. The reference orbit only moves 6.24 mm

at the foil and has a 16.4 mrad angle toward the centerline. The middle chicane dipole will be used to merge the incoming H<sup>-</sup> with the proton orbit. Its field is limited by a loss rate due to magnetic field stripping and has been chosen to be 2.0 kG resulting in the loss of  $1.3 \times 10^{-6}$  ( $8.7 \times 10^{-7} \text{ m}^{-1}$ ). The field in the third chicane was chosen to be 8.333 kG such that it will strip any H<sup>-</sup> emerging from the foil or missing it. It will also strip higher excited states of H<sup>0</sup> coming out from the foil. Most of them will be accepted to the beam but some, which penetrated deep into B3 field before stripping, will be lost in the collimation system located immediately downstream of the injection region. To reduce the angular spread due to stripping in the magnetic field the field edge of the dipole has to be short. For symmetry, the first chicane dipole has the same field as the third. Figure III-33 presents layout of the injection region. Magnetic field of the chicane dipoles is not changed during acceleration. It excites  $\pm 5\%$  betatron wave in the vertical plane that, if required, can be easily corrected by trim quadrupoles.

**Table III-14: Injection Area information**

Structure of Injection Half Cell			
Name	L[cm]	B[kG]	G[kG/cm]
Q4	79.4		0.4595
oInj	160		
B1	18	-8.33	
oInj1	60		
B2	150	2	
oInj2	30		
FOIL	0		
oInj2	30		
B3	18	-8.33	
oInj	577.122		
Q5	79.4		-0.4585

Corrector Strength for Injection Bumps		
	Injection Bump (kG cm)	Injection bump max painting Bump (kG cm)
C1x	8.75	-3.29
C1y	8.94	-11.54
C2x	8.21	-10.47
C2y	0	2.65
C3x	0	3.87
C3y	4.33	-6.85
C4x	16.7	-17.61
C4y	4.75	-2.04

Four fast correctors (in each plane) perform transverse beam painting. Such a scheme allows one to have the independent control of the closed orbit position and angle for both planes at the foil location. The correctors are located near quads 132, 3, 6 & 7. The orbit bump consists

of two constituents: the painting bump (changing during injection) and the injection bump designed to minimize the required aperture in the injection region quadrupoles.

presents the corrector strength required to create such bumps. After painting the beam is moved horizontally inward out of the foil and is parked at -7.61 mm relative to the reference orbit. With further acceleration the value of this displacement is decreasing together with the beam size resulting in that the beam does not touch the foil even if values of the injection bump correctors stay unchanged during acceleration. The injected  $H^-$  beam does not move during injection. Relative to the reference orbit (which takes into account the beam displacements in the injection dogleg) it has the following coordinates on the foil:  $x = 11.80$  mm,  $y = 5.85$  mm,  $\theta_x = -0.527$  mrad and  $\theta_y = 0.284$  mrad. The coordinates of the foil corner are  $x_f = 9.25$  mm,  $y_f = 3.38$  mm. Figure III-34 and Figure III-35 show the beam and vacuum chamber cross-sections on the foil and the beam envelopes in the injection region. To have enough room for the injection bumps the aperture of four quads (Q3-Q6) is increased from 25 to 45 mm.

The foil thickness has been chosen to be  $600 \mu\text{g}/\text{cm}^2$ . This is thick enough to strip the major fraction of  $H^-$  to protons leaving about 0.5% particles as  $H^0$  and negligible fraction as  $H^+$ . Further increase of the thickness would result in larger particle loss due to scattering in the foil and larger foil heating. However both these problems stay on the manageable level. To minimize the number of secondary passages through the foil the beam is parked quite close to the foil edges ( $2.32\sigma$  in both planes) resulting in that about 2% particles will be missing the foil. They will be converted to  $H^0$  in the field of B3 and go to the beam dump. The finite length of B3 edge field increases the angular spread of field stripped  $H^-$ . The RMS width of this angular distribution is about 1 mrad, which is about 5 times larger than the RMS horizontal angular spread of the  $H^0$  beam. The center of the distribution is shifted by  $\sim 3$  mrad. Figure III-36 shows the distribution of  $H^0$  beam after stripping of  $H^-$  in the field of B3 dipole.

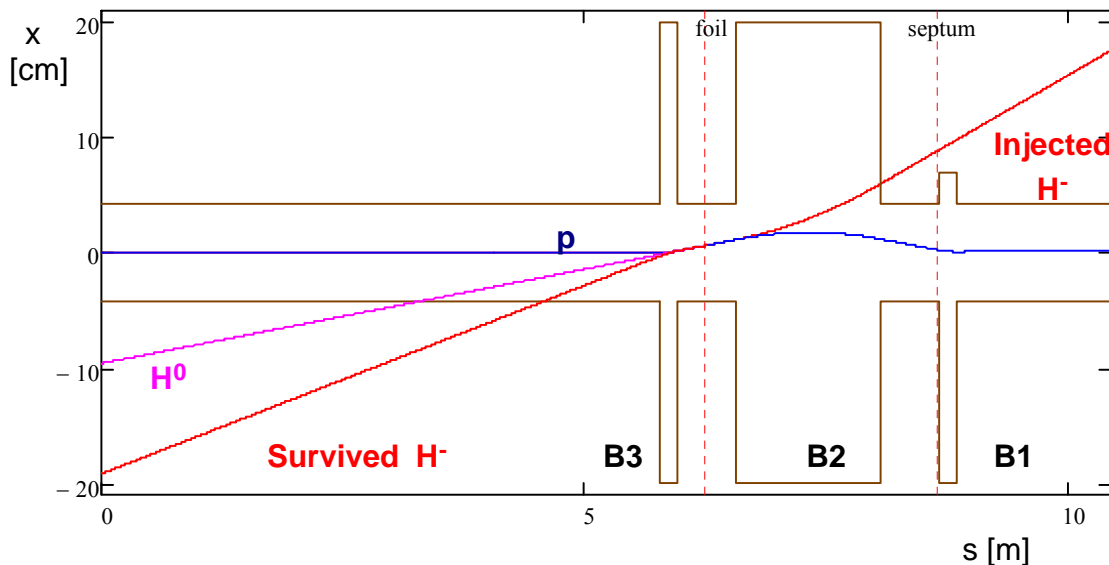


**Figure III-33:** The trajectories of the circulating proton and incoming  $H^-$  beams. The brown lines show aperture of vacuum chamber and positions of chicane dipoles.

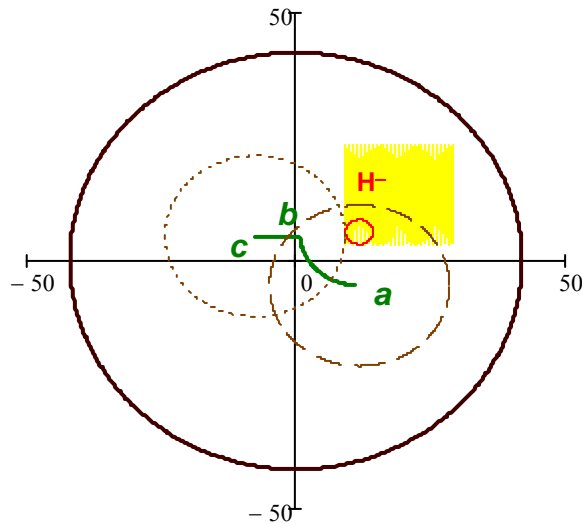


**Figure III-34:** The beam and vacuum chamber cross-sections on the foil. The green line shows displacement of the closed orbit in the course of painting. It starts at point *b*, goes to point *a*, then goes back to *b*, and finally it is moved to point *c* to prevent further beam interaction with the foil. The yellow square shows position of the stripping foil. The red ellipse shows boundary of injected  $H^+$  beam. The brown dashed and dotted lines present boundary of stored proton beam when the closed orbit is located in points *a* and *c* for machine acceptance of 40 mm mrad (normalized). The internal radius of vacuum chamber is 42 mm.

The total power of the injected beam is about 85 kW. About 4% of these particles are lost during injection: ~2% miss the foil, 0.5% are not completely stripped in the foil, 0.15% are single scattered in the foil, and ~1% are outside of 40 mm mrad RCS acceptance and are lost in the scraping system. In normal operating conditions it results in the heat load on the injection beam dump being about 3 kW and 1.5 kW intercepted by the collimation system. Prudent design (confirmed by SNS experience) would have both the injection waste beam absorber and the collimation system designed to handle 10% of total beam power or 8.5 kW.

Stripping of  $H^+$  also yields two 1.1 MeV electrons per each stripped  $H^+$ . These electrons carry sufficiently large power of about 90 W that needs to be intercepted by the electron beam dump. After leaving the foil the electrons are reflected from the B3 dipole where they are bent by its magnetic field. It results in the bending angle of 180 deg (reflection) and the beam shift of about -9 cm in the horizontal plane. That minimizes interference between the stripping system and the electron dump. The B3 field also results in a vertical defocusing of the electron beam and, consequently, a reduction of peak heat load. A design of the electron dump has to prevent the interaction of secondary electrons with the circulating beam.

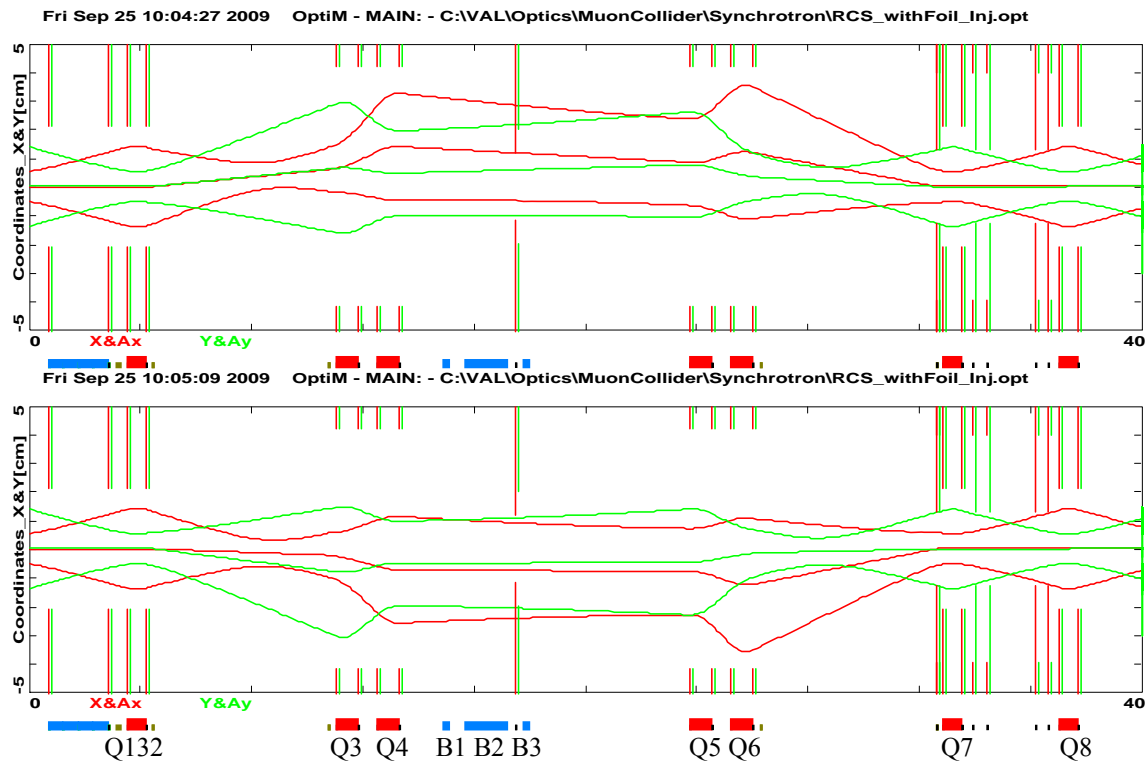


**Figure III-35:** Beam envelopes through the injection bump region for parameters of **Figure III-27**; top – injection bump only, bottom – injection bump + maximum amplitude for X&Y painting bumps. Vertical green line near Q7 shows primary horizontal scraper.

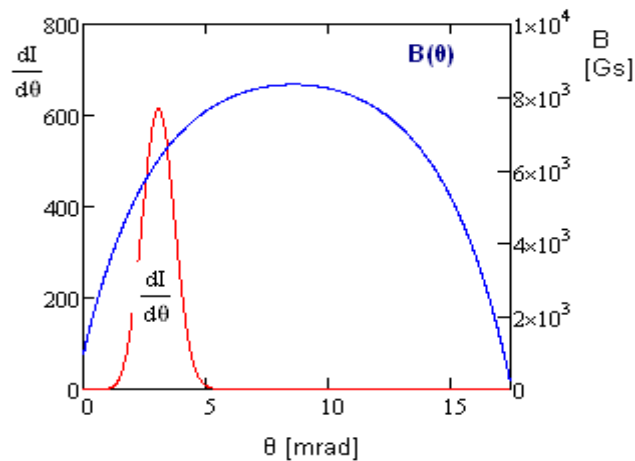


**Figure III-36:** Angular distribution of  $H^0$  after  $H^-$  stripping in field of B3 dipole (red line). Blue line presents the magnetic field in the corresponding stripping point.

### III.3.5.2 Transverse and longitudinal injection painting

We considered a few possible transverse painting schemes. In this document we present a scheme that minimizes the foil heating, is sufficiently simple, and has the beam distribution close to the desired KV-distribution. The above infrastructure of the injection region is sufficiently flexible and does not prevent us from using other painting methods in the future.

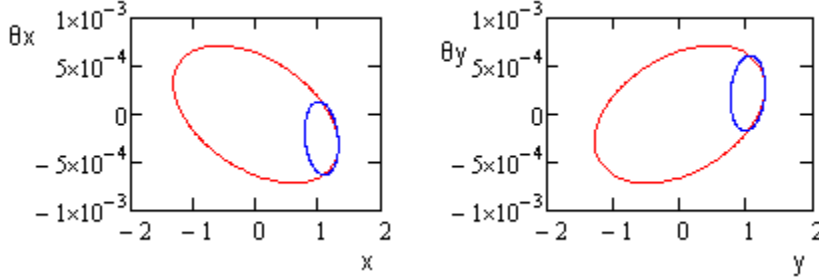


**Figure III-37:** Phase space boundaries of the linac (blue lines) and RCS (red lines) beams. The linac beam boundaries correspond to the normalized boundary emittance of 3 mm mrad ( $2.45\sigma$  of 0.5 mm mrad RMS emittance) the RCS beam boundaries correspond to the normalized emittances of 25 mm mrad.

The following criteria were used to create a particle distribution: (1) create a KV-like distribution which would have approximately constant particle density across the beam, (2) make the beam cross section in  $x$ - $y$  plane elliptical with semi-axes corresponding to horizontal and vertical emittances of 22 mm mrad, and (3) minimize the number of secondary passages through the foil. The time dependence of closed orbit position on the foil for the first half of the painting cycle can be described by the following equations,

$$\begin{aligned} A_x(t) &= -A_{x0} \cos(\varphi(t)), \\ A_y(t) &= -A_{y0} \sin(\varphi(t)), \end{aligned} \quad \varphi(t) = \begin{cases} \phi_0 + 2(\pi/2 - 2\varphi_0)t/T_{inj}, & t \leq T_{inj}/2, \\ \phi_0 + 2(\pi/2 - 2\varphi_0)(T_{inj} - t)/T_{inj}, & t > T_{inj}/2, \end{cases} \quad (3.8)$$

where  $A_{x0} = 11.1$  mm,  $A_{y0} = 10.8$  mm,  $\phi_0 = 79$  mrad,  $T_{inj} = 4.3$  ms. In the second half of the painting cycle the closed orbit motion is inverted so that it comes to the initial point at the cycle end. To minimize the number of passages through the foil all beta- and alpha-functions of the linac beam are scaled from corresponding values of RCS by a factor of 0.345 so that the linac phase space would be inscribed into  $x$  and  $y$  machine acceptances as shown in Figure III-37. To paint on the surface of KV-distribution (in the 4D phase space) the angles and positions of the injected linac beam are scaled together so that:

$$\begin{aligned} \theta_x &= x/L_x, \\ \theta_y &= x/L_y, \end{aligned} \quad (3.9)$$

where  $L_x = -42$  m and  $L_y = 46$  m. Such correlation also reduces the number of passages through the foil. All these measures resulted in the distribution quite close the desired KV distribution. Figure III-38 presents particle positions at the end of painting. One can see that the almost all particles are inside the ellipse corresponding to the horizontal and vertical normalized emittances of 35 mm mrad. Figure III-39 presents the single dimensional particle densities for horizontal and vertical planes at the foil location and their comparison to the KV distribution with for  $\varepsilon_{xn} = \varepsilon_{yn} = 22$  mm mrad. One can see a good coincidence for the main part of the distributions. The distribution tails are related to the

finite value of linac emittances. Figure III-40 presents the integral particle distributions over 2D and 4D Courant-Snyder invariants:

$$\begin{aligned}
 I_x &= \theta_x^2 \beta_x + 2\alpha_x x \theta_x + (1 + \alpha_x^2) x^2 / \beta_x, \\
 I_y &= \theta_y^2 \beta_y + 2\alpha_y y \theta_y + (1 + \alpha_y^2) y^2 / \beta_y, \\
 I_{4D} &= I_x + I_y.
 \end{aligned}
 \tag{3.10}$$

The total number of particles outside of machine acceptance of 40 mm mrad (normalized) is about 1%. Initial optimization and tracking were done neglecting the beam space charge. Tracking studies with the beam space charge taken into account were done using ORBIT code. They exhibited small effect of beam space charge on the final distribution and particle loss.

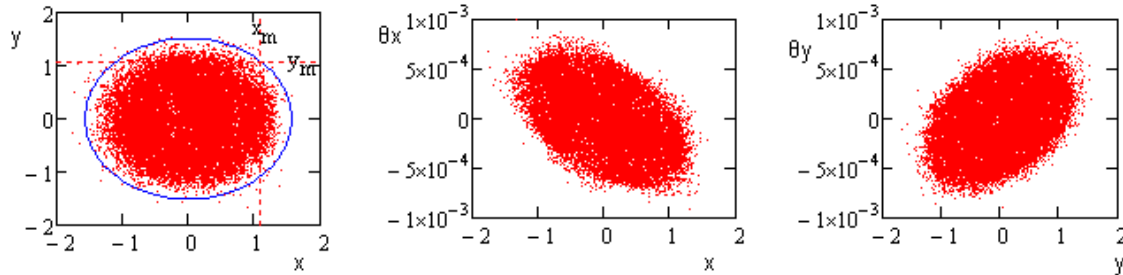


**Figure III-38:** Particle coordinates at the end of painting. Blue line is shown for the horizontal and vertical normalized emittances of 35 mm mrad.

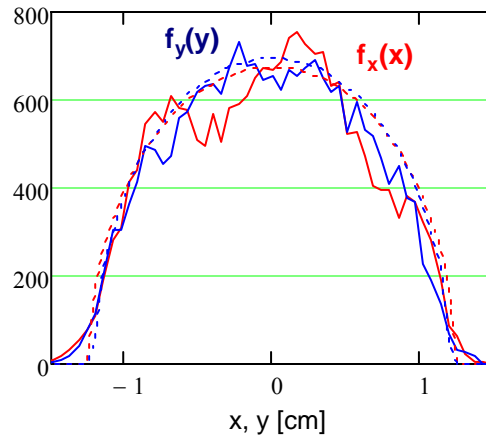


**Figure III-39:** Dependence of single dimensional particle densities on transverse coordinates at the foil location. The dotted lines show the corresponding densities for the KV-distribution with  $\epsilon_{xn} = \epsilon_{yn} = 22$  mm mrad.

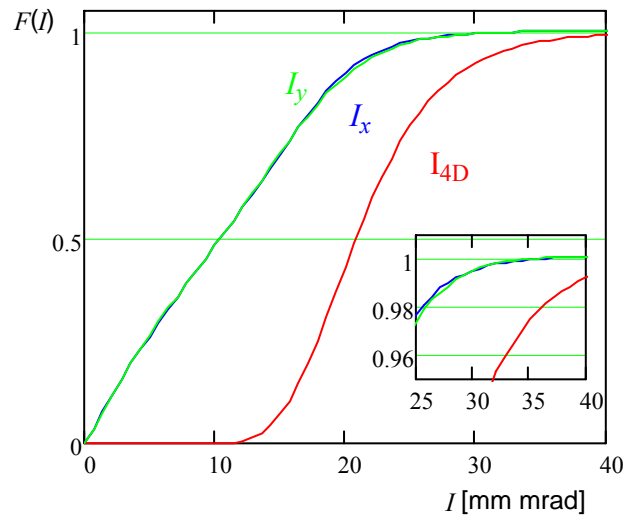


**Figure III-40:** The integral particle distributions over Courant-Snyder invariants. Inset shows the upper end of the same curves.

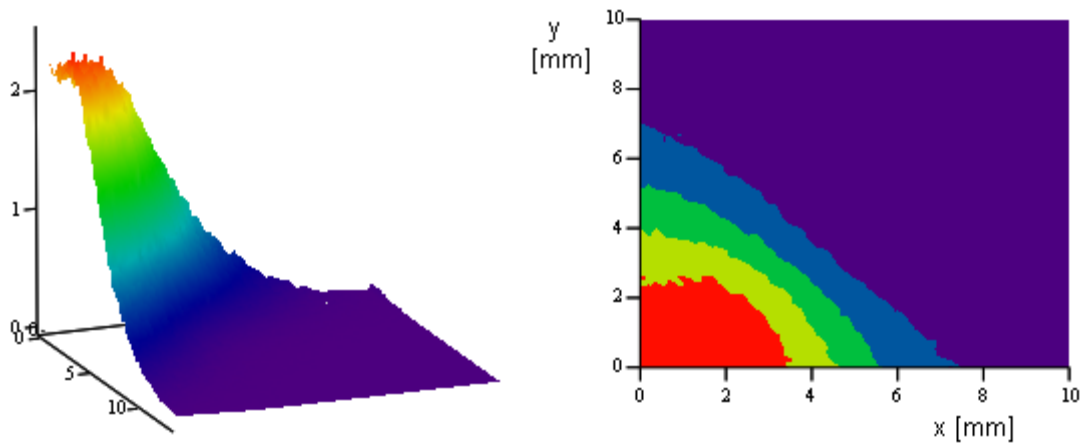


**Figure III-41:** Distribution of secondary passages on the foil surface; the peak of the distribution corresponds to 2.2 passages per  $\text{mm}^2$  per injected particle.

From the simulations, the number of secondary passages through the foil is about 50. Figure III-41 presents the distribution of secondary passages on the foil surface. The use of double pass painting described above resulted in more uniform power distribution on the foil and, corresponding, reduction of peak power density by  $\sim 20\%$  relative to a single pass painting. The maximum of the distribution is achieved on the foil corner and is equal to  $\sim 2.2$  passages per  $\text{mm}^2$  per incoming particle. The density of the incoming  $\text{H}^-$  beam is  $0.14 \text{ mm}^{-2}$  per particle. It is shifted from the foil edges and does not change the maximum of power deposition located at the foil corner. To improve the foil cooling the foil of  $420 \mu\text{g}/\text{cm}^2$  thickness is rolled by  $45^\circ$  so that it would have the stripping power of  $600 \mu\text{g}/\text{cm}^2$  foil. Taking into account that about 25% of heating power is removed by  $\delta$ -

electrons and that the foil is cooled by the black body radiation on both, the foil peak temperature is  $\sim 1200\text{ C}^\circ$ .

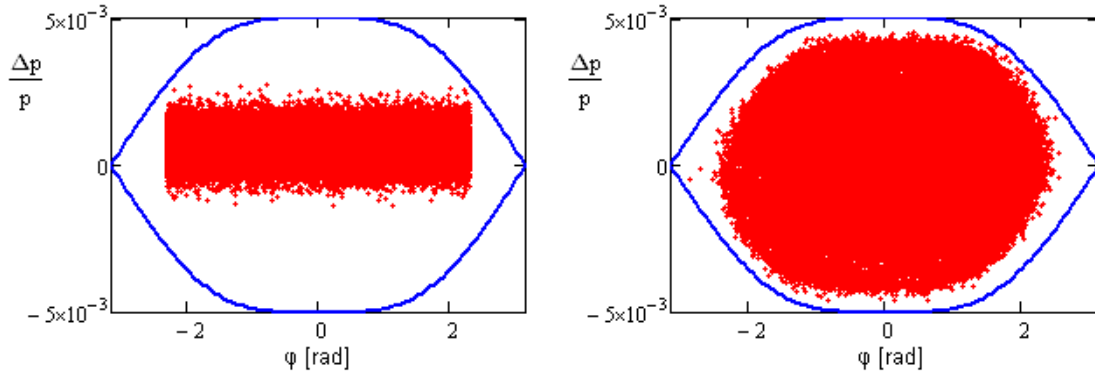


**Figure III-42:** The phase space positions of the injected particles (left) and the particle positions at the end of injection ( $\sigma_p=5\times 10^{-4}$ ,  $\Delta p/p=7\times 10^{-4}$ ,  $T_w=14.6\text{ ns}$  (73%))

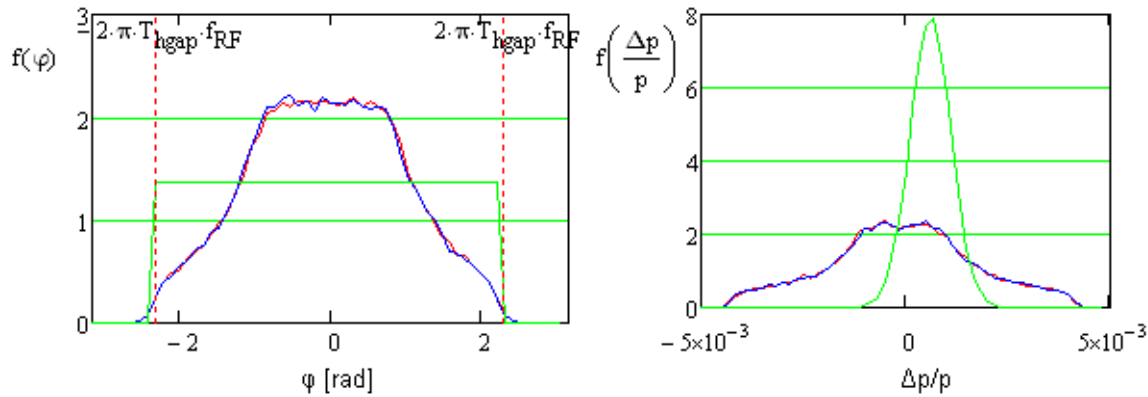


**Figure III-43:** Particle distributions over RF bucket length (left) and over momentum (right); green lines – for injected particles, red lines – after injection, blue lines - 500 turns after injection.

The painting of the longitudinal distribution is performed by the momentum offset of linac beam relative to the RCS RF bucket center. The dual harmonic RF system is used to flatten the bucket. The nominal voltage of 1 MV (first harmonic) is on at the beginning of injection. The value of the offset is equal to  $7\times 10^{-4}$  ( $\Delta p/p$ ) while the bucket height is  $5\times 10^{-3}$ . To prevent particle injection outside of the RF buckets, the linac bunches are chopped to an appropriate pattern (see section III.1.1). The chopper is synchronized with the RCS RF and chops off particles located outside  $\pm 7.3$  ns window (relative to bucket center) corresponding to 73% of the bucket length. Simulation results are shown in Figure III-42 and Figure III-43. The bunch is sufficiently flat at the top of the distribution. Its bunching factor is equal to 2.2. The contribution of the beam space charge and the vacuum chamber impedance are small and were neglected in these simulations.

### III.3.5.3 Beam extraction

Beam extraction from the RCS has been located in the downstream end of the injection/extraction straight section as shown in Figure III-44. The extraction plane is vertical,

where the beam is kicked vertically into a horizontally bending Lambertson magnet. There are two kickers located between quads 10 and 12. The Lambertson magnet is located between quads 13 and 14. This configuration will be responsible for all extractions from the RCS.

In normal operating conditions the RCS extraction energy is matched to the Recycler energy that cannot be changed because Recycler has dipoles built from permanent magnets. The initial configuration does not include a RCS beam abort system to dump the beam during acceleration. In the case of an accident the beam energy will be absorbed by the beam collimation system that is not designed to withstand permanent loss of full intensity beam but can withstand infrequent loss of single full intensity pulse with stored energy of 34 kJ.

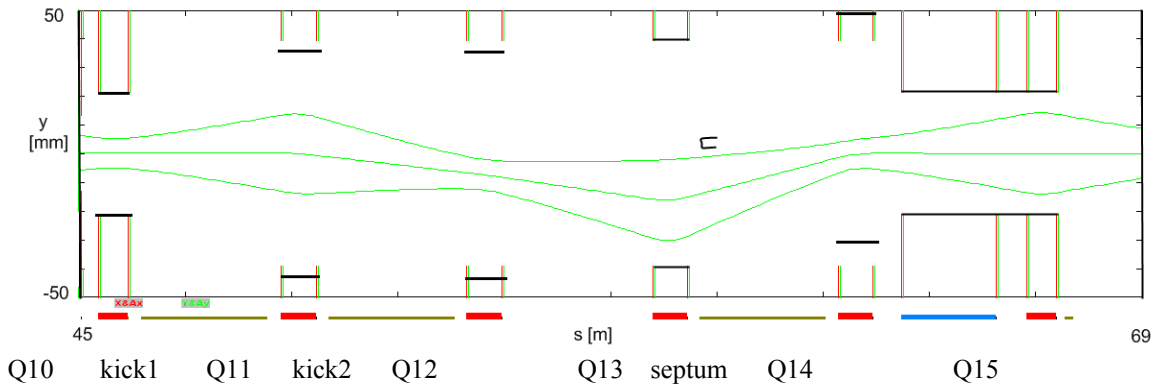


**Figure III-44:** Vertical beam envelope ( $40\pi$ ) of injected beam in the extraction region. Beam displacement at septum is 14.3 mm. Horizontal black lines show aperture in displaced quads: Q11 = -4.8 mm, Q12 = -6.39 mm, Q14 = 9.84 mm.

The vertical orbit displacement below the Lambertson septum is achieved by displacement of 3 quadrupoles (Q11, Q12 and Q14) making permanent extraction bump. Figure III-44 shows the vertical beam envelope of injected beam with its displacement taken into account. It also shows the position of the septum. The Lambertson septum is assumed to be 5 mm thick and a minimum of 5 mm is left between the septum and circulating beam at all energies. To have enough room, 4 quads (Q11 – Q14) have increased aperture of 45 mm (radius). They have the same design as the injection quads.

Figure III-45 shows the extracted beam orbit and 8 GeV beam envelope due to the  $\sim 4.5$  mrad vertical kick of the extraction kicker pair. This produces a 24 mm displacement at the entrance of the Lambertson with a 6 mrad angle toward the centerline. The horizontal Lambertson has been rolled by  $\sim 7$  degrees to compensate the downward kick from the quadrupole just upstream of the Lambertson. For the initial layout, the Lambertson horizontal bend angle has been chosen to be 96 mrad to be able to install the first quadrupole magnet of the extraction line in the space between the RCS quad and dipole. This angle requires a dipole field of approximately 1 Tesla for a magnet length of 2.85 meters. Reusing an existing Lambertson magnet for this purpose is being investigated. The vertical offset of quad upstream of the Lambertson or its aperture needs further evaluation. The aperture and magnet choices of this configuration will be re-evaluated if this system will need to be utilized as a RCS abort system.

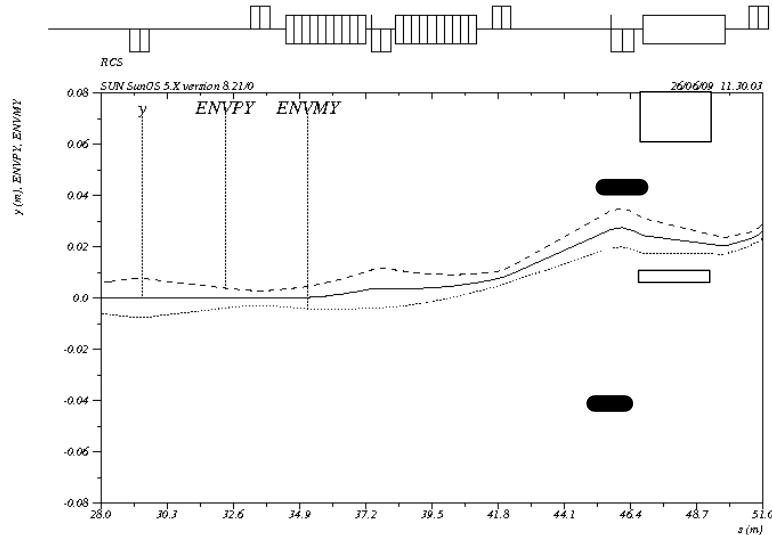


**Figure III-45: 8 GeV extraction beam envelope through the Lambertson field region.**

#### III.3.5.4 Injection Beam Dump and Beam Collimators in RCS

The injection dump and the collimation system localize the beam loss. They are well protected from radiation excited by the beam. It results in significant reduction of the residual radiation in the RCS tunnel. The injection dump is installed immediately downstream of the injection chicane (before quad Q5). It intercepts  $H^0$  that were not stripped to the protons. The dump design (see Section IV.2.2) allows routine operation with 4 kW beam loss and can operate up to 10 kW during limited time (hours).

An initial design of the collimation system suggests that it will consist of a primary momentum collimator, primary betatron collimators, and 4 main collimators. The primary momentum collimator is located downstream of quad Q130 and has 2 jaws allowing to scrape the beam horizontally on both sides. The horizontal and vertical primary betatron collimators are located downstream of quad Q7. Each of them scrapes the beam on 2 sides. The four main collimators (2 horizontal and 2 vertical) are located between quads Q8 and Q10, so that each half cell would have one horizontal and 1 vertical collimator. Each collimator has two jaws and scrapes both sides of the beam. The jaws of each main collimator have an independent control of their angle and position so that they could be aligned along the beam envelope.

#### III.3.5.5 8 GeV Extraction Beam dump/Recycler Switch

The first part of the extraction line mimics the lattice of the RCS with the use of RCS elements. Approximately  $360^\circ$  downstream of the Lambertson a dump switch, producing the same angle as the Lambertson, is used to apply a reverse bend to the trajectory for transport to the Recycler. If this switch magnet is off, the extracted beam travels straight ahead to the RCS extraction dump. A quarter-wave transformer is utilized to create a round diverging beam for the dump. The initial layout transports the beam approximately 16 meters after the dump switch before expanding the beam. The dump absorber is located approximately 20 to 25 meters downstream of the last dump line quad. At this distance the lattice functions are between 100 and 140 meters for each plane. This would produce a spot size on the face of the dump of 40 to 50 mm in diameter. Figure III-46 shows the layout.

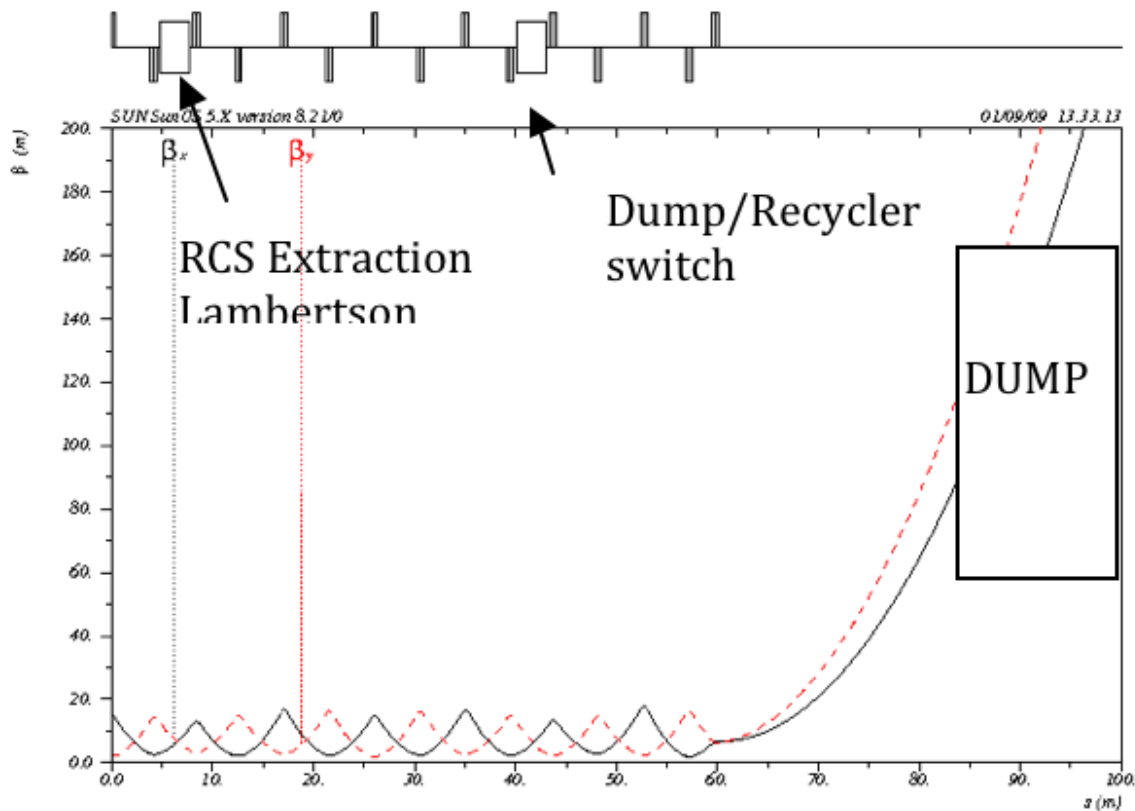


**Figure III-46: Lattice functions in the RCS 8 GeV dump line.**

The expected maximum power of the extracted beam is 340 kW with the RCS accelerating all cycles. This corresponds to accelerating  $5.15 \times 10^{21}$  particles per year. The initial concept was that the dump switch magnet runs DC and acts as a critical device for the Recycler. The current design shows that this dipole should be pulsed with a resonant pulser. This way if the beam permit for the Recycler is removed before the switch magnet is ramped, the waveform can be inhibited. The absorber design should allow for routine 10% beam power with short periods, of 1 hr or so, of full intensity.

### III.3.6 8-GeV transport to Recycler

Due to siting constraints, the present plan calls for utilizing the Recycler 62 straight section to inject 8 GeV protons from the RCS. This straight section in the Recycler is currently used for instrumentation and mimics the design of the MI 62 straight section currently used for 150 GeV antiproton transfers to the Tevatron. When the Collider Run is terminated the transfer line between the Main Injector and Tevatron will be decommissioned and the tunnel between the two enclosures will be available to be used to transport 8 GeV protons from the RCS to the Recycler. The footprint of the transfer line from the Main Injector to the Tevatron enclosure is fixed. However, the challenge will be siting the transport line from F0 to the RCS without interfering with the existing P1 line and not going directly under the F0 building. The P1 line is presently used for the Pbar source, Switchyard and injection to the Tevatron and will not be decommissioned together with the Tevatron collider.

Figure III-47 shows an initial attempt to bring the transfer line into the A1 enclosure. Here the transport line is shown approaching the F0 building just under the north corner of the building with the actual connection to the existing tunnel in a cast-in-place section away from the building itself. Also, this layout keeps the new transport line away from the Tevatron RF and P1 line. Since the transport line has to cross the Tevatron beam line and the P2 line it should not block the tunnel. The elevation of the RCS2RR transport line at this tie-in location is approximately 720'6", which is close to the Recycler elevation and midway between the lower and upper floors in the F0 enclosure. Figure III-48 shows a cartoon of relevant elevations and geometries at the location of the tie-in to the F0 enclosure.

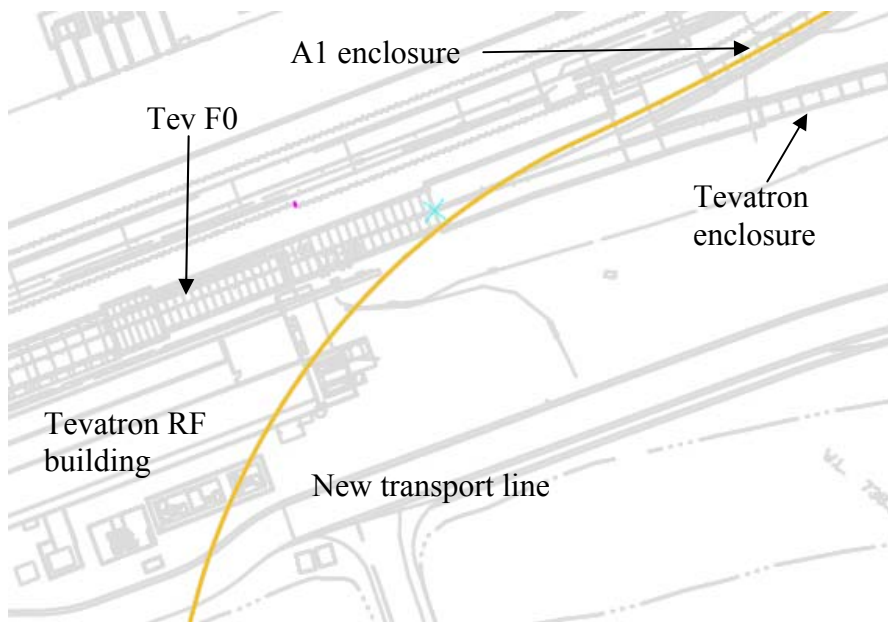


**Figure III-47: Relationship of new transport line to Tevatron RF building, Tevatron enclosure and the existing A1 transport line enclosure.**

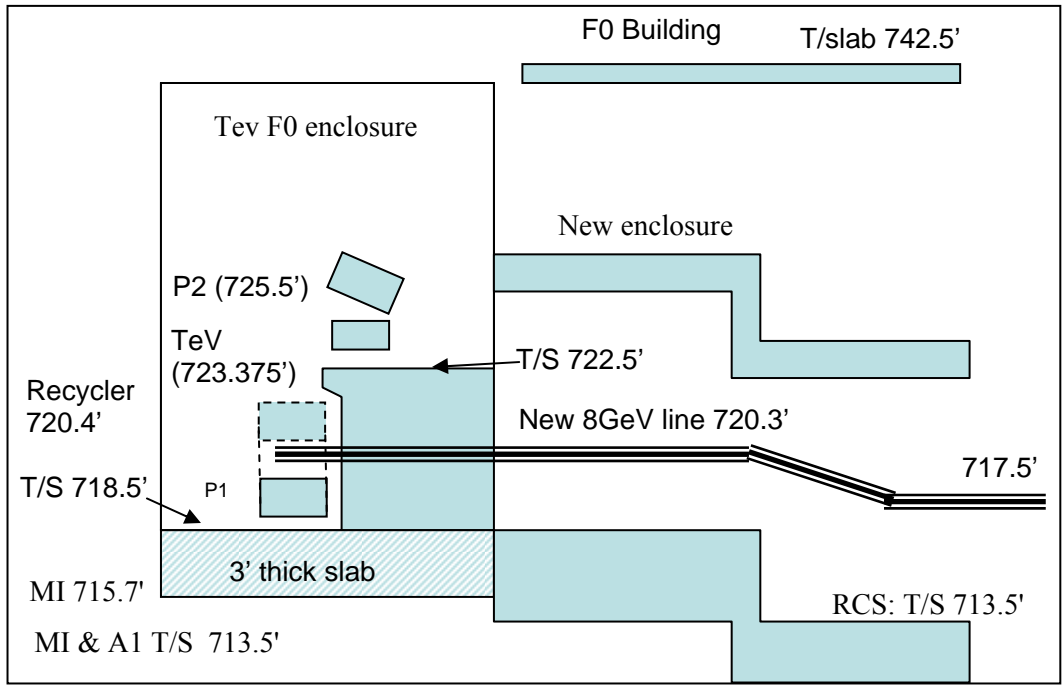


**Figure III-48: Tunnel cross section at the location of the tie-in. Relevant elevations of enclosures, rings, and the proposed new transport line. The location of the elevation change of the transport line is much closer to the RCS and is only shown here to indicate relative elevation changes from the RCS to F0.**

The transport line has a potential of transporting up to 340 kW (as compared to 64 kW for the current Booster to MI transport line). The length of the transport line between the RCS and Recycler is approximately 550 meters, with approximately 150 meters inside existing beam-line enclosure. To maintain proper shielding level, the transport line enclosure remains at the same elevation as the RCS and MI until close to the F0 tie-in. Shielding over the tunnel where it crosses the F0 enclosure should be investigated. Since this line will be transporting protons, the single particle loss mechanisms due to Lorentz stripping or black body radiation are not applicable. The major contributor to single particle loss will be due to interaction with residual gas particles.

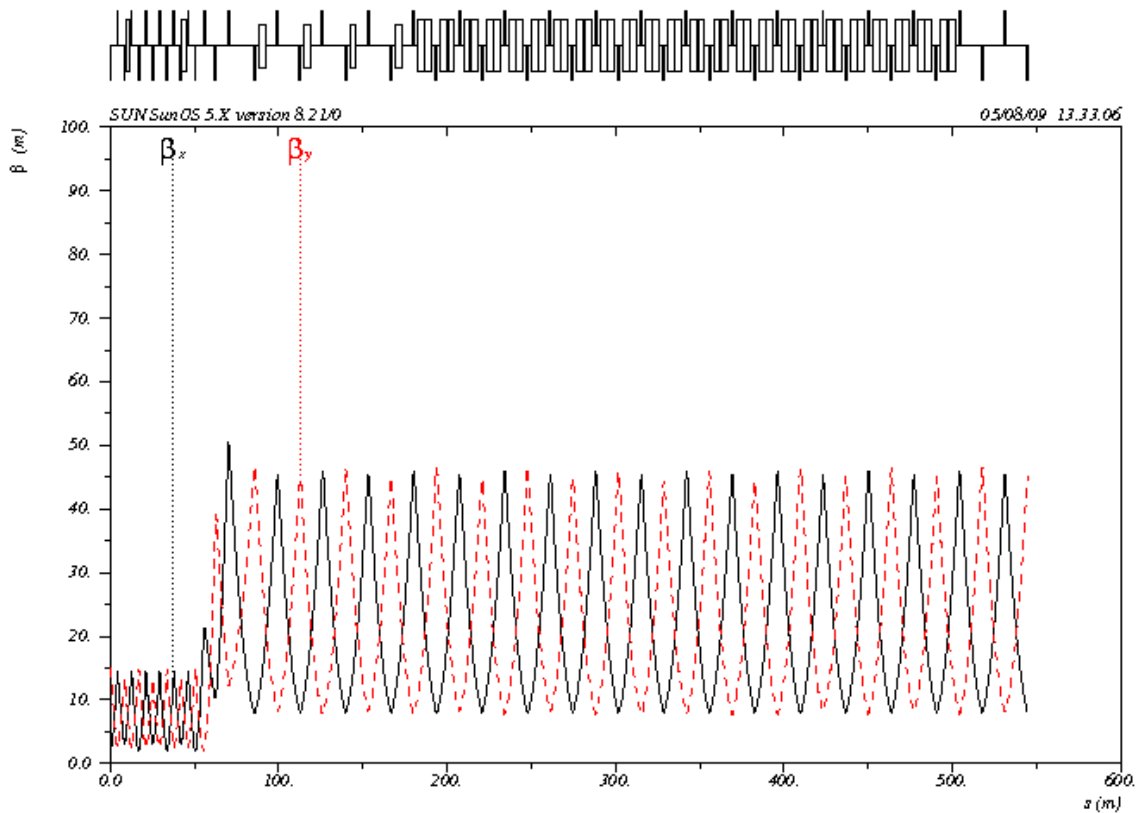
To keep residual activation levels low, a criterion on the uniform loss rate of  $8 \times 10^{-5}$  is suggested (0.05 w/m). To accomplish this level of residual activation, the vacuum level of  $< 10^{-7}$  Torr is sufficient; the transport line should have adequate aperture, and transverse and momentum collimation.

**III.3.6.1 Optics of 8 GeV Transport**

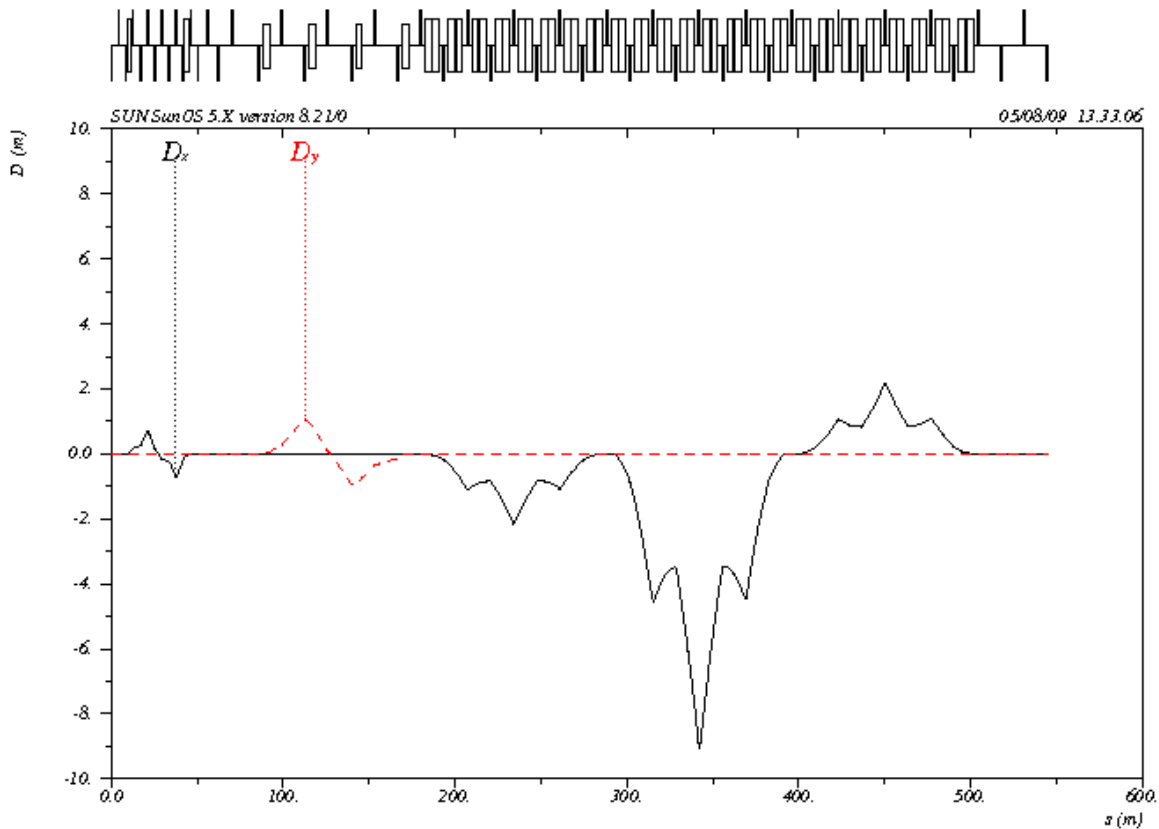
The Recycler is located 60 inches above the MI while in the initial configuration the elevation of the RCS is the same as that of the MI. Therefore the line goes up coming into the F0 building and then stays at the same level up to the Recycler injection. The transport line will be a FODO lattice with achromatic horizontal and vertical bend strings.

Figure III-49 shows the lattice functions for the RCS2RR transport line. The transport line starts with the extraction Lambertson. The RCS FODO lattice is maintained until after the dump

switch. With this dipole activated beam will go to the Recycler, with it off beam goes to the 8 GeV RCS dump. Once the beam passes the dump switch it is matched to a lattice with larger cell length (to reduce number of elements). A vertical achromat brings the transport line to the Recycler elevation. The transport line consists of three horizontal achromats. Since the energy of the Recycler is fixed at 8 GeV kinetic, the magnet design of choice is that of a permanent magnet. To approximate the trajectory of the current A1 line between the MI and Tevatron, a 4 cell, 360° achromat with two 4-meter dipoles at 1.05 kG have been assumed. The number, length, and strength, need further optimization. To create a trajectory that matches into the A1 line enclosure and minimizes interference to F0 (building, enclosure, beam-lines, etc.), an achromat of the same design with a 57° bend angle is used. This achromat uses 16 four meter dipoles with a field of 4.6 kG. Since this field is too strong for permanent magnet technology, this string is to be powered. The number of magnets could be reduced to 8 at 9.2 kG. The large bend creates a horizontal dispersion of ~9 meters. The third achromat (closest to RCS) determines the siting of the RCS inside the Tevatron ring infield and is the first horizontal bend string encountered by the 8 GeV protons from the RCS. The strength of this bend string was chosen to match that of the string in the A1 enclosure to minimize the number of dipole designs.



**Figure III-49: RCS to Recycler transport lattice**



**Figure III-50: Horizontal and vertical dispersion functions showing the three types of achromats.**

Figure III-50 shows the dispersion function of the RCS to Recycler transport line. Although other achromat designs, such as a missing dipole of  $\theta/2$ , have a smaller dispersion, their trajectory goes further under the RF building. The reduced dispersion from 9 to about 6 meters of the other achromat options makes only a small impact on the required horizontal aperture.

Figure III-51 shows the  $6\sigma$  envelope which produces ample aperture for a beam tube of 2" in the vertical and 3" to 4" in the horizontal plane.

Due to the high beam power and potential halo generated in the RCS, the transfer line should provide the transverse and momentum collimations. Neither system has been installed in the lattice. Since the lattice is packed with dipoles, the most logical place to install transverse collimation would be right after the dump switch by extending the length of the RCS cell structure before matching to the longer cells. This can alter the location of the RCS and linac and is left to optimization. The obvious location for the momentum collimation primary is at the peak of the large dispersion. With two dipoles per half cell, there is little room for secondary collimators in the arc, so creating the bend with a single 4 or 5 meter dipole (with dipole fields of 9.2 kG or 7.3 kG, respectively) will provide room for secondary momentum collimator absorbers. Details of these collimators are left for optimization phase.

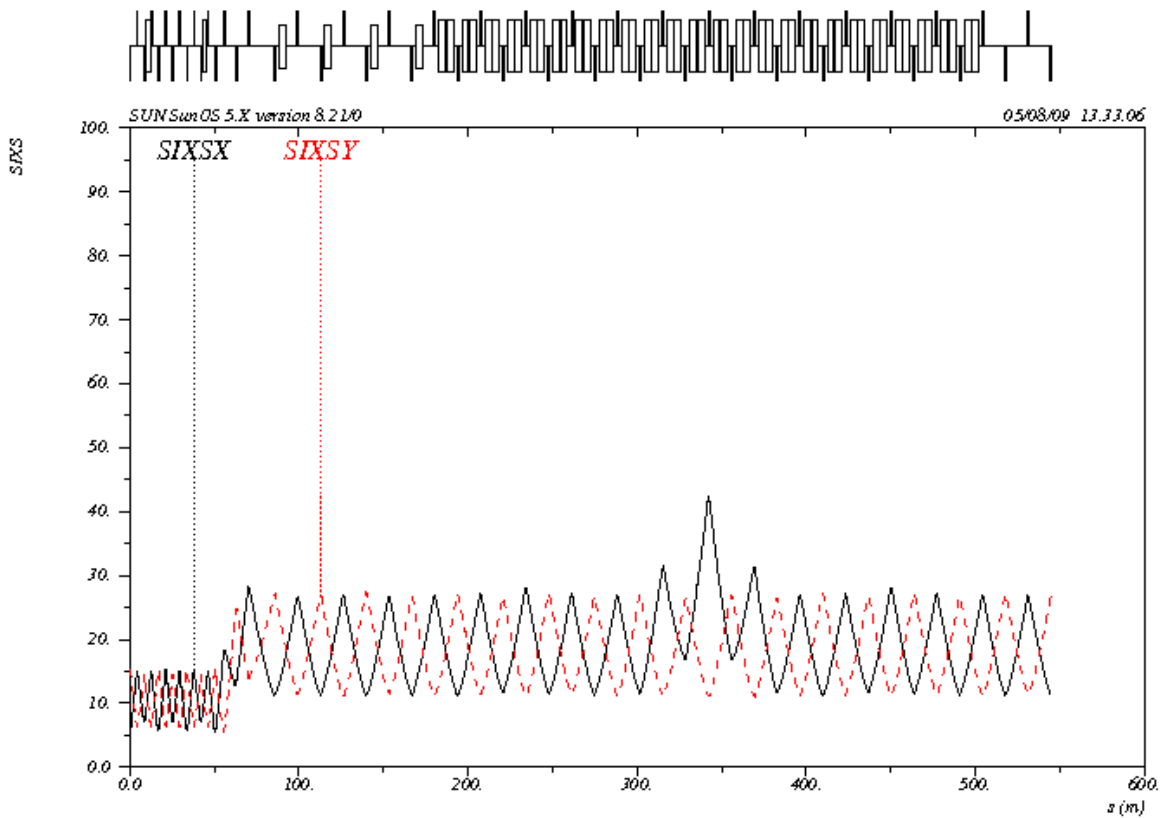


**Figure III-51:  $6\sigma$  beam envelopes in the RCS to Recycler transport line. Assume 95% transverse emittance of  $25 \pi$ -mm-mr and  $\sigma_{p/p}$  of  $3 \times 10^{-4}$  ( $dp/p \sim 1.5 \times 10^{-3}$ ). Recycler matching and injection is not shown.**

All quad locations contain trim dipoles and BPMs for the specific plane. Multiwire profile monitors will be installed at each end of the transport line and in the arc for matching and emittance and momentum spread monitoring.

### III.3.6.2 Recycler Injection

The Recycler injection design will follow the injection design at RR 10 for the Nova Project. This design is documented in Nova doc 1495. It will consist of a horizontal Lambertson with vertical injection kickers, similar to the configuration utilized for 8 GeV proton injection into the Main Injector from the Booster.

Figure III-52 shows the Recycler lattice functions and the location of the Lambertson and kickers.

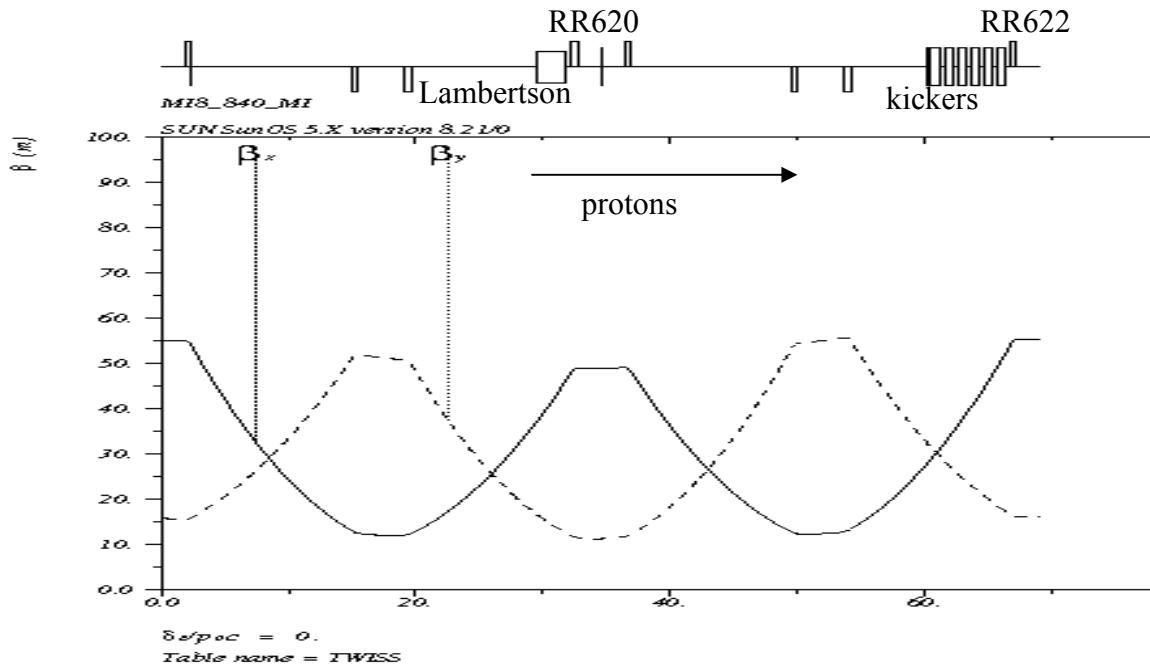


**Figure III-52: Recycler injection layout at RR62.**

The transport line will approach the Recycler at a horizontal angle of 15 to 30 mrad tangentially from the outside and approximately 50 mm below the Recycler. The Lambertson removes the horizontal angle and places the protons on the Recycler horizontal closed orbit, but 50mm below the vertical centerline. The kickers located 90° downstream, remove the vertical offset. This configuration will require replacement of the RR620 quads with RQE style quads with 4.25 inch pole tip diameter to accommodate vertical offset of the injected beam through RRQ620. For a 50 mm vertical offset, the kicker strength needs to be approximately 1.25 mrad. The kickers will operate at 10 Hz and must have a rise time of about 60 ns and a flattop length of approximately 1.85 microseconds. The Lambertson will run DC.

### III.4 Recycler/Main Injector

The Recycler and Main Injector have the same requirements as in ICD-1. The main difference in ICD-2 with the RCS is the injection scheme to the Recycler. In this case we will have a bucket-to-bucket transfer from the RCS to Recycler. In order to minimize the space charge effects especially during transition crossing in Main Injector the longitudinal beam emittance per bunch should be ~0.4 eV-sec. We plan to blow-up the longitudinal emittance in the RCS before injecting in the Recycler. The beam will be injected in a bucket with 800KV of 53 MHz and 20 KV of 106MHz. The second harmonic voltage will be adiabatically raised from 20-400KV improving the bunching factor (Figure III-53 and Figure III-54).

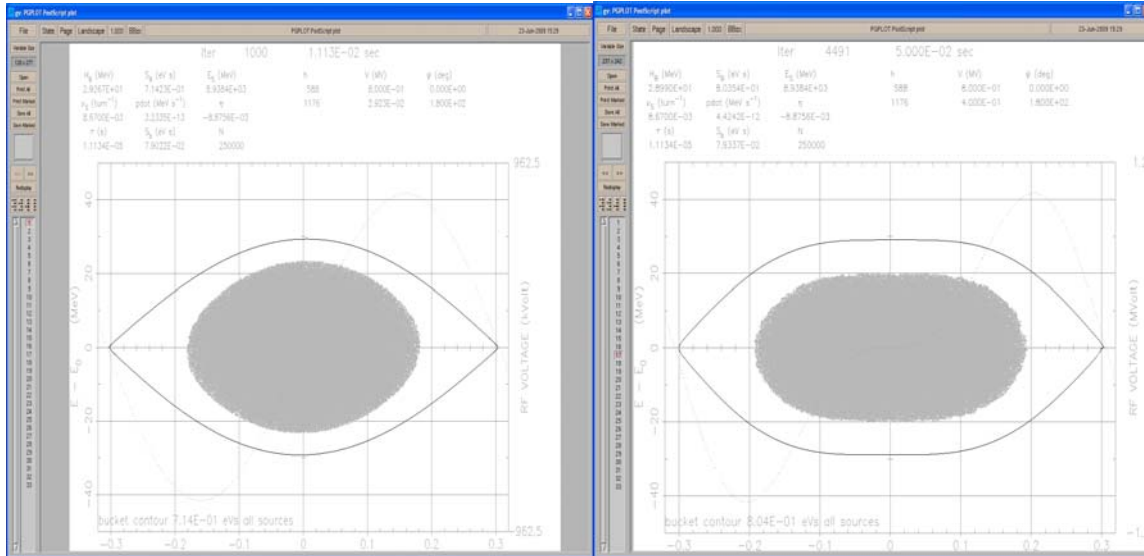


**Figure III-53:** Longitudinal phase space of a 0.4 eV-sec bunch injected in RR from the RCS. On the left is injection in a 53 MHz bucket with 20KV of second harmonic. On the left the change in bunch shape after ramping the second harmonic to 400KV in 50 msec.

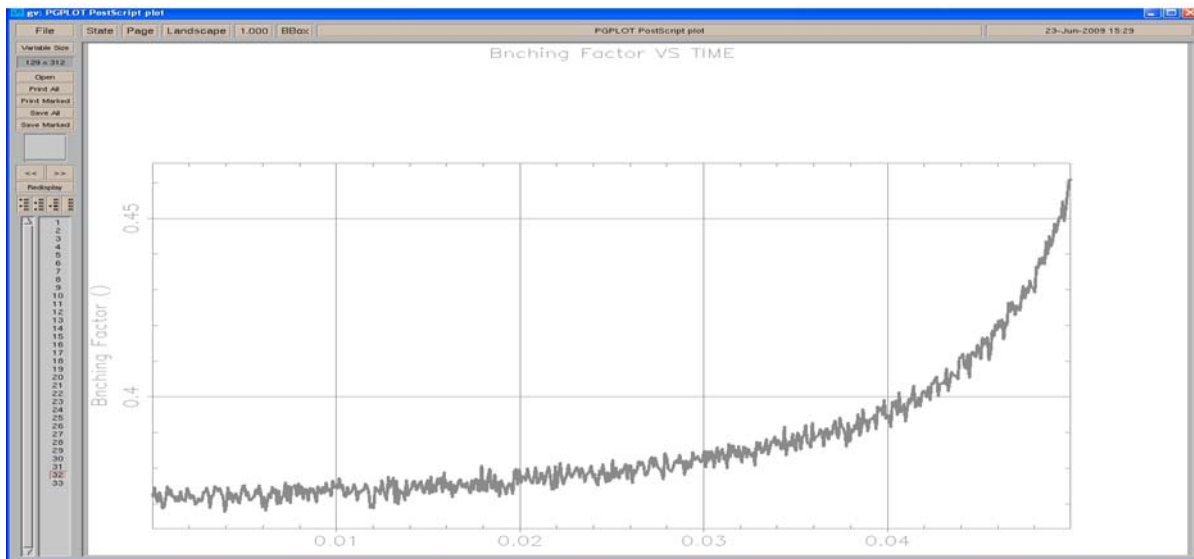


**Figure III-54:** Evolution of the bunching factor during the 50msec ramping of the second harmonic amplitude.

## IV Requirements and Initial Configuration of Major Subsystems

## IV.1 CW Linac

### IV.1.1 RFQ

There is a number of CW RFQs operating at room temperature for beam currents of up to 100 mA and energies of up to ~7 MeV. The LBNL group has conducted preliminary CW RFQ studies based on their experience with the SNS front end system.

The RFQ is an electrostatically focused FDFD strong-focusing lattice with accelerating field ( $E_z$ ) added as a perturbation. The energy bandwidth of the focusing lattice allows unaccelerated beam to be transported to the exit. About 90% of the beam is typically captured and accelerated to full energy. However, there is a low-energy tail that needs to be removed in the MEBT prior to injection into the SRF linac, possibly by a dipole magnet-based energy selector. The output longitudinal beam emittance is somewhat dependent on the beam current and can increase at lower currents. Two RFQs were studied, 162.5 MHz and 325 MHz. The requirements for both were 2.5 MeV, 10 mA beam current, and 0.25 mm-mrad emittance (norm RMS). The design was optimized to meet both beam requirements and thermal management requirements. The thermal management is critical because of high wall power density, which can lead to material stresses and geometric deformations, difficulties with maintaining frequency, and field distribution. It is also important to manage “hot spots” in the RF structure. This can be accomplished by a careful selection of cooling fluid passages configuration.

The RFQs are based on the so-called kick-bunching principle<sup>16</sup>, which has several advantages for the low-current designs. This design approach is used in the IUCF RFQ. Table IV-1 presents several representative RFQs. Two last columns are the proposed RFQ parameters for this concept.

	CRITS	KOMAC	LEDA	IUCF	Proj-X 162	Proj-X 325	
Frequency	267	350	350	213	162.5	325	MHz
Injection Energy	50	50	75	20	35	30	keV
Output Energy	1270	3000	6700	700	2500	2500	keV
Current	86	23	110	1	10	10	mA
Length	147	324	800	118	385	287	cm
Length/Lambda	1.3	3.8	9.3	0.8	2.1	3.1	
Vane-Vane Voltage	78	100	102	35	90.8	64.2	kV
Peak E-field	28.8	33.1	33.6	13.8	20.7	27.6	MV/m
E-field/Kilpatrick	1.75	1.8	1.83	0.91	1.52	1.55	
Cavity Power	159	350*/417	1200	8.4*/12	155*	149*	kW
Power/Length	107	108	150	7.1	40	52	kW/m
Avg Wall Power Density	4.6	13	11.4	0.7	2.1	5.2	W/cm <sup>2</sup>
Max Wall Power Density	116.7		65				W/cm <sup>2</sup>
$r_0$ (transverse vane tip radius)				0.31	0.61	0.31	cm
minimum longitudinal radius				0.52	1.2	0.69	cm
Output rms Momentum Spread					0.15	0.15	percent
Output Longitudinal Emittance		0.246	0.174	0.024	0.056	0.046	MeV-Degree
Output Transverse Emittance		0.023	0.022	0.010	0.031	0.028	cm-mrad
Transmission			90	85	94	90	percent

\*=Calculated

Thanks: Dale Schrage for CRITS, LEDA

**Table IV-1: The RFQ parameters**

Both concepts have similar power requirements; however one clear advantage of the 162.5 MHz RFQ is the lower wall power density and larger transverse acceptance. Coupling RF into

<sup>16</sup> Staples, Linac94

the 325 MHz structure may require iris couplers, which are more difficult to design and to adjust. The 162.5 MHz structure would use loop couplers.

The RF source for a CW RFQ of up to  $\sim 1$  MW power is available at both 162.5 MHz and 325 MHz.

#### IV.1.2 CW linac cavities and cryo-modules

The ICD-2 version of Project X uses the current R&D on both the HINS and ILC programs to provide a basis for the SRF components and cryomodules from 2.5MeV to 2GeV. As specified in Section III.1.3, single spoke resonators with  $\beta_G$  ranging from 0.11 to 0.4 are used to accelerate the beam to 117MeV, and triple spoke resonators with a  $\beta_G$  of 0.6 are used to reach 466 MeV. Above 466 MeV ICD-2 transitions to 1.3GHz, 9-cell cavities with  $\beta_G = 0.81$  to 1.2GeV and  $\beta_G = 1$  to 2GeV (section III.1.4).

In the 325 MHz region, the single spoke accelerating structures used for  $\beta_G = 0.11, 0.22$  and 0.4 are assumed to be closely related to the  $\beta_G = 0.22$  structures fabricated and tested as part of the HINS program and are estimated as such. Though it is noted that the coupler will need to be redesigned for the higher average power in ICD-2, it and the remainder of the components of the cryomodule are estimated as in ICD-1 with the belief that the ICD-1 provides enough of an envelope that the final design can be engineered to that cost. Development of the new coupler will be covered by the Project X RD&D plan.

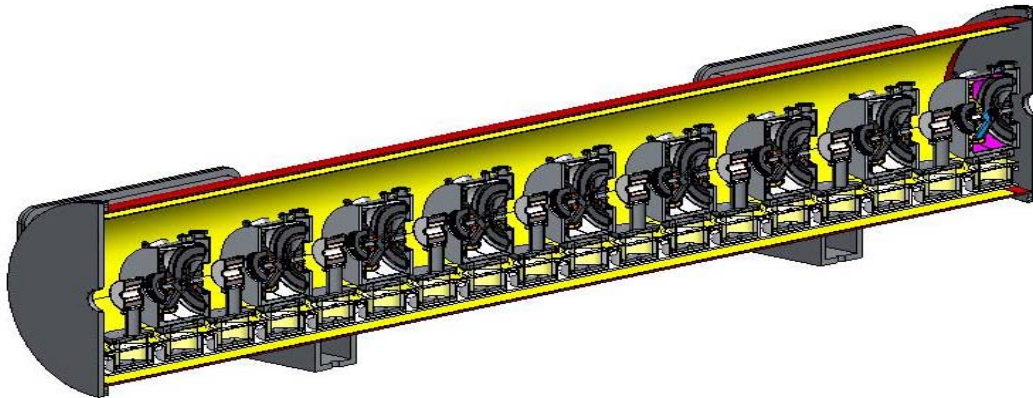


**Figure IV-1: 325 MHz Cryomodule**

For the  $\beta_G = 0.6$  section, the triple spoke resonators have been designed, but there are currently no concrete plans to develop and test prototypes though several expressions of interest have been received from collaborating laboratories. Currently within ICD-2 the TSR structures and all associated cryomodules are estimated by scaling from the SSR-1 experience.

Aside from the structures themselves, several collaborators have expressed interest in assisting with the 325 MHz cryomodule design, and potential alternative accelerating structures. These alternatives will be explored during the R&D phase.

For the 1.3GHz system, the cavities and cryomodules, as in ICD-1, follow closely the development work already underway for the ILC Type IV cryomodules. For the  $\beta_G = 1$  section, the cavities remain the standard ILC 9 cell design. The coupler will be redesigned for the higher average power, and the cryomodule modified to accommodate magnets at slots 2, 5 or 8 depending on need. This modification is a duplication of the port that currently exists at point 5 at the other points, and with the use of the ILC EDMS system not a major design challenge. The required coupler redesign will use the envelope of the current ILC coupler and not require major modifications to the other components in the cryomodule.

For the  $\beta_G = 0.81$  cavities, ICD-2 extends the compatibility by using the same cavity slot length as in the  $\beta_G = 1$  cryomodule. This may result in an 11-cell cavity design, for instance, or a cavity design with slightly longer than optimal ends; however, the cryomodules will be completely interchangeable along the 1.3 GHz section in this case, simplifying design and integration of the system as a whole.



**Figure IV-2: 1.3 GHz Cryomodule.**

#### IV.1.3 RF power

The ICD-2 version of Project X includes a continuous wave (CW) 2 GeV Linac, which consists of an RFQ front end followed by Superconducting RF (SRF) cavities of six varieties. At 325 MHz there are Single Spoke Resonators of three beam betas = 0.117, 0.22, 0.4 (SSR0, SSR1, SSR2). Also at 325 MHz Triple Spoke Resonators (TSR) have a beta = 0.6. A transition at 466 MeV to 1300MHz with two species of SRF cavities with betas = 0.81 and 1.0 a “squeezed” version of ILC cavities and ILC design (SILC and ILC). In all SRF systems, a circulator will be used to isolate the cavity from the power amplifier (PA). A block diagram of the RF systems has been created<sup>17</sup>. Low Level RF (LLRF) will be covered separately.

<sup>17</sup> <http://ProjectX-docdb.fnal.gov:8080/cgi-bin/ShowDocument?docid=274>

A klystron capable of 500 kW to 1 MW will be necessary to drive the RFQ at 325 MHz. Klystrons close to this frequency and at these power levels operate CW at the APS at Argonne National Lab.

Each of the cavities in the CW Linac will be powered by an independent RF system similar to what was done at SNS in Oakridge, TN. Power levels vary from a few hundred watts to 30 kW. Pricing of the RF systems was done by obtaining quotes from vendors with standard catalog items meeting the project specifications. Solid-state amplifiers have been chosen for power levels below 1 kW tetrode amplifiers for power levels between 1-5 kW and inductive output tube amplifiers (IOT) for higher power levels.

The SSR0 systems will have a 1 kW solid-state amplifier as the final PA. SSR1 and SSR2 will utilize a 5 kW tetrode amplifier at 325 MHz. For the TSR cavities at 325 MHz, a 30 kW IOT is the preferred amplifier. IOTs have efficiencies approaching 60% and excellent saturation characteristics. Unfortunately, IOTs have inherent low gain and require a drive amplifier capable of several hundred watts. It has been decided to utilize a 200 W solid-state amplifier.

For the 1300 MHz systems, IOTs are the desired choice due to efficiency (klystrons have continuous power consumption in the absence of RF drive). CPI has a catalog 30 kW CW 1300 MHz IOT. L3 and Thales have been contacted and currently make a 20 kW IOT at 1300 MHz, and both companies have submitted a preliminary bid for 30 kW units.

## **IV.2 Collimators and Beam Dump**

### **IV.2.1 Collimators**

There are a large number of beam collimators and beam dumps in the ICD-2 complex. The beam collimation starts at the LEPT, continues in MEPT, where the beam chopper is located, a few collimators will be placed in the linac, and finally they will be located in the RCS and all transport lines (linac-to-RCS, linac-to-experiments, RCS-to-Recycler.) There are also three beam dumps: the linac beam dump, the RCS injection beam dump, and the RCS beam dump. The closest existing collimation systems are those of SNS and JPARC. JPARC has a 3-GeV proton ring to operate at 0.6 MW. It has two primary (1-mm tungsten foils) and seven massive secondary collimators (iron).

The RCS injection beam dump has “not-quite standard” design and therefore it is the only beam dump described in this document in any details. There is a comparatively straightforward approach to the design of other beam collimators and beam dumps, based on the existing units already operating in the Fermilab accelerator complex. The design is based on iron and/or tungsten jaws that encounter the beam first. The radiation shielding is done with thick radial and axial outer iron plates, surrounded by marble and/or concrete. Cooling is performed with borated water (2000 parts of  $^{10}\text{B}$  per  $10^6$ ) that removes several tens of kW. Table IV-2 lists requirements for high energy collimators, absorbers and beam dumps.

### **IV.2.2 RCS Injection beam absorber**

Energy deposition calculations for the ICD-2 injection absorber were performed with the MARS code. The absorber is designed to localize the beam loss at injection and meet the requirements of the Fermilab Radiological Control Manual (FRCM). The following issues were addressed: (i) surface water activation; (ii) residual activation; (iii) survival of the magnets around the absorber; (iv) cooling. Current design of the absorber with an inner radiation trap is shown in Figure IV-3. The beam intensity is  $2.67 \times 10^{13}$  2-GeV proton/pulse at the repetition rate

of 10 Hz, which corresponds to the beam power of 85 kW. It is assumed that 4% of the beam is deposited in the absorber. The beam pipe radius is equal to 4 cm.

**Table IV-2: Collimators, Absorbers, and Beam Dumps**

Energy [GeV]	Function	Species	Beam fraction [%]	Beam Power [kW]	Survive (peak)
2	Linac Dump	H <sup>-</sup> , H <sup>+</sup>	10	200	Full int. 1 hr
2	Trans. collimation	H <sup>-</sup>	5	4.25	2 pulses full int.
2	Mom collimation	H <sup>-</sup>	5	4.25	2 pulses full int.
2	Ring collimation	H <sup>+</sup>	10	8	
2	Injection Absorber	H <sup>-</sup>	10	8.5	Full int 10 pulses
8	Extraction Dump	H <sup>+</sup>	10	34	Full int. 1 hr
8	Trans collimation	H <sup>+</sup>	5	17	2 pulses full int.
8	Mom collimation	H <sup>+</sup>	5	17	2 pulses full int.

According to the Fermilab Concentration Model, activation of the surface water for the given beam intensity reaches its permitted maximum approximately every 6 months, so that the collected water must be replaced twice a year. Calculated residual dose around the absorber is shown in Figure IV-4. There are a couple of hot spots on the tunnel wall and side surface of the quadrupole with residual dose about 200 and 700 mRem/hr, respectively, while typical requirement for hands-on maintenance is 100 mRem/hr. The issue can be resolved by means of extra marble shielding layers. Power density was calculated for the coils of the 1<sup>st</sup> magnet both upstream and downstream of the absorber. The power density in the 1<sup>st</sup> magnet upstream is pretty low, so that it can survive for about 100 years. The 1<sup>st</sup> quadrupole downstream of the absorber can survive for about 8 years. In the estimate it is assumed that, according to empirical observations, lifetime of a magnet depends on lifetime of epoxy used in its coils and the latter corresponds to absorbed dose of 400 Mrad.

Finally, passive cooling of the absorber with airflow appears to be adequate. Using the passive cooling rate of about  $10^{-3}$  W/(cm<sup>2</sup> K) and the outer surface of the absorber of  $2.2 \times 10^5$  cm<sup>2</sup>, one can see that the absorber's temperature will exceed temperature of the surroundings by approximately 10 K.

The length of the absorber is determined mostly by the requirement to keep the absorbed dose in the coils of the 1<sup>st</sup> quadrupole downstream of the absorber at an acceptable level. Transverse dimensions depend mostly on residual activation and surface water activation. The total weight of the absorber is about 58 tons including 32 tons of iron, 20 tons of concrete and 5.6 tons of marble. Further optimization of the design can be performed.

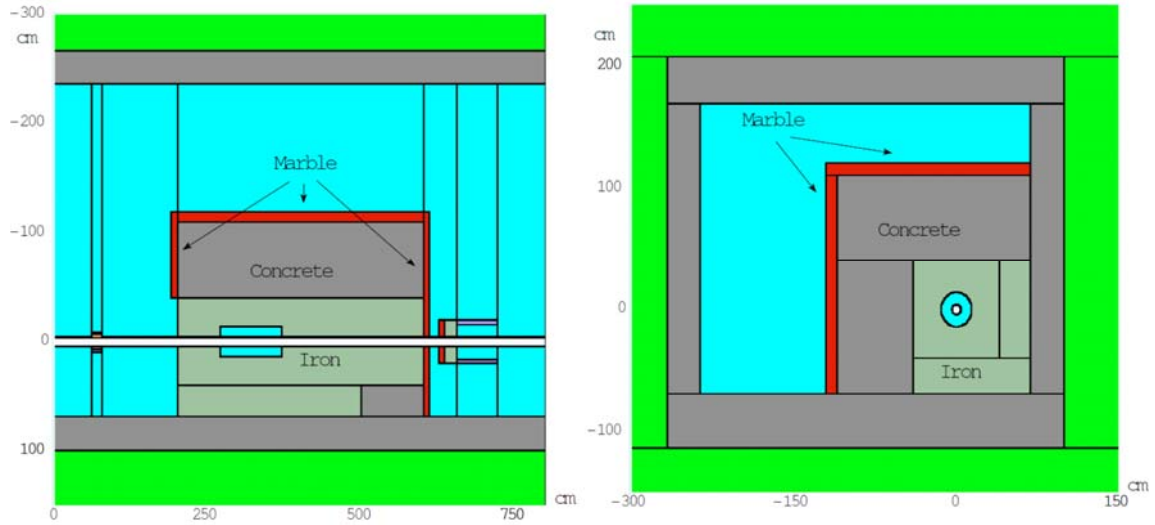


**Figure IV-3: Plan view (left) and cross section (right) of the injection absorber in the tunnel. The following color coding is employed: white, blue, green, light gray, dark gray, red and violet correspond to vacuum, air, soil, iron, concrete, marble and yoke, respectively.**

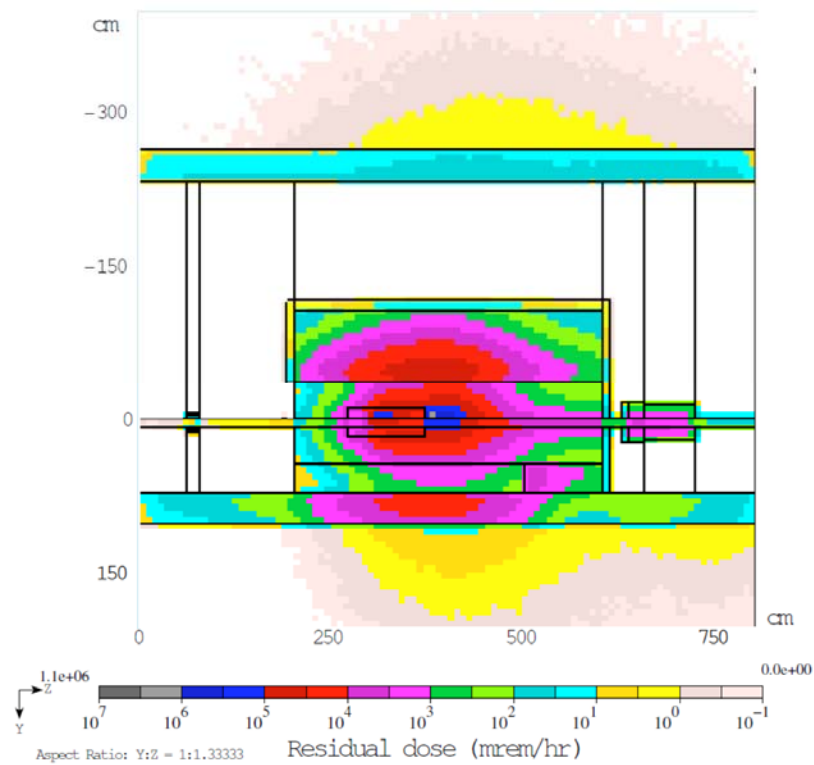


**Figure IV-4: Calculated residual dose distribution (plan view) around the injection absorber for standard irradiation conditions: 30-day irradiation followed by a 1-day cooling.**

## IV.3 Rapid Cycling Synchrotron

### IV.3.1 Magnets

In previous studies<sup>18,19</sup> of 16 GeV and 8 GeV Booster Synchrotrons, the magnets had large good field areas: 127 mm x 228.6 mm in Study I, and 101.6 mm x 152.5 mm in Study II. In the ICD-2 the beam aperture is substantially reduced to 40 mm diameter, which leads to smaller magnets, lower stored energy, and lower operational expenses.

The RCS optics is based on a separated function lattice and magnets with 100 ring dipoles and 132 quadrupoles connected in series and powered by a resonant power supply (see Section IV.3.3). Magnet yokes are laminated and made from M17 coated low carbon steel.

#### IV.3.1.1 Ring Dipoles

The RCS dipole is an iron dominated magnet and has a conventional H-magnet design. A proper pole tip shimming with minimization of pole tip width and peak field optimizes field homogeneity. The magnet cross-section is shown in Figure IV-5 and parameters in Table IV-3.

#### IV.3.1.1 Ring Quadrupoles

The RCS quadrupole magnet parameters are shown in Table IV-4 and its cross-section is shown in Figure IV-6. The quadrupole integrated strength will be corrected  $\pm 2.6\%$  ( $\pm 0.3$  T) by a shunting power supply or an additional trim winding wound over main coils or trim quads.

#### IV.3.1.2 Multipole Correctors

Multipole correctors have vertical or horizontal dipole, and sextupole windings. Corrector parameters are shown in Table IV-5. The magnet design and fabrication technology is similar to new Booster correctors<sup>20,21</sup> which are in an operation now. The number of poles is reduced from 12 to 6, which is enough for the combined dipole and sextupole correctors. In this case the horizontal corrector (vertical field) and vertical corrector (horizontal field) have different winding configurations to explore the six pole yoke geometry. The quadrupole correction combined with the main quadrupole by using trim coils or shunting power supplies. The corrector magnet has two modifications: horizontal corrector with sextupole and vertical corrector with sextupole. The quantity and corrector positions in lattice is described in Section III.3.

Correctors have laminated yokes that are split in the vertical direction and have indirect water cooling. Laminations are coated to reduce the eddy current effects and provide proper half yokes curing. Coils could be randomly wound into slots between poles around the yoke. Finally the magnet is assembled from two sets into a single solid package impregnated with epoxy.

---

<sup>18</sup> The Proton Driver Design Study, Fermilab-TM-2136, December 2000.

<sup>19</sup> Proton Driver Study II, Part 1, Fermilab-TM-2169, May 2002.

<sup>20</sup> V.S. Kashikhin, *et al.*, "A New Correction Magnet Package for the Fermilab Booster Synchrotron," PAC05, May 2005.

<sup>21</sup> E.J. Prebys, *et al.*, "New Corrector System for the Fermilab Booster", PAC07, 2007.

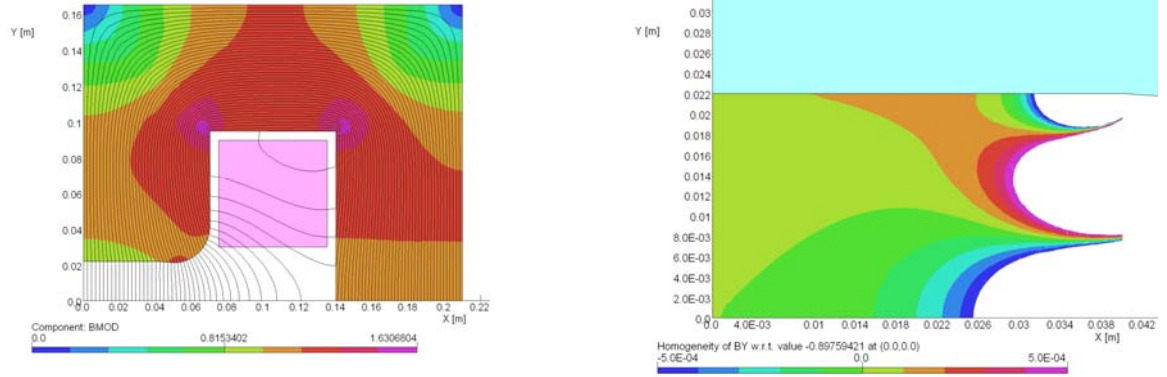


**Figure IV-5: Dipole magnet geometry with flux lines and flux density at 667 A current (left) and field homogeneity in range of  $\pm 5$  units for the magnet aperture (right).**

**Table IV-3: Parameters of dipoles**

Parameter	Unit	Value
Number of magnets		100
Peak field	T	0.87375
Field at injection	T	0.2184
Magnet gap	mm	44
Good field area diameter	mm	40
Field homogeneity		0.02 %
Effective length	m	2.13216
Peak current	A	667 A
Current form		Shifted up sine wave
Current frequency	Hz	10
Duty factor	%	100
Number of turns/pole		24
Copper conductor	mm x mm	12.5 x 12.5
Conductor cooling hole diameter	mm	7
Number of pancake coils/pole		2
Lamination material		M17
Lamination thickness	mm	0.35
Inductance	H	0.025
DC resistance	Ohm	0.021
Stored energy	kJ	5.47
Power losses RMS (without eddy currents)	kW	4.3
Peak inductive voltage	V	390
Number of cooling circuits/magnet		1
Water pressure drop	MPa	0.5
Water flow	l/min	2.8
Water temperature rise	C°	22

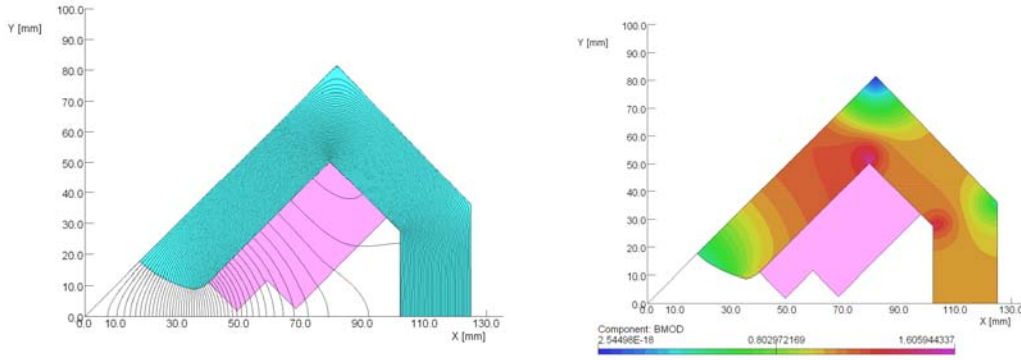


**Figure IV-6: Quadrupole geometry, flux lines (left), and the yoke flux density(right) at 672 A current.**

**Table IV-4: Parameters of quadrupoles**

Parameter	Unit	Value
Peak field gradient	T/m	17.43
Field gradient at injection	T/m	5.47
Pole tip radius	mm	25
Good field area diameter	mm	40
Field nonlinearity (2D)		0.03 %
Effective length	m	0.612
Peak current	A	672 A
Current form		Shifted up sine wave
Current frequency	Hz	10
Duty factor	%	100
Number of turns/pole		7
Copper conductor	mm x mm	10 x 10
Conductor cooling hole diameter	mm	5
Number of coils/pole		1
Lamination material		M17
Lamination thickness	mm	0.35
Inductance	mH	1.15
DC resistance	Ohm	0.012
Stored energy	J	260
Power losses RMS (without eddy currents))	kW	2.0
Peak voltage	V	40
Number of cooling circuits/magnet		1
Water pressure drop	Mpa	0.5
Water flow	l/min	1.9
Water temperature rise	C°	16

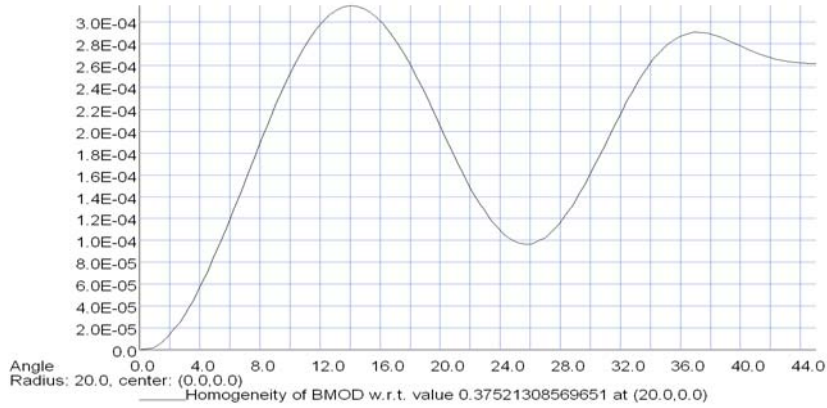


**Figure IV-7: Quadrupole field homogeneity at radius 20 mm and 672 A current.**

**Table IV-5: Parameters of trim magnets**

Parameter	Unit	Vertical (normal) dipole field	Horizontal (skew) dipole field	Sextupole (normal)
Number of magnets		66	66	132
Peak dipole field	T	0.047	0.054	
Peak sextupole gradient	T/m <sup>2</sup>			200
Magnet aperture diameter	mm	44	44	44
Effective length	m	0.2	0.2	0.2
Peak current	A	10	10	10
Current form		Shifted up sine wave	Shifted up sine wave	Shifted up sine wave
Current frequency	Hz	10	10	10
Duty factor	%	100	100	100
Number of turns/pole		90	90	50
Copper conductor area	mm <sup>2</sup>	3	3	3
Lamination material		M17	M17	M17
Lamination thickness	mm	0.35	0.35	0.35
Inductance	H	0.03	0.03	0.018
DC resistance	Ohm	1.2	1.2	1.0
Stored energy	J	1.5	1.5	0.9
Power losses RMS	W	60	60	50
Peak inductive voltage	V	20	20	12
Water cooling		indirect	indirect	Indirect

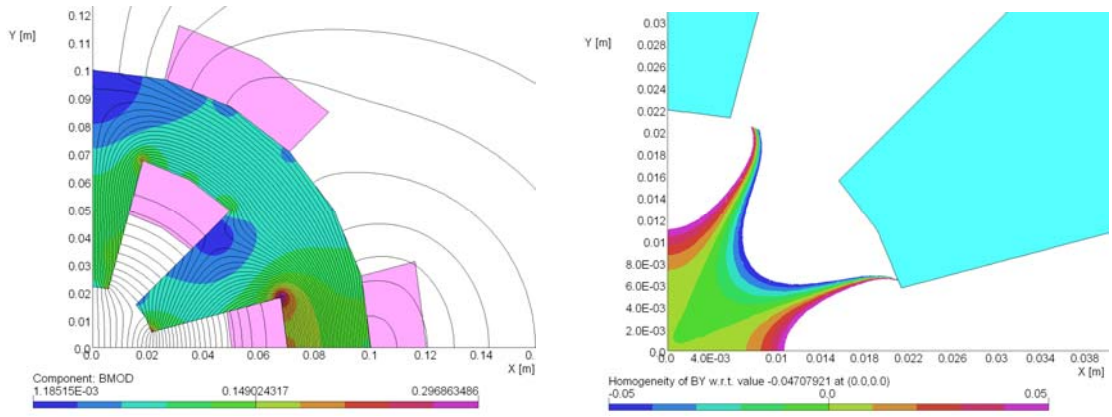


**Figure IV-8: Horizontal dipole corrector field (left) and field homogeneity  $\pm 5\%$  (right).**

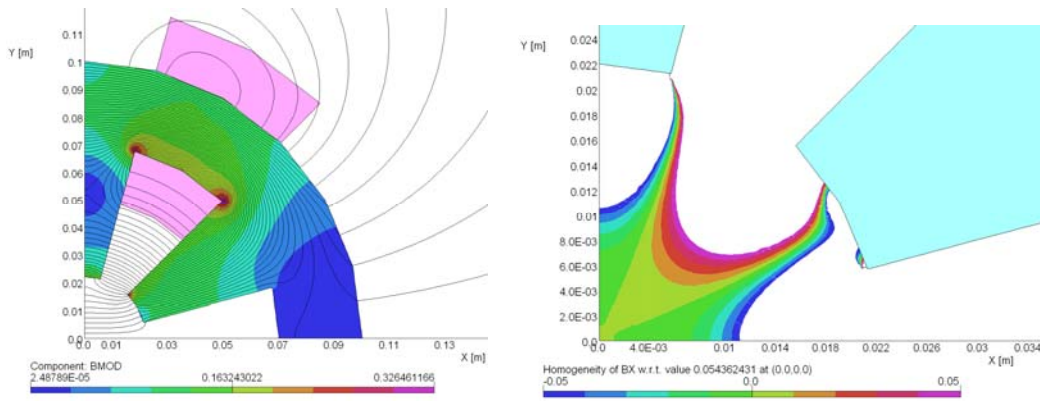


**Figure IV-9: Vertical dipole corrector field (left) and field homogeneity  $\pm 5\%$  (right).**

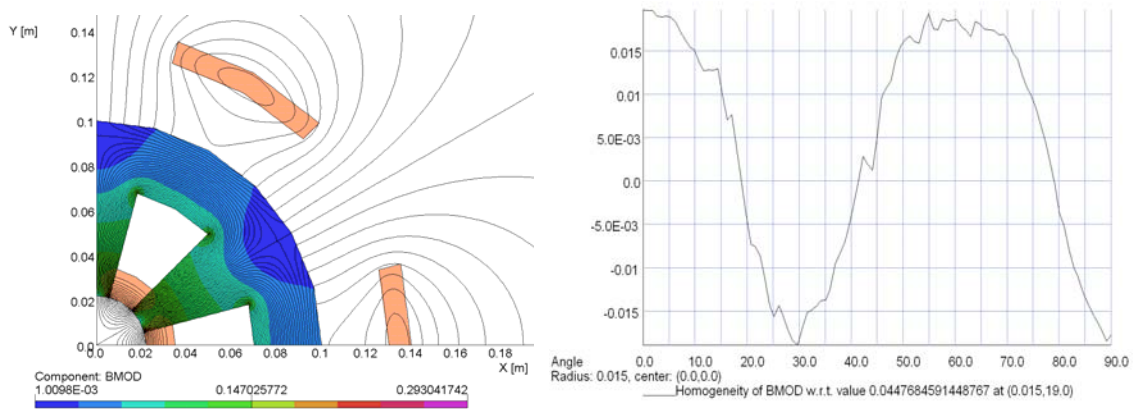


**Figure IV-10: Sextupole corrector field (left) and field homogeneity  $\pm 2\%$  at radius 15mm (right).**

## IV.3.2 RF System for Rapid Cycling Synchrotron RF

### IV.3.2.1 Fundamental harmonic cavities

The fundamental RF system is a completely new system with RF drive controls similar to that of the present Main Injector RF system. The philosophy of the baseline design is based on handling a high beam current under conservative assumptions about beam stability and feedback requirements.

**Table IV-6: Main Beam and Fundamental RF System Parameters**

Beam Current @ injection	2.2	Amps
Repetition rate	10	Hz
Acceleration Ramp Slope	165	GeV/s
Frequency Min	50.33	MHz
Frequency Max	52.81	MHz
Frequency sweep	2.5	MHz
Number of First Harmonic RF stations (h=98)	16	Stations
Peak accelerating voltage	1.6	MV
Cavity peak voltage	100	kV / cavity
Peak Power Dissipation Cavity	50	kW /cavity
Peak Power: beam + cavity	1.5	MW
Peak Power per cavity: beam + cavity	93.75	kW / cavity
Cavity Rs	100	k $\Omega$
Cavity Q	~2857	
Cavity Rs/Q	~35	
Cavity Tuner Geometry		Perpendicular Biased

#### ***IV.3.2.1.1 New Cavity Design for Rapid Cycling Synchrotron***

The cavity reference design is shown in Figure IV-11. It is based on the SSC Low Energy Booster cavities that were quarter wave cavities with low R/Q to reduce the effects of beam loading. Providing adequate cooling to the garnets will be the major engineering challenge in this design. Each cavity is ~ 1.25 meters in length. The total length required for the 16 fundamental frequency cavities is ~ 20 meters.

#### ***IV.3.2.1.2 Modulator Requirements***

Each RF station would require a modulator that would be identical to those presently used in the Main Injector (see Figure IV-12). They will provide efficient power amplifier plate voltage control along with protection and isolation for connecting multiple stations to a common anode power supply. The modulators would be located in the surface building's RF equipment gallery. Dimensions of the modulator are 36 inches wide by 60 inches deep and 84 inches high.

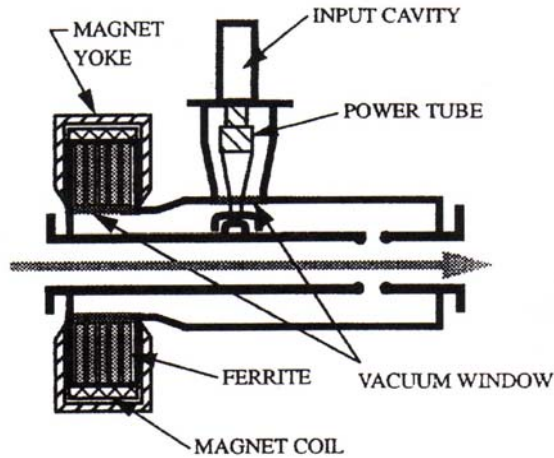


**Figure IV-11: LEB Prototype cavity**



**Figure IV-12: MI modulator racks**

#### ***IV.3.2.1.3 Ferrite Tuner Bias Power Supplies Requirements***

The ferrite bias supply must be a fast slewing high current power supply with active filter for good regulation to achieve accurate control of cavity tuning. These supplies could be similar to the present Booster ferrite bias supplies but with the capability of higher output voltage. The present Booster supplies operate from the 480 V pulsed power feeder and can slew 150,000 amps per second (0 to 2500 amps).

#### ***IV.3.2.1.4 Power Amplifier Requirements***

The power amplifier will be a modified version of our standard MI 150 kW amplifier. It will be cathode driven from the solid state driver amplifier located in the surface building, with grid grounded for RF, but biased to allow dynamic programming through the cycle. This amplifier will have power supplies (grid, screen, plate, & filament) located upstairs in the equipment gallery and multiple “Heliac” cables will carry the voltages from the remote power supplies to the tunnel.

#### ***IV.3.2.1.5 SS Driver requirements:***

This will be a broadband solid state driver amplifier identical to those used in the Main Injector’s RF system. These are housed in a standard relay rack and over the years have a proven track record for being highly reliable. These would be the 8 kW driver versions that are now used for all MI RF stations. The solid state drivers would be located in the surface building’s RF equipment gallery.

#### ***IV.3.2.1.6 Anode Supply requirements:***

Two large anode supplies will be required to power the fundamental RF system. It will be divided into two groups of 8 stations. The supplies will be very similar to the existing MI-60 anode supplies presently power the MI RF system. Each supply will consist of a fused disconnect to the 13.8 kV line, a fast step start vacuum circuit breaker, 2 MW main rectifying transformer, rectifier stack, interphase reactor, capacitor bank, crowbar, and individual DC vacuum switches connecting each modulator to the anode supplies DC bus (8 station per supply).

#### ***IV.3.2.1.7 RF Controls requirements:***

Much of the RF controls would be very similar to that of the MI 53MHz RF system. This would include; cavity tuning controller, possible direct RF feedback controller, etc. A similar form of direct RF feedback could be employed as it is in the present MI system along with transient beam loading (feed forward).

### **IV.3.2.2 Second Harmonic Cavities**

#### ***IV.3.2.2.1 Second Harmonic Cavity Design for Rapid Cycling Synchrotron***

This cavity design would be similar to the fundamental frequency cavities including the use of perpendicular biased tuner arrangement. Each cavity is ~ 1.0 meters in length. The total length required for the 10 second harmonic frequency cavities is ~ 10 meters.

**Table IV-7: Main Parameters of Second Harmonic RF System**

Frequency Min	100.66	MHz
Frequency Max	105.62	MHz
Frequency sweep	5.0	MHz
Number of second Harmonic RF stations (h=196)	10	Stations
Peak accelerating voltage	0.7	MV
Cavity peak voltage	70	kV / cavity
Peak Power Dissipation Cavity	24.5	kW /cavity
Peak Power: beam + cavity	0.43	MW
Peak Power per cavity: beam + cavity	43	kW / cavity
Cavity Rs	100	k $\Omega$
Cavity Q	2850	
Cavity Rs/Q	~35	
Cavity Tuner Geometry		Perpendicular Biased

#### ***IV.3.2.2.2 Modulator Requirements***

Each RF station would require a modulator that would be identical to those presently used in the Main Injector. They will provide efficient power amplifier plate voltage control along with protection and isolation for connecting multiple stations to a common anode power supply. The modulators would be located in the surface building's RF equipment gallery.

#### ***IV.3.2.2.3 Ferrite Tuner Bias Power Supplies Requirements***

The ferrite bias supply must be a fast slewing high current power supply with active filter for good regulation to achieve good control of cavity tuning. These supplies could be similar to the present Booster ferrite bias supplies with the capability of higher output voltage. The present Booster supplies operate from the 480 V pulsed power feeder and can slew 150,000 amps per second (0 to 2500 amps).

#### ***IV.3.2.2.4 Power Amplifier Requirements:***

The power amplifier will be a modified version of our standard MI 150 kW amplifier. It will be cathode driven from the solid state driver amplifier located in the surface building, with grid grounded for rf, but biased to allow dynamic programming through the cycle. The operating frequency is near the upper limit for this tube and further measurements would have to be done to validate the tube operating at high power level under these conditions. This amplifier will have power supplies (grid, screen, plate, & filament) located upstairs in the equipment gallery and multiple "Helix" cables will carry the voltages from the remote power supplies to the tunnel.

#### ***IV.3.2.2.5 SS Driver requirements:***

This will be a broadband solid-state driver amplifier but different from our standard amplifiers (due to operating frequency band) and probably could be bought commercially for this project. The solid-state drivers would be located in the surface building's RF equipment gallery.

**IV.3.2.2.6 Anode Supply requirements:**

One large anode supply will be required to power the second harmonic RF system. The supply will be very similar to the existing MI-60 anode supplies presently power the MI RF system. The supply will consist of a fused disconnect to the 13.8KV AC line, a fast step start vacuum circuit breaker, 2MW main rectifying transformer, rectifier stack, interphase reactor, capacitor bank, crowbar, and individual dc vacuum switches connecting each modulator to the anode supplies DC bus (10 stations).

**IV.3.2.2.7 RF Controls requirements:**

Much of the RF controls would be very similar to that of the MI’s 53MHz RF system. This would include; cavity tuning controller, possible direct RF feedback controller, etc. A similar form of direct RF feedback could be employed as it is in the present Main Injector’s system along with transient beam loading (feed forward).

**IV.3.2.3 LCW Requirements:**

<b>95 degree LCW</b>		<b>Per Station LCW Requirements</b>	<b>Total LCW RF System Requirements</b>
<b>Fundamental</b>			
16	Ferrite Bias Supply	15 gpm	240 gpm
16	Series Tube Modulator	25 gpm	400 gpm
16	Power Amplifier # 1	30 gpm	480 gpm
16	SS Driver Amplifier	13 gpm	208 gpm
2	Anode Supplies	25 gpm	50 gpm
16	RF Cavity	30 gpm	480 gpm
	<b>Total</b>		<b>1858 gpm</b>
<b>Second Harmonic</b>			
7	Ferrite Bias Supply	15 gpm	105gpm
7	Series Tube Modulator	25 gpm	175gpm
7	Power Amplifier #2	30 gpm	210gpm
7	SS Driver Amplifier	13 gpm	91gpm
1	Anode Supplies	25 gpm	25gpm
7	RF Cavity	30 gpm	210gpm
	<b>Total</b>		<b>816 gpm</b>

**IV.3.2.4 AC Power Requirements:**

13.8 KV		Total
3 Anode Power Supplies	2 MW	6 MW
2 Pulse Power 480:120 Transformers	1.5MW	3MW
2 Conventional 480:120 Transformers	1.0MW	2MW

### IV.3.3 Power supplies

#### IV.3.3.1 Power supplies and resonant excitation of the dipoles and quads

The RCS power supply consists of the power supplies and the capacitors and inductors necessary to resonantly excite the main dipole and quadrupole magnets. A resonant system, similar to Fermilab's Booster, is used to reduce the cost of the power components that would be necessary in order to ramp the magnets at the high  $dI/dt$  required for 10 Hz operation.

The magnets are divided into 50 independent cells each tuned to 10 Hz. All the cells would be connected electrically in series. A typical cell (shown in Figure IV-13) consists of 2 dipole magnets, a quadrupole, a capacitor bank, and choke.

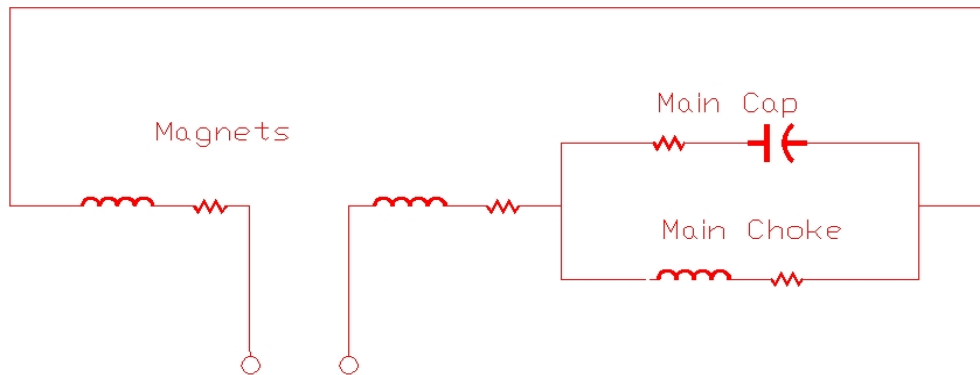


**Figure IV-13: Typical Magnet Cell**

Like the present Booster, the components in a typical cell will all be mounted on a steel girder. The electrical bus within the cells on either side of the straight sections would be extended to include the additional quadrupole magnets evenly spaced throughout the straight section.

Two main power buses (designated "upper" and "lower") would run completely around the ring and "folded" or connected to each other at one location. Thus the buses form a continuous loop around the ring with the magnet cells connected at uniform intervals. The currents in each bus would run in opposite directions to minimize the net magnetic field. Every other cell would be connected to the upper bus and the remaining cells connected to the lower bus. Although, owing to its series connection, the distributed resonance circuit provides a basic uniformity in magnets currents, the effect of leakage capacitance currents to ground can distort this current equality to a degree that is significant. Since these leakage paths are distributed around the network in a generally uniform manner, it is necessary to ensure that the AC potentials of the corresponding points in the network attain a similar value. This is achieved by matching equivalent cell magnet inductances, close tolerances of each resonant cell components and auxiliary windings in chokes  $L_{ch}$  connected in parallel with each other.



**Figure IV-14: Fermilab Booster magnet girder**

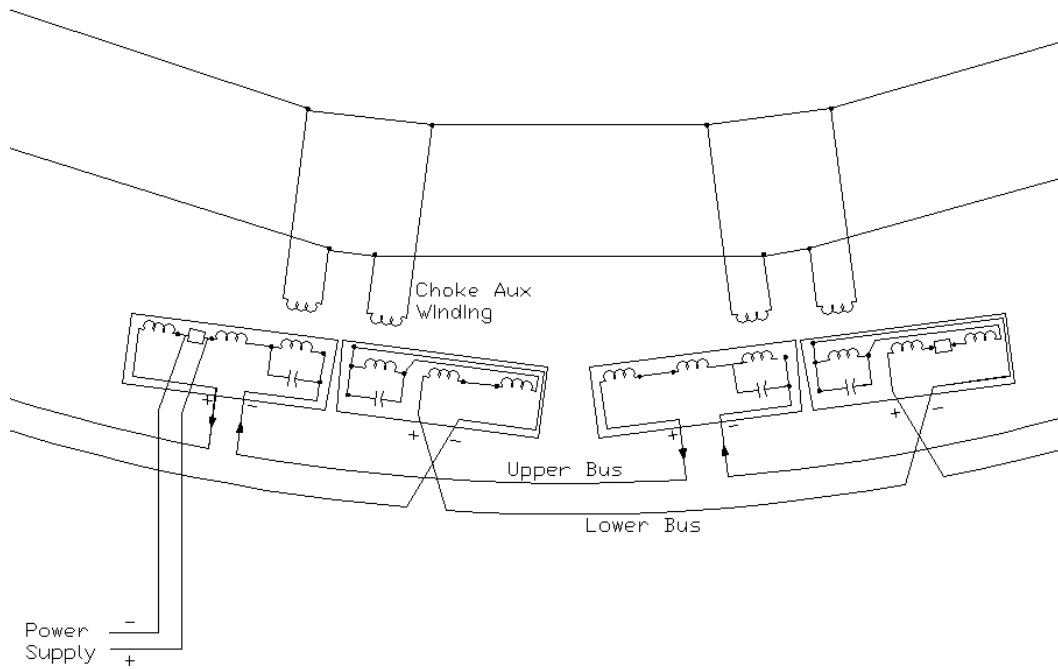


**Figure IV-15: Tunnel schematic showing 4 resonant cells**

Four main power supplies installed in 2 different locations will be connected in series with the magnets. In each power supply location one power supply will be connected to the upper bus and the other to the lower bus. In this way the maximum voltage to ground seen by any magnet will be less the 600 volts. The power supplies are connected near virtual ground of the distributed resonant circuit. Each power supply will be rated for 700 volts that will allow for normal operations with one power supply off-line. As with the present Booster, the power supplies will be phased-control units operating in 12-pulse (720 Hz) mode.

The regulation system will consist of transducers to measure the magnet current in a couple of locations and an embedded computer system to control the amplitude and phase of the 10 Hz current.

#### **IV.3.3.2 Power supplies for Trim Magnets (Correctors, Sextupoles, Trim quads)**

There are numerous correction power supplies needed to operate the RCS. Table IV-8 lists the various kinds of magnets and the proposed power supplies.

The sextupole, dipole corrector, and skew quad trims are individual magnets inserted into to the lattice at the appropriate points. The quad trims and optics quads consist of trim coils built into the main magnet quads. The power supplies for these quads will have to have sufficient voltage to buck the existing 10 Hz voltage induced from the main coils as well as provide the necessary voltage to produce the desired current in the trim coils. A similar system exists in the Main Injector where the large aperture quad magnets have internal trim coils for field correction. All the correction power supplies will be 4-quadrant, switch-mode units based on existing Fermilab designs.

The 50 volt units will be copies of correctors recently installed in a Booster upgrade project. The higher voltage units will be new designs based on the sextupole power supplies designed and built for the Main Injector.

<b>MAGNET TYPE</b>	<b># OF MAGNETS</b>	<b># OF POWER SUPPLIES</b>	<b>VOLTAGE/CURRENT</b>
<b>F Quad trims</b>	<b>48</b>	<b>1</b>	<b>400V/20Amp</b>

<b>D quad trims</b>	<b>48</b>	<b>1</b>	<b>400V/20Amp</b>
<b>F Sextupoles</b>	<b>50</b>	<b>2</b>	<b>600V/10Amp</b>
<b>D Sextupoles</b>	<b>48</b>	<b>2</b>	<b>600V/10Amp</b>
<b>Regular Dipole Correctors</b>	<b>128</b>	<b>128</b>	<b>50V/10Amp</b>
<b>Injection Dipole Correctors</b>	<b>8</b>	<b>8</b>	<b>50V/10Amp</b>
<b>Optics Quad Correctors</b>	<b>36</b>	<b>36</b>	<b>50V/40Amp</b>
<b>Skew Quad Correctors</b>	<b>12</b>	<b>12</b>	<b>50V/10Amp</b>

**Table IV-8: Trim power supplies required for the RCS**

#### **IV.3.3.3 Pulsed power supplies (kickers, septa)**

?????

### IV.3.4 Vacuum system

Proton scattering on the residual gas atoms results in the particle loss and emittance growth. The particle loss is mainly determined by single scattering. For energies 2 GeV and above the scattering cross section is dominated by nuclear scattering. In this case the probability of particle loss in the course of acceleration is:

$$W = n_a \sigma_s \int_0^T (\beta c) dt \approx n_a \sigma_s c T .$$

Assuming that molecular nitrogen dominates the scattering and taking into account that the cross section is  $\sigma_s = 330$  mbarn/atom, the cycle time is  $T=50$  ms, and the average pressure is  $10^{-7}$  Torr ( $n_a=7 \cdot 10^9$  cm<sup>-3</sup>) one obtains  $W=3.5 \cdot 10^{-6}$ . The normalized RMS emittance growth is determined by the multiple scattering and is equal to:

$$\Delta \varepsilon_{nx} = 2\pi r_p^2 c Z^2 n_a L_c \beta_x \int_0^T \frac{dt}{\gamma \beta^2} ,$$

where  $r_p$  is the classical proton radius,  $Z$  is the nuclear charge,  $L_c$  is the Coulomb logarithm, and  $\beta_x$  is the average  $\beta$ -function. For the above parameters and  $\beta_x = 4.8$  m one obtains the emittance increase of  $3.4 \cdot 10^{-3}$  mm mrad. Thus for vacuum levels of  $10^{-7}$  Torr or better (N<sub>2</sub> equivalent), the scattering on the residual gas scattering is not an issue. The electron multipactoring and related deterioration of vacuum is expected to be the more important limitation.

The RCS is composed of 132 half cells. The vacuum layout for a half cell is shown schematically in Figure IV-16. As one can see from the above estimate the required vacuum level in this accelerator is not stringent:  $\leq 10^{-7}$  Torr. However, this system does require some novel features such as titanium nitride (TiN) coating (to suppress multipactoring) and RF shielding on ports and bellows (to reduce the ring impedance). Experience from existing accelerators will provide a basis for design and cost estimation.

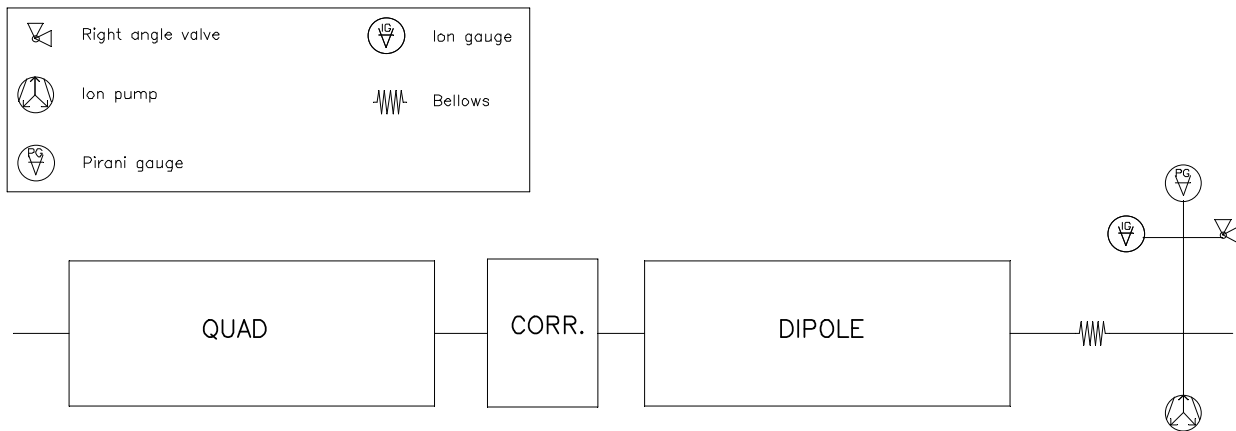


**Figure IV-16: Typical vacuum layout for an RCS half cell.**

The required beam tube size for the quadrupoles and dipoles is 44 mm OD, transitioning to 2 inch OD for the rest of the vacuum chamber. The wall thickness is 0.7 mm inside magnets. It can be larger at other places. Bellows and pumping ports will require RF shielding. In order to

minimize the secondary emission yield from the chamber wall, the entire vacuum chamber will be coated with TiN. This has been done successfully at the SNS and the PEP II B-Factory.

Because of magnetic permeability requirements, the vacuum chamber will be constructed of 316LN stainless steel. It will be electropolished and hydrogen degassed prior to coating with TiN. Alternatively, Inconel 718 is being considered as a promising choice of material for the quadrupole and dipole beam tube. It has high electrical resistivity for reducing eddy current effects and high strength for structural stability. Disadvantages include the high cost and the challenge of coating with a thin and highly uniform copper layer (which would not be required for the stainless steel option).

Vacuum levels will be maintained with ion pumping. Additional pumping may be needed in some areas depending upon out gassing rates of specific accelerator components or special needs in certain areas (interfaces between accelerators, diagnostic components, etc.). The system will not require an *in-situ* bake. Ion gauges and convection gauges will provide vacuum read back.

## IV.4 MI/RR

### IV.4.1 Requirements

The Fermilab Recycler is a fixed energy 8 GeV storage ring using strontium ferrite permanent magnets in the Main Injector tunnel. For the NOvA program, the Recycler will be converted from an antiproton storage ring to a proton accumulator for single turn injection into the Main Injector. We assume these upgrades are complete.

The Recycler will boxcar stack 6 cycles from the RCS and perform a single turn extraction into the Main Injector for neutrino operations. The Main Injector will receive  $1.6 \times 10^{14}$  protons from the Recycler in a single turn and will accelerate them to 120 GeV in 1.4 seconds. This intensity is about 3 times the beam intensity the Main Injector will be required to accelerate for the NOvA program.

### IV.4.2 Configuration

As the Recycler is built with permanent magnet quadrupoles, permanent magnet combined function devices, powered dipole correctors, and a tune trombone of powered quadrupoles, we anticipate the need for more flexibility in the lattice design. The installation of new powered quad elements allows for lattice flexibility.

Both the Recycler and Main Injector will need new RF systems. The current Main Injector RF system does not have the power to accelerate the required beam intensity to 120 GeV in 1.4 seconds (even with the addition of a second power tube per station). We include an upgraded RF system capable of handling the required intensity. To achieve the required bunching factor a substantial second harmonic RF system is also needed. An initial design exists for the primary system cavities but not for the second harmonic cavities. For the Recycler, a new 53 MHz RF to capture the injected beam is included in the project. As in the Main Injector, a second harmonic RF system is necessary.

The maximum peak current required assumes three times the protons per 53MHz bunch in Main Injector of the current operation. Electron cloud instabilities could be a limitation to the maximum Recycler and Main Injector intensities. We are investigating the threshold of the instability, and its dependence on various parameters (bunch spacing, bunch length, SEY, etc.) with simulations. Meanwhile we are developing a plan of coating the Recycler and Main Injector beam pipes in-situ with TiN, as there is no easy way of replacing the Main Injector

beam pipe without disassembling the magnets. The TiN coating can decrease the secondary emission yield (SEY) of the Main Injector beam pipe by 40%

For high efficiency acceleration through transition, the Main Injector also needs a first order matched  $\gamma$ -t jump system consisting of 8 sets of pulsed quad triplets. The system can provide a maximum  $\gamma$ -t jump of 2 units in 0.5 ms, 16 times faster than the normal ramp.

## IV.5 Cryogenics

### IV.5.1 Cryogenics Requirements

The cryogenic system scope for Project X includes a new cryogenic plant, a cryogenic distribution system, and the necessary ancillary systems (purification system, cryogenic storage, etc.) to support the plant. A conceptual layout for the cryogenic system is shown in Figure IV-17.

The cryogenic distribution system accommodates a range of steady state and transient operating modes including RF on/RF off, cool down, and warm-up and fault scenarios. The system includes feed boxes, cryogenic transfer lines, bayonet cans, feed and end caps, string connecting and segmentation boxes, gas headers, etc. It will be capable of supporting operation of the linac within cool down and warm-up rate limits and other constraints imposed by accelerating SRF components. Protecting the superconducting RF cavities from over pressurization beyond the component's maximum allowable working pressure during fault conditions will be accommodated by the cryomodules and cryogenic distribution system. Liquid helium at 4.5K will be transported to the crab cavities in the 2 GeV transport line with a dedicated cryogenic distribution system similar to the existing Tevatron transfer line. Components of the cryogenic distribution system contain cryogenic control and isolation valves, cryogenic instrumentation, safety valves, etc.

It is assumed that on the time scale of the Project X, a large portion of the Tevatron ancillary cryogenic components will be available for use by the project. These components include cryogenic nitrogen and helium dewars, gas storage tanks, purifier compressors, cryogenic transfer line and parts of the inventory management system.

### IV.5.2 Cryogenics Configuration

The 325 MHz linac (Low  $\beta$  section) components are cooled by two-phase superfluid liquid helium at 1.8 K. There is a single unit for the cryomodules containing spoke resonators. For the spoke resonators, the dynamic heat load (due to RF power dissipation) at 1.8 K dominates the static heat load (due to conduction and radiation).

The 1300 MHz linac components consist of saturated He II cooled cavities to 1.8 K with two He gas thermal shields in the ranges of 5-8 K and 40-80 K. The dynamic heat load at 1.8 K is an order of magnitude greater than the static heat load. The 1300 MHz linac is divided in two cryogenic units; one containing cryomodules of type S-ILC ( $\beta=0.81$ ) and one of type ILC ( $\beta=1$ ). There are fourteen S-ILC and ten ILC cryomodules in each respective unit. The cryogenic feed point will be between the two units.

A preliminary heat load estimate has been performed and the estimated uncertainty of the calculations is 20% for the 1.8K load and 50% for the 5-8K and 40-80K loads. For the design study, an additional 20% is applied to the estimated heat loads to ensure the system could meet all operational requirements. With these two factors, the total equivalent design capacity at 4.5 K for the entire linac is approaching 30 kW. The physical size of a plant of

this capacity is too large to house in a single cold box. As a result, two cold boxes are envisioned; one to support the 1.8K loads and one to support the two shield loads.

A wide range of possible cryogenic plant design solutions that satisfy all requirements and constraints for Project X will be studied further. Combining effective use of the existing Fermilab infrastructure with commercially available components requires further study. The solution will be based on cycles with cold compression, or hybrid – cold and ambient temperature compression. Ease of operation, reliability, ability to operate efficiently over a wide range of loads, capital and operational costs, and other factors will be considered in selecting technology for the Project X cryogenic plant.

Operation of Project X in a continuous wave mode results in very high dynamic heat loads to the cryogenic system. A study will need to be performed to ensure that the Project X cavity operating temperature is optimized for a minimum combined capital and operating cost while maintaining system reliability.

## IV.6 Instrumentation

As described in the ICD-1 (v1.1), we will need various beam instrumentation and diagnostics systems to characterize the beam parameters and the performance in all Project X sub-accelerators. For startup and initial beam commissioning we need to provide, at a minimum, beam instruments in order to observe:

- Beam intensity
- Beam position / orbit
- Transverse beam profiles
- Beam phase / timing

The high beam intensity / power and the presence of superconducting technologies also require a reliable, fail safe machine protection system (MPS) to prevent quenches in cryogenic elements or damages due to an uncontrolled loss of the high power beam. This system will be based on beam loss monitors (BLM) and other beam detection systems e.g. toroids (beam intensity).

Beside these core beam instrumentation systems, more specialized beam diagnostics need to be provided, e.g. to characterize the longitudinal bunch profile and tails, transverse beam halo, and more advanced beam emittance monitors. Even though some types of beam monitors (e.g. BPMs, toroids, etc.) can be standardized for most areas, the H<sup>-</sup> source, the synchrotron, and injection / ejection areas demand some dedicated beam diagnostics (Allison scanner, fast Faraday cup, e-beam scanner, vibrating-wire, etc.).

A complete set of “beam instrumentation requirements” has to be established. Each sub-accelerator (linac, transport lines, RCS, MI, RR) needs to address the operating modes with the nominal, as well as non-standard beam parameters, and all requirements for the different beam instruments (resolution, precision, dynamic range, etc.).

For ICD-2, the required beam instrumentation systems are almost identical to those listed in ICD-1 (BPMs, toroids, BLMs, beam profile monitors, special and “exotic” beam monitors). There are however some substantial differences in operation and data acquisition, as of the quasi CW operation of linac and transport lines, and the added rapid cycling synchrotron (RCS):

### **Linac and transport-lines**

Internal calibration systems, as well as data acquisition, and transport cannot make use of a long pause in the beam pulse (there is none in CW operation). The integration times of some of the measured parameters, e.g. beam intensity, and their time stamping has to be discussed in detail.

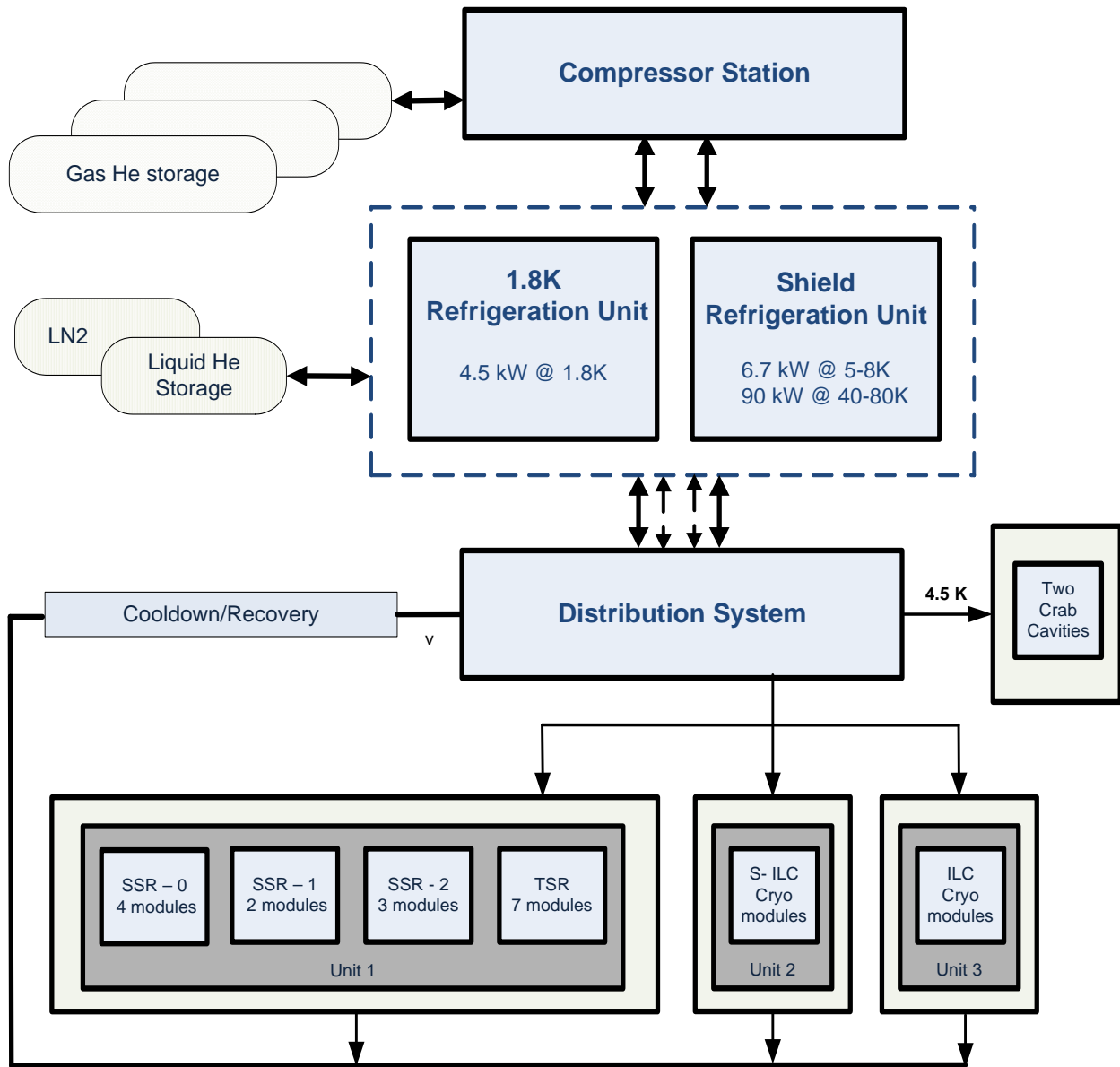


**Figure IV-17: Conceptual Layout for the Project X Cryogenic System**

### RCS

The synchrotron will be equipped with 132 BPMs. All will have a high resolution ( $\sim 50 \mu\text{m}$ ) turn-by-turn mode, being able to capture all orbits of a complete cycle (2-8 GeV). Other diagnostics systems in the RCS include beam intensity (toroid, WCM) and profile (wire-scanner, e-beam scanner, OTR) monitoring. As of the high beam intensities, transverse and longitudinal beam damping systems will be provided to mitigate instabilities.

Sufficient physical space will be made available to accommodate the required beam detection elements. At some critical, real-estate limited locations, e.g. LEPT, MEPT,

injection / ejection, and SRF areas, a compromise has to be worked out, which enables a decent way to sense the beam without compromising its quality in the diagnostic sections.

## **IV.7 Controls:**

The control system for the ICD-2 configuration of Project X would be fundamentally the same as for ICD-1. This would be a single integrated control system for the entire complex based on an evolution of the current Fermilab system augmented to support EPICS based subsystems. The operational scenarios for the linac described in Section II.2, with repeating short intervals of fixed bunch patterns, can be accommodated within the same timing framework as for ICD-1. The RCS would be controlled using similar technology as in the Main Injector and current booster accelerators. The CW nature of the linac would require the machine protection system, and any trajectory stabilization or other fast feedback systems, to operate without the long gaps present in the ICD-1 design.

## **IV.8 LLRF**

The Low Level RF system encompasses the programming and regulation of the cavity field amplitude and phase as required by longitudinal beam dynamics in the machine. It also controls or interfaces to much of ancillary equipment that is involved in the generation of RF. Hardware and software modules includes Cavity Field Controllers, PZT Controllers, Master Oscillator, Phase Reference Line, LO distribution, transfer synchronization and the interfaces to interlocks, timing systems and the control system. This section will cover first the 2 GeV CW 325MHz and 1300MHz Linac followed by the 2-8 GeV 53 MHz RCS requirements and system description.

### **IV.8.1 LLRF for the CW 2 GeV SRF LINAC**

The proposed high level RF configuration for the CW linac provides a single power amplifier for each of the 251 cavities as opposed to the “one klystron drives many cavities” scheme of ICD-1. While this increases the number of LLRF controllers it does not greatly increase the component count and reduces project risk by following a more traditional control scheme. The design beam current field gradients determine the loaded cavity Qs and the cavity bandwidths. Analysis of the 1mA beam current and cavity gradients show that loaded Qs may be kept down in the low  $10^7$  range where control of cavity microphonics will not create excessive RF power demands, nor large field disturbances. In addition, CW operation eliminates the dynamic effects of Lorentz force detuning and modulator droop. In many ways ICD-2 will operate in a regime similar to the 12GeV upgrade of CEBAF. The largest disturbance to the cavity fields will be the beam structure produced by the beam chopper. The LLRF system will provide the chop pattern and will therefore have the information required for accurate beam loading compensation. The ICD-2 linac does not present any great challenges for field control beyond that of the Project X ICD-1 linac. A comparison of the ICD-1 and ICD-2 proposals is shown below.

For cost savings and hardware simplicity, the LLRF controllers will be grouped into stations that will cover two cryomodules (nominal 16 cavities) and the associated RF equipment. Fermilab has been extensively involved in SRF LLRF Control Systems for the ILC and the varied ongoing SRF programs on site. Two types of digital controllers have been developed and are in use, each of which could be modified to meet ICD-2 requirements.

RF and microwave hardware has also been developed for HINS and ILCTA that directly apply to Project X. Ongoing R&D will determine the details of the beam-based calibration and of the phase reference distribution system.

**Table IV-9: RF Control Parameter Comparison**

	ICD-1	ICD-2
Duty Factor	pulsed 10 Hz, 2ms	CW operation -Chopped
Beam Current	25mA	1mA
Cavity/PA Ratio	16:1	1:1
Regulation	1 Deg., 1%	1 Deg., 1%
Control loops	GDR	GDR, SEL

#### IV.8.2 LLRF for the Rapid Cycling Synchrotron

The details of the RCS RF system may be found in sections III.3.3 and IV.3.2. Basic RF and beam control will be handled by a conventional beam phase lock loop nested inside a radial position loop. Feedforward programming for dynamic frequency and phase settings will be calculated from beam momentum programming. These loops provide for mode 0 dipole damping and beam energy regulation. The RCS RF is switched to the control loops at the very beginning of injection. The linac beam chopper is phase locked to the RCS RF so that all injected particles would be inside RF buckets. Just before extraction the RCS RF will be locked to the Recycler Ring RF. There are 16 fundamental cavities operating between 50.33 MHz and 52.8 MHz and ten second harmonic cavities slaved to fundamental cavities with a required tracking of better than 5 degrees between systems. As discussed in section III.3.3, this tracking requirement combined with the 2.2 A of beam current and the 50 to 1 voltage swing over the acceleration cycle provide a large challenge for the control system.

For example, at extraction, a second harmonic cavity will be required to maintain a gradient on the order of 1kV while the beam induced voltage will be 220 kV. Maintaining the required phase will require regulation to 100V or about 67dB of disturbance suppression. Learning feedforward systems may provide 30 dB, leaving 37dB of suppression to the feedback systems. Achievement of this specification will require a FPGA based digital IQ feedback system in combination with a direct RF feedback system that has 120 ns latency or less. It is likely that a 1-turn delay or comb filter feedback system will be required to suppress the first few revolution lines in the spectrum produced by the 10-bunch kicker notch. These demanding feedback systems require a highly linear, wideband HLRF power amplifier. The hardware and system design for the RCS LLRF may be derived from much of the same hardware and software used in the CW linac and the present Main Injector RF control systems.

#### IV.9 Safety and radiation shielding

Operation of accelerators and beam transport lines at the significantly higher beam power envisioned for Project X ICD-2 presents some new challenges. Simple extrapolation of the methods used at Fermilab to design existing, relatively low power accelerators will be not

sufficient. Fortunately, techniques developed at megawatt power accelerators such as SNS can be readily applied to Project X. Such techniques are already being applied at Fermilab to enhance operation of existing accelerators and beam transport lines. It will be shown that radiation protection can be realized for Project X through the straightforward process methods currently in use along with a supplemental machine protection or beam loss management system.

There are two basic requirements for radiation protection to be observed. First are the regulatory requirements from the Code of Federal Regulations, DOE Orders, and the State of Illinois that are enumerated in the Fermilab Radiological Controls Manual (FRCM). These requirements are related to health and safety of workers, the public, and the environment. Second are the practical machine control requirements that are necessary to protect machines from short term and long term damage due to beam loss. Prevention of excessive losses improves machine reliability, reduces the frequency of breakdowns, and simplifies required maintenance due to the need for less complex radiation protection procedures. While the methods for achieving these radiation protection requirements may be overlapping, the requirements for personnel and environment protection methods tend to be more rigorous and prescriptive than those required for meeting machine protection requirements. Controls designed primarily for machine protection may not be sufficiently rigorous for the regulatory mandated personnel and environmental protection. However, a machine protection system installed throughout the complex will be of utmost importance in order to prevent catastrophic failures. The details for the manner in which such a system is implemented (e.g., a safety system or controls system) will need to be addressed.

An electronic berm system has been considered for ICD-2. The E-berm systems that have been conceptualized to date are capable of detecting a 1 to 2% beam loss. Since many parts of ICD-2 are rated for 2 MW beam power, this means a 20 to 40 KW beam loss could persist without detection by an E-berm system until some permanent damage occurs to otherwise disable the accelerator complex. In order to protect Project X ICD-2 machines, a more sensitive and pervasive beam loss monitoring system will be required to be installed in accelerator and beam transport enclosures. A continuous argon-filled heliix cable acting as an ion chamber installed, for example, at the ceiling of accelerator/beam transport line enclosures could be used to not only identify that a loss condition exists but also pinpoint the location of the loss. Such systems have been considered for other high power accelerators.

Some important aspects of radiation and environmental protection are discussed in the following sections. No issues have been identified which would preclude construction and operation of the Project X ICD-2 concept.

#### **IV.9.1 Prompt radiation shielding**

Earth shielding for accelerator/beam transport enclosures can be easily determined for when the expected beam power loss is defined. In the case of ICD-2, one could design the shield so that limits for uncontrolled access to berm surfaces could be allowed under conditions of full beam power loss. For example (see Table IV-10), for a 2 GeV, 2 MW beam loss in an enclosure with a distance of 5 feet from an accelerating cavity to tunnel ceiling, the shielding required to limit radiation levels at the surface to 1 mRem/hr is approximately 26.7 feet.

Beam enclosure	Cossairt Criteria	Beam energy	Beam Power	Component to ceiling distance	Required shielding
2 GeV linac	1a	2 GeV	2 MW	5	26.7 feet
RR/MI	1a	8 GeV	340 KW	1	28.1 feet
RR/MI	1a	120 GeV	2.1 MW	5	25.7 feet

**Table IV-10: Shielding requirements for several beam power/enclosure geometries**

It is feasible, for example, to build the 2 GeV linac enclosure with a 26.7 foot earth shield. However, if such an accident condition were to occur, catastrophic damage would result to an accelerating structure, beam pipe, or magnet. It will be possible to develop a plausible beam power loss strategy that could be used as a basis for the final shield design for the 2 GeV linac as well as the remainder of the complex for the ICD-2 era.

A machine protection system or beam loss management system which is capable of detecting low power beam loss and interrupting beam operation will be required for a number of purposes, some of which are described further below. Such a system could be used as a basis to establish shielding criteria.

#### IV.9.2 Collimation systems to control beam losses

Collimation systems are a fundamental requirement for high power accelerators, beam transport lines, and the ion stripping injection region used in Project X. Multiple stage collimation systems are designed and strategically placed to remove beam halo in controlled, shielded locations. With proper optics and orbit control following collimation systems, beam losses in accelerators, in transport lines and at injection/extraction regions become relatively small, permitting high power operation in conjunction with a relatively safe working environment for beam enclosure maintenance related activities. Collimation systems have been incorporated upstream in the MI8 line and in the Main Injector accelerator with the remarkable result that residual radiation levels in the associated accelerator and beam line enclosures have decreased while beam power has increased. Collimation systems have also been used at the SNS with similar result. An H<sup>-</sup> stripping foil/collimation system will also be included at RCS injection system. Collimation systems must be designed with shielding to allow personnel access for maintenance and to prevent excessive air, ground and surface water activation. While collimation systems are designed to meet machine protection requirements, they also provide intrinsic radiation protection necessary for feasible operation of high power accelerators and beam lines.

#### IV.9.3 Electronic berm

The existing passive shielding for the Recycler Ring and Main Injector enclosure may not be sufficient for operation at 2 MW. High intensity losses might be tolerated by devices such as Lambertson magnets at injection or extraction regions that could lead to excessive radiation dose rates on the shielding surface. An electronic berm could be used to compare beam intensity injected into Recycler Ring with that extracted from the Main Injector. A 1 to 2% difference could be detected on a pulse-to-pulse basis which would lead to a beam

inhibit. Other controls such as radiation fences, radiation postings, and entry controls may also be a feasible alternative radiation protection option. Finally, a machine protection system could be considered for the RR/MI enclosure which could provide an even more sensitive level of control.

#### **IV.9.4 Accelerator component activation and residual radiation levels in accelerator/beam line enclosures**

Residual radiation levels in beam transport lines and accelerators due to operational beam losses must be controlled in order to conduct maintenance activities while keeping personnel radiation exposure as low as reasonably achievable (ALARA). For the beam power associated with ICD-2, small fractions of a percent loss will result in very high residual radiation levels which would render beam enclosure access difficult and maintenance at loss points extraordinarily difficult. A sensitive machine protection system which inhibits beam operation when significant losses are present will be required to allow access and maintenance activity modes historically enjoyed at Fermilab.

For design purposes, a loss rate of 3 to 10 watts/meter results in a dose rate of about 100 mR/hr at one foot from beam line components such as magnets and accelerating cavities following a 30 day irradiation period and 1 day of cool down. A loss of 0.25 watts/meter results in a dose rate of about 100 mR/hr at one foot from low mass components such as beam pipes for the same irradiation/cooling period. Radiation levels are typically at least a factor of 5 less than these levels. For example, for a typical magnet beam loss location at 2 watts per meter, the fractional beam power loss is 1 ppm. A sensitive machine protection system will be required to quickly identify and suspend operation in the event such losses occur.

#### **IV.9.5 Surface and ground water activation and air activation**

##### **IV.9.5.1 2 GeV Linac, Experimental Halls, RCS, and Transfer Line to RR Enclosures**

The site chosen for these enclosures is presently at the center of the Tevatron beam enclosure. In order to evaluate ground water activation, a geological survey (core borings) will be required to understand ground water migration rates at this site since no data presently exists. It would be prudent to begin characterization of the proposed site in order to confirm its suitability for ICD-2. In addition, the results of such characterization will be required in order to proceed with design of collimation system shielding and enclosure elevation determination.

Surface water and air activation must also be characterized. In order to calculate surface water and air activation, it will be necessary to know what type of machine protection system will be employed so that limits for surface water discharge can be understood. That is, the machine protection system will serve to limit the total beam loss which would also determine the level of surface water and air activation. Integration of these activation levels over the projected operating period would yield an estimate of annual surface water and air activity to be released from the facility. This estimate is necessary in order to ensure compliance with regulatory discharge permit limits for surface water and air.

#### IV.9.5.2 Recycler Ring and Main Injector Enclosures

Surface water, ground water, and air activation have been studied for the existing Recycler/Main Injector rings. Scaling from existing conditions and assuming the use of additional controls (e.g., E-berm or machine protection system) to limit uncontrolled losses in the Recycler and Main Injector machines, the surface water activation, ground water activation and air activation should remain well within acceptable limits. The design for the RR/MI machine protection system will need to be understood in order to actually evaluate air, surface water, and ground water activation.

### IV.10 Conventional Facilities

This Chapter outlines the conventional facilities required to house and support the proposed 2-GeV superconducting H<sup>-</sup> linac and 8 GeV Rapid Cycling Synchrotron (RCS). Civil construction for the proposed facility includes all below-grade beam-line enclosures. All above-grade buildings, roads, parking, utilities and services to accommodate the equipment for the operation of the linac on the Fermilab site are also included.

Construction of the below-grade linac and RCS beam line and beam transport line to the Main Injector as well as the above-grade service buildings are similar to previously utilized and proven construction methods previously executed at Fermilab. Construction of all below-grade enclosures consists of conventional open-cut type construction techniques. The architectural style of the new buildings reflects, and is harmonious with, the existing buildings. Currently, the layout has been optimized for the accelerator requirements. Future layouts will consider existing topography, sustainability, watersheds, vegetation, natural habitat, and wetlands. All the aspects will be thoroughly addressed in the Environmental Assessment for this project.

#### Site Construction

##### 1. Site work

- a. Site Drainage will be controlled by ditches and culverts while preserving the existing watershed characteristics both during construction and subsequent operation.
- b. Road Construction includes a new temporary construction road providing access to Butterfield Road. This road will provide direct access for construction traffic during construction only – roadway will be restored to original condition upon completion of the project. New Service Road will provide permanent access to all service buildings and utility corridor.
- c. Landscaping includes the restoration of disturbed areas. Construction yards and stockpile areas will be removed after completion of the construction phase of the project. All disturbed areas will be returned to a natural state or landscaped in a similar manner as found at other Fermilab experimental sites. Erosion control will be maintained during all phases of construction.
- d. Wetlands Mitigation includes the avoidance or minimization of adverse impacts to wetlands in the project area. Environmental consultants would delineate wetlands, and a Clean Water Act permit application prepared for submittal to U.S.

Army Corps of Engineers for impacts that cannot be completely avoided.

Compensatory mitigation would be provided according to terms and conditions of the permit. This may be in the form of purchased wetland bank credits, restoration or enhancement of existing wetlands on site, or creation of new wetland areas. The permit would dictate the amount and type of mitigation, which must be in place prior to the initiation of construction. A

Floodplain/Wetland Assessment pursuant to 10 CFR 1022 would be incorporated into the Environmental Assessment.

## 2. Utilities

The following utilities are required to support the operation of the facility. The list incorporates current assumptions and will require further refinement as the design process progresses.

- a. Electrical Power includes new duct banks and utilization of existing duct banks from two sources including Kautz Road Substation (KRS) and Master Substation (MSS). Separate high-voltage feeders with backup will be provided for conventional, machine and cryogenic power.
- b. Communications include new duct banks tied into the existing communication network along Kautz Road.
- c. Chilled Water (CHW & CHWR) for machine and building cooling will be supplied via new supply and return lines from the existing Central Utility Building (CUB).
- d. Low Conductivity Water (LCW) for machine cooling will be supplied via new supply and make-up water from the existing Main Injector ring LCW system.
- e. Industrial Cooling Water (ICW) for fire protection will be supplied via new supply and return lines from the existing D-0 Utility Corridor.
- f. Domestic Water Supply (DWS) for potable water and facilities will be supplied via new supply line from the existing D-0 Utility Corridor.
- g. Sanitary Sewer (SAN) for facilities will be supplied via new sewer main and lift station from to the existing D-0 Utility Corridor.
- h. Natural Gas (NGS) for building heating will be supplied via new supply lines from the existing D-0 Utility Corridor.

## 3. Facilities Construction

Conventional facilities will be constructed with future upgrade capabilities considered in the initial design phase. Equipment galleries, enclosures and surface buildings will be designed to accommodate future expansion of the technical components of the facility. See Figure IV-18 for a site map and facilities locations and Table IV-11 for description of facilities.

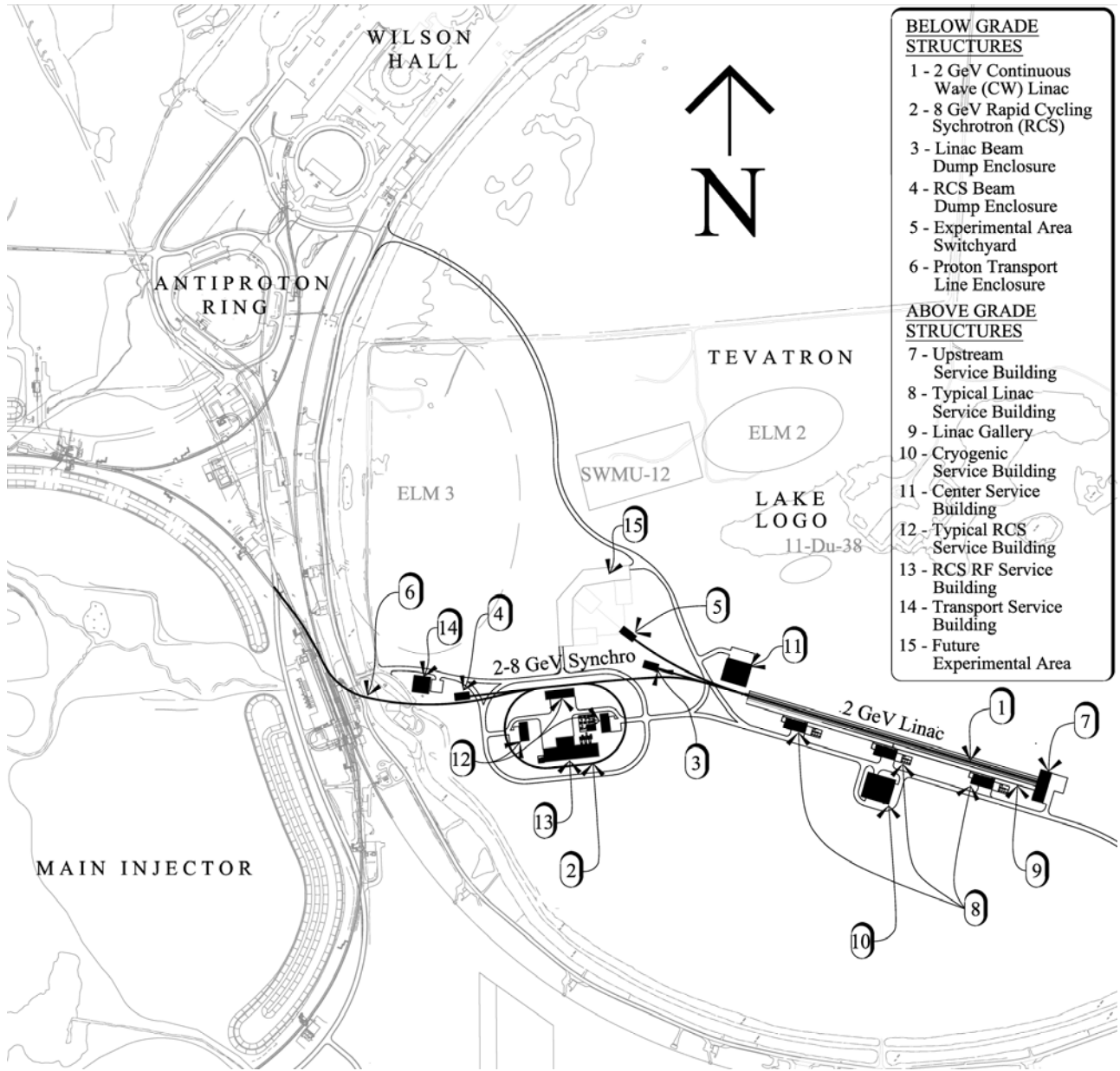


**Figure IV-18: Site Plan**

<b>Item No.</b>	<b>Facility Name</b>	<b>Function</b>	<b>Contents</b>
<b>BELOW GRADE STRUCTURES</b>			
<b>1</b>	2 GeV Continuous Wave (CW) Linac Beam Line Enclosure	Below-grade enclosure for equipment/controls for linac H- accelerator components	H- source, RF cavities, magnets, beam instrumentation and utilities
<b>2</b>	8 GeV Rapid Cycling Synchrotron (RCS) Beam Line Enclosure	Below-grade enclosure for equipment/controls for RCS accelerator components	RF cavities, magnets, beam instrumentation and utilities
<b>3</b>	Linac Beam Dump Enclosure	Below-grade enclosure for equipment/controls for linac H- abort components	Concrete block and steel shielding and utilities for linac abort system
<b>4</b>	RCS Beam Dump Enclosure	Below-grade enclosure for equipment/controls for RCS abort components	Concrete block and steel shielding and utilities for linac abort system
<b>5</b>	Experimental Area Switchyard	Below-grade enclosure for transport of H-beam to Experimental Area, stripping, and RF separation to experiments	Beam transport magnets, collimation, RF separation and utilities
<b>6</b>	Proton Transport Line Enclosure	Below-grade enclosure for proton transport from RCS to the Recycler	Beam transport magnets, collimation and instrumentation
<b>ABOVE GRADE STRUCTURES</b>			
<b>7</b>	Upstream Service Building	Building for personnel/equipment access for installation and operation of low-energy support equipment and tech space	Electrical equipment and controls, utility services and H- source support equipment
<b>8</b>	Typical Linac Service Building	Building for LCW pumps, electrical services, power supplies and controls	Heat exchangers, pumps, electrical equipment, power supplies and controls
<b>9</b>	Linac Gallery	Building for equipment for RF power generation	RF amplifiers, modulators, controls and utilities
<b>10</b>	Cryogenic Service Building	Building for equipment for helium refrigerator plant	Compressors and helium cold boxes
<b>11</b>	Center Service Building	Building for personnel/equipment access for installation of linac	Crane bay, hatch and staging area
<b>12</b>	Typical RCS Service Building	Building for LCW pumps, electrical services, power supplies and controls	Heat exchangers, pumps, electrical equipment, power supplies and controls
<b>13</b>	RCS RF Service Building	Building for equipment for RF generation and accelerator control	RF amplifiers, modulators, magnet power supplies, utilities, controls, and local control room
<b>14</b>	Transport Service Building	Building and enclosure for correction power supplies and controls - 8 GeV Proton power supplies, instrumentation and controls	Power supplies and controls
<b>15</b>	Future Experimental Area	Site dedicated to future H- experimental halls	Future

**Table IV-11: Facilities Description**

## V Appendix A: Longitudinal Beam Motion in a Flat-Bottom Potential Well

The equation of motion is

$$\ddot{\phi} + \Omega_{s,0}^2 F(\phi, \phi_0) = 0, \quad \Omega_{s,0} = \omega_0 \sqrt{\frac{eV_0 q \eta}{2\pi m c^2 \gamma \beta^2}}, \quad (\text{A.1})$$

where  $q$  is the harmonic number,  $\eta$  is the slip factor,  $\omega_0$  is the revolution frequency,  $e$ ,  $m$ ,  $\gamma$  and  $\beta$  are the particle charge, mass and relativistic factors,  $V_0$  is the voltage of the first harmonic RF system, and  $\phi_0$  is the accelerating phase of the first harmonic RF system. In a general case of the two harmonic RF system the function  $F(\phi, \phi_0)$  can be presented in the following form

$$F(\phi, \phi_0) = \sin \phi - \sin \phi_0 - v_s \sin(2(\phi - \phi_0)) - v_c \cos(2(\phi - \phi_0)) + v_c, \quad (\text{A.2})$$

which was constructed so that it would satisfy  $F(\phi_0, \phi_0) = 0$ . The flat bottom potential well is determined by requirements of zeroing the first two derivatives:

$$dF(\phi, \phi_0)/d\phi|_{\phi=\phi_0} = d^2F(\phi, \phi_0)/d\phi^2|_{\phi=\phi_0} = 0. \quad (\text{A.3})$$

It results in

$$v_s = \frac{\cos \phi_0}{2}, \quad v_c = \frac{\sin \phi_0}{4}. \quad (\text{A.4})$$

Consequently, the total and accelerating voltages of the second harmonic RF system are:

$$V_1 = V_0 \sqrt{v_s^2 + v_c^2} = \frac{V_0}{4} \sqrt{1 + 3 \cos^2 \phi_0}, \quad (\text{A.5})$$

$$V_{a1} = -V_0 v_c = -\frac{V_0}{4} \sin \phi_0.$$

One can see that for the case  $\phi_0 = 0$  (no acceleration)  $V_1 = V_0 / 2$  and both the first and second harmonic RF systems do not transfer energy to the beam. In the case of beam acceleration the second harmonic decelerates the beam with decelerating voltage equal to  $1/4$  of the voltage of the first harmonic RF system. Thus the one quarter of the power transferred to the beam from the first harmonic RF is transferred back to the second harmonic RF system.

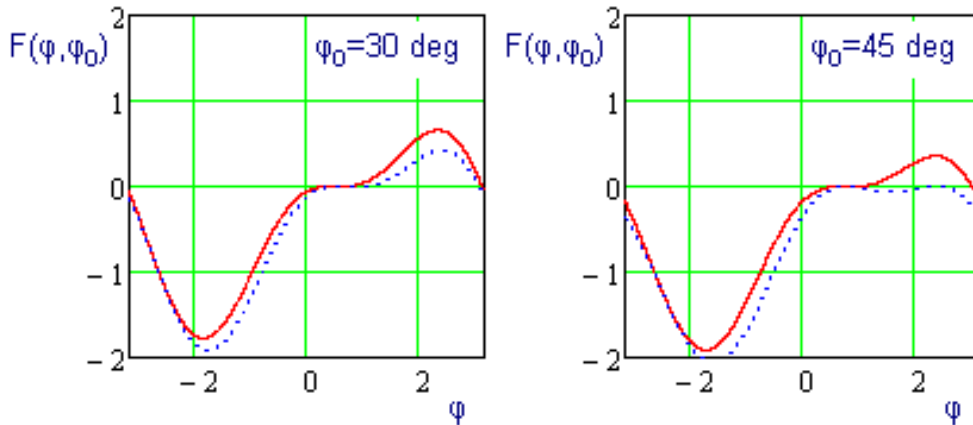


Figure A1.1. Dependence of  $F(\phi, \phi_0)$  on  $\phi$  for  $\phi_0 = 30$  and  $45$  deg and for the cases of the flat bottom potential well (red solid line) and the case of  $v_c = 0$  (blue dashed line).

To avoid the beam deceleration by the second harmonic RF system, use the requirements of zero derivative (first Eq. (A.3)) and  $v_c = 0$ . This situation is similar to the flat bottom case that results in  $v_s = \cos \phi_0 / 2$ . In this case, for small values of accelerating phase, the bottom of the well is still sufficiently flat. In contrast to the flat bottom case, such a scheme makes the bucket of finite size for  $\phi_0 < \pi / 4$  only (see Figure A.1.1.)

The total area of the RF bucket is:

$$\varepsilon_L \equiv \oint p(s) ds = \frac{8mcC}{\pi q\beta} \sqrt{\frac{eV_0 \gamma \beta^2}{2\pi mc^2 q \eta}} \Phi(\phi_0) . \quad (\text{A.6})$$

The form factors  $\Phi(\phi_0)$  were computed by numerical integration for the cases of (1) the single harmonic acceleration, (2) the flat bottom well, and (3) the case of  $v_s = \cos \phi_0 / 2$  and  $v_c = 0$ . Corresponding plots are presented in Figure A1.2. The dependences can be also approximated by the following equations:

$$\Phi(\phi_0) \approx 1.145 \frac{1 - \sin \phi_0}{\left(1 + \frac{1}{2} \sin \phi_0\right)^2} , \quad (\text{A.7})$$

$$\Phi(\phi_0) \approx 1.145 \frac{\left(1 - \frac{2}{\pi} \phi_0\right)^{1.8}}{1 - \frac{1}{4} \phi_0^6} , \quad (\text{A.8})$$

$$\Phi(\phi_0) \approx 1.145 \left(1 - \frac{2}{\pi} \phi_0\right) . \quad (\text{A.9})$$

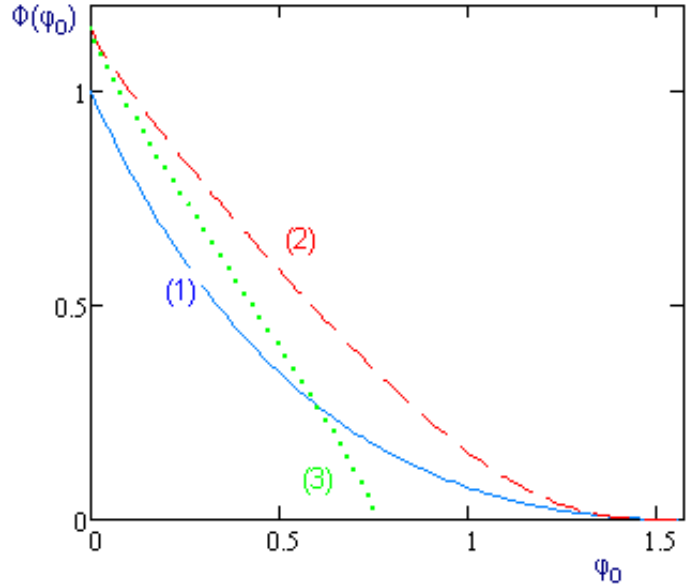


Figure A1.2. The form factors  $\Phi(\phi_0)$  for the cases of (1) the single harmonic acceleration, (2) the flat bottom well, and (3) the case of  $v_s = \cos \phi_0 / 2$  and  $v_c = 0$ .